Technical Report
TR-18-02
June 2019

Full-scale test of the Dome Plug for KBS-3V deposition tunnels

Project summary and evaluation of the final results

Jonas Enzell
Richard Malm

SVENSK KÄRNBRÄNSLEHANTERING AB

SWEDISH NUCLEAR FUEL
AND WASTE MANAGEMENT CO

Box 3091, SE-169 03 Solna
Phone +46 8 459 84 00
skb.se

SVENSK KÄRNBRÄNSLEHANTERING

ISSN 1404-0344
SKB TR-18-02
ID 1701635
June 2019

Full-scale test of the Dome Plug for KBS-3V deposition tunnels

Project summary and evaluation of the final results

Jonas Enzell, Richard Malm
Sweco Energuide AB

Keywords: Dome plug, Deposition tunnel end plug, Pressure test, Gas tightness test, Bentonite seal, Backfill transition zone, Filter, Gravel, Concrete dome, B200, KBP1016, DOMPLU.

Preface

This report summarizes the test results and conclusions from the full-scale test DomPlu, performed at the Äspö Hard Rock Laboratory regarding the system development for the KBS-3V deposition tunnel end plugs. The design, construction and initial pressurization of the DomPlu test was previously described in the report by Grahm et al. (2015). In this report, the results from three years of monitoring during constant water pressure of 4 MPa is presented. In addition, the test results from a gas tightness test, a strength test and finally the demolition of the plug are evaluated.

The formal name of the project is “Demolition and evaluation of the dome plug” (KBP1016) and the main project team consisted of the following people;

SKB:	Matti Nord (project leader), Patrik Hagman, Jens Rohwedder, Anna Pettersson, Pär Grahm, Mats Lundqvist, Karin Nilsson, Thomas Grybäck
Betong & stålteknik:	Carsten Vogt
Clay Technology:	Mattias Åkesson, Torbjörn Sandén
SWECO:	Richard Malm, Jonas Enzell, Manouchehr Hassanzadeh

The DomPlu project has included several different disciplines and is far too extensive to be reported in detail in this report. Therefore, several project reports have been developed during this project. This main report summarizes the project reports from the respective disciplines and presents additional results. Several others, in addition to the main project team listed above, have contributed to the project and performed work that has been published in the project reports.

Abstract

This is the final project report that summarizes the dome plug full-scale test (DomPlu) intended to evaluate the design concept of the deposition tunnel end plugs for the KBS-3V reference disposal system. The DomPlu full-scale test, was carried out at the Äspö Hard Rock Laboratory (Äspö HRL) and tested the plug system in a realistic environment with realistic and excessive loads.

The current SKB reference design and the DomPlu design for a deposition tunnel end plugs are similar, except for a few experimentally related modifications. The DomPlu therefore represents a more detailed iteration of the basic design rather than a fundamental change to the earlier plug experiments undertaken by SKB.

In this project, the behaviour of the plug has been evaluated when subjected to a constant water pressure load of 4 MPa for three years. After this, a gas tightness test was performed to evaluate the gas tightness of the plug. The last test was a strength test intended to test the load carrying capacity of the concrete dome during high pressure loads. Finally, the dome plug was demolished, and the included systems and materials were evaluated.

To evaluate the dome plug, monitoring has been performed since construction where about 100 sensors were installed in the different material zones in the dome plug. Besides this, other types of measurements have also been conducted such as; leakage measurements, non-destructive test methods and a large amount of material tests on concrete and bentonite. As a complement to all these measurements, numerical analyses have also been performed to predict and to obtain greater understanding of the results.

During the gas leakage test, the filter of the plug was drained to remove the water. After this, the filter was filled with helium and the gas pressure was continually recorded and a sniffer was used to track leakage downstream of the plug. The results from this test showed that the plug can be considered to satisfy the requirements of gas tightness.

In the strength test, the water pressure was temporarily increased to 8.1 MPa, resulting in a total pressure about 10 MPa. The results showed that the concrete dome behaved as expected and some nonlinear deformations occurred. The deformations did not, however, result in significant cracking or damages within the concrete dome.

The measurements of the leak tightness of the plug showed that the leakage varied between one and two litres per hour (17–33 ml/min). This should be considered as an upper limit of the expected leakage of the DomPlu design, since the natural pressure from the groundwater was lower than the artificial pressure applied in this full-scale test. In addition, the results showed that leakage to a great extent by-passed the bentonite seal through fractures in the rock. Therefore, it is of great importance to choose a plug location with limited fractures. The swelling pressure in the bentonite seal was lower than expected and varied between 0.2 and 1.9 MPa. The results also showed that the water content in the central parts was lower than expected. This has likely been a result of the leakage by-passing the seal in the rock.

During demolition, great experience was obtained from material test sampling of concrete and bentonite. A larger waterfilled cavity was also detected in the top of the concrete dome, which had not been seen with the non-destructive test methods.

Overall, the DomPlu full-scale test has showed that the plug design is robust and could sustain high water pressures and obtain quite low rates of leakage despite the fractures in the rock and the cavity in the top of the concrete dome. The full-scale test has also showed that it is possible to build and (if necessary) breach and demolish a plug.

Sammanfattning

Föreliggande rapport sammanfattar DomPlu-försöket med en kupolformad plugg avsedd för att utvärdera designkonceptet för förslutning av deponeringstunnlar vid KBS-3V förvaret för radioaktivt avfall. DomPlu-försöket genomfördes vid Äspö laboratoriet och utvärderade pluggsystemet under realistiska förhållanden samt med realistiska och överdrivna laster.

SKB:s nuvarande referensdesign och DomPlu pluggen för förslutning av deponeringstunnlar är lika, med undantag för vissa mindre experimentrelaterade modifieringar. Jämfört mot tidigare fullskaleförsök som SKB har genomfört så representerar DomPlu pluggen en mer detaljerad iteration av designen snarare än en fundamental förändring.

I detta projekt utvärderats pluggens respons efter att den varit belastad med ett konstant vattentryck på 4 MPa under tre års tid. Efter detta, genomfördes ett gastäthetstest som syftade till att utvärdera gastätheten hos pluggen. Det avslutande testet som genomfördes avsåg att utvärdera bärförmågan hos betongpluggen då den utsätts för hög tryckbelastning. Slutligen demonterades pluggen och försöket utvärderades.

Fullskaleförsöket har övervakats med ca 100 sensorer som installerats i de olika ingående materialen i pluggen under dess uppförande. Utöver detta så har även flera andra typer av mätningar genomförts så som; läckagemätningar, oförstörande provningsmetoder samt ett stort antal materialtester på betong och bentonit. Som komplement till alla dessa mätningar har även numeriska analyser genomförts i syfte att prediktera och få ökad förståelse för resultaten.

Vid gastäthetstestet, dränerades pluggens filter för att leda bort allt vatten. Därefter trycksattes filtret med helium, där gastrycket övervakades kontinuerligt och en sniffer användes för att spåra läckage nedströms om pluggen. Resultatet från detta test visade att pluggen kan anses uppfylla de krav som finns formulerade avseendes dess gastäthet.

Vid bärförmågetestet ökades vattentrycket temporärt till 8,1 MPa, vilket resulterade i ett totaltryck på ca 10 MPa. Resultatet visade att betongkupolens beteende var som förväntat och att ickelinjärt beteende uppstod till viss del men detta resulterade inte i signifikanta sprickor eller skador i betongkupolen.

Mätningarna av läckaget genom pluggen visade att det varierade typiskt mellan en och två liter per timme (17–33 ml/min). Detta bör anses vara en övre gräns för vilket läckage som kan förväntas vid DomPlu-pluggen, dels eftersom det naturliga trycktillståndet var avsevärt lägre än det artificiella trycket under testet. Dessutom, visar resultaten att läckaget till stor del gick i bergssprickor intill pluggen och därmed kortslöt bentonitfiltret. Kortslutningen visar att det är mycket viktigt att välja pluggens läge med avseende på sprickläget i berget. Svälltrycket i bentonittätningen var lägre än förväntat och varierade mellan 0,2 och 1,9 MPa. Resultatet visade även att vattenkvoten i de centrala delarna av bentonittätningen vara lägre än förväntat. Dessa effekter kan sannolikt vara ett resultat av att läckaget kortslöt bentonittätningen.

Demonteringen av pluggen och materialtesterna för betong och bentonit bidrog till en stor ökning av kunskapen om pluggen. Vid rivningen upptäcktes ett större vattenfyllt hålrum i toppen av betongkupolen, som inte hade observerats vid de oförstörande provningarna.

Sammanfattningsvis så visade fullskaleförsöket DomPlu att pluggdesignen är robust och kan bära höga vattentryck samtidigt som den ger upphov till relativt låga läckage trots sprickor i berget och kaviteten i toppen av kupolen. Fullskaleförsöket har även visat att det är möjligt att bygga och (om nödvändigt) bryta eller riva pluggen.

Contents

1 Introduction

This is the final project report that summarizes the dome plug full-scale test (DomPlu) intended to evaluate the design concept of the deposition tunnel end plugs for the KBS-3V reference disposal system. The DomPlu full-scale test, was carried out at the Äspö Hard Rock Laboratory (Äspö HRL) and tested the plug system in a realistic environment with realistic and excessive loads. This report summarizes results and conclusions from the activities performed since the previous report by Grahm et al. (2015). The report by Grahm et al. (2015) presented the design, construction and the pressurization of the plug up to 4 MPa water pressure.

In the current report, the following activities are described:

- Behavior of the plug during three years of sustained water pressure of 4 MPa.
- Gas tightness test of the plug.
- Final pressure test including drainage of the plug and re-pressurization with a water pressure of 8 MPa, resulting in a total pressure about 10 MPa (strength test).
- Demolition of the concrete dome.
- Material tests of concrete and bentonite.

Monitoring, evaluation and technical reporting of DomPlu was a part of the Full-Scale Demonstration of Plugs and Seals (DOPAS) Project between 2012–2014. The DOPAS project was a European Commission (EC) programme of work jointly funded by the Euratom Seventh Framework Programme and European nuclear waste management organizations. The purpose of the DOPAS project was technology development for testing plugging and sealing systems for geological disposal facilities for radioactive waste and included full-scale experiments, laboratory tests and performance assessments studies of several plugs and seals.

This chapter gives a brief overview of the KBS-3V systems and the function of the plug. An overview of the design and the development of the design basis is also given. The purpose and scope of the report is finally stated.

1.1 Background

The KBS-3V system has been proposed for final deposition of spent nuclear fuel in Sweden. The method has been developed by SKB to ensure long term safety by storing the spent fuel in copper canisters with cast iron inserts. The copper canisters will be stored in a crystalline host rock in a non-seismically active area. A site has been selected in Forsmark, Sweden to accommodate the Swedish repository. The site has good crystalline rock and the deposition will take place at a depth of 470 m below the ground surface. For further reading, the KBS-3V method is summarized in SKB (2010a).

The design aims to ensure long-term safety by isolation and containment of the spent fuel. This is achieved by selecting engineered barriers which will result in a stable geological environment inside the host rock.

Copper canisters are placed in vertical boreholes in the deposition tunnels and are surrounded by a buffer of bentonite blocks and pellets. The deposition and access tunnels are filled with bentonite blocks and pellets. To keep the backfill in place, the deposition tunnel is closed with a dome-shaped concrete structure that acts as mechanical resistance and transfer the loads to the surrounding rock, as illustrated in Figure 1-1.

The aim of the repository is to contain radionuclides. This relies heavily on the function of the copper canister. The main function of the buffer and deposition tunnel backfill is therefore to protect the copper canister. The repository will be in operation for approximately 100 years, thereafter all access tunnels will be filled with bentonite. The main function of the concrete dome will therefore be to ensure the safety during the operation.

If water can flow freely, it tends to create channels and erode the bentonite. This is especially problematic before the bentonite is saturated and the conductivity is lower. There is therefore a high demand for water tightness of the concrete dome. The initial water tightness is achieved by injection grouting along the abutment of the plug. To relieve any potential water pressure before the concrete dome has cured and the injection grouting is finished, a filter section with drainage pipes is included in the design, see Figure 1-4.

To ensure a water tight seal for the entire life span of the plug (100 years), a swelling bentonite section was incorporated in the reference design. After the bentonite section is saturated, the water tightness of the concrete dome will be redundant, and the main function will be to retain the swelling pressure of the bentonite and the water pressure. The conductivity of the plug system will also depend largely on fractures in the rock mass.

As the deposition of spent nuclear fuel is finished and the deposition tunnels are backfilled and plugged, the main tunnel, directly adjacent to the deposition tunnel will also be backfilled with bentonite. Thereby, the plug will have bentonite on both sides which means that the deposition-tunnel plugs (the DomPlu) no longer have any function in the repository. Finally, all tunnels in the repository all the way up to ground level will be filled with materials such as bentonite or crushed rock.

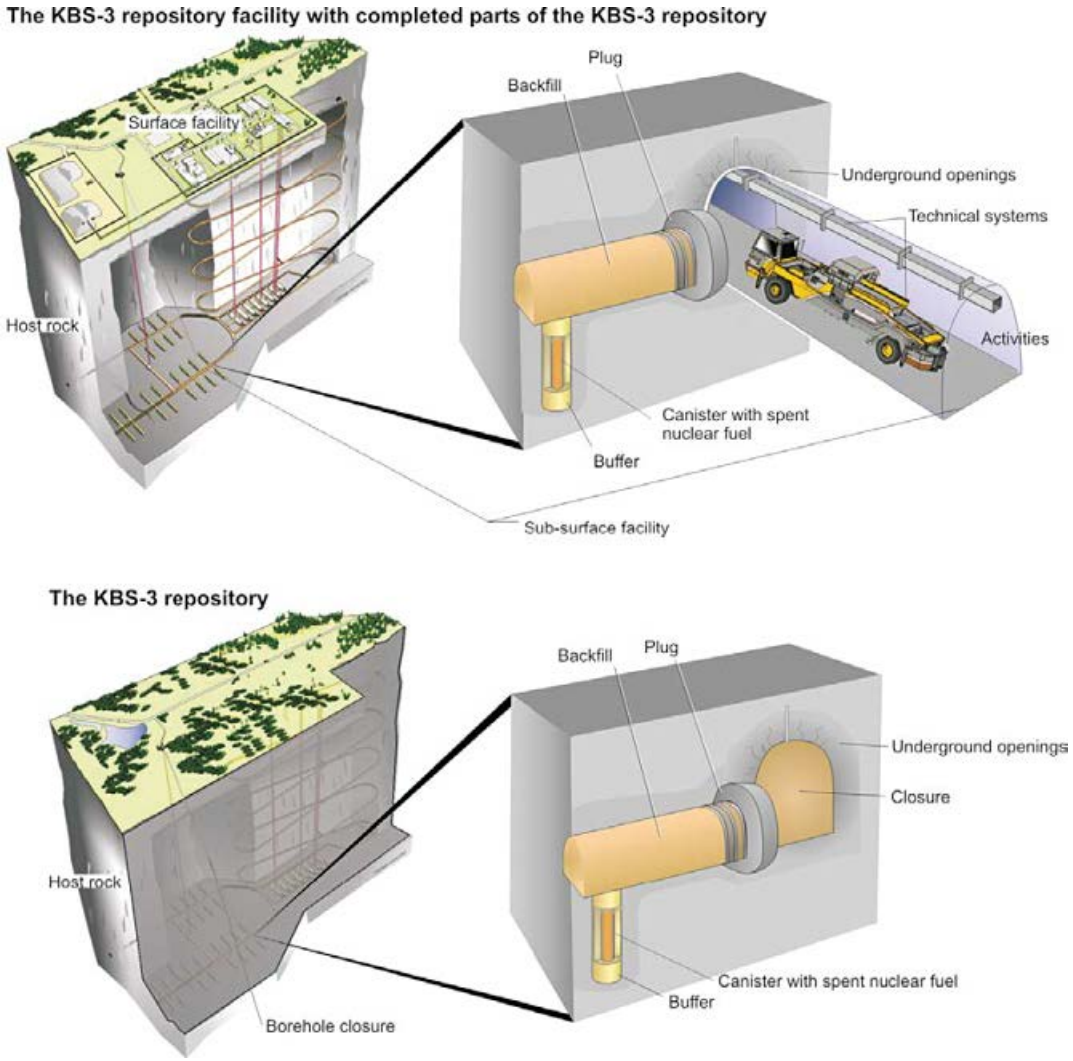

Figure 1-1. *Principal sketches of the KBS-3V facility and KBS-3V repository, SKB (2010a).*

1.1.1 Development of the design bases for deposition tunnel plugs

The need for a way to hold the backfill in place and maintain a higher water head than in the open access-tunnels was recognized early in the development of the Swedish repository program. The design base for the deposition tunnel plugging concepts has therefore been under development for many decades. The concepts have been driven by increased knowledge of the site-specific conditions of the repository, laboratory tests, and previous full-scale tests in Sweden and internationally. The full-scale tests undertaken by SKB has been in collaboration with Posiva and has also contributed to develop the plugging system in the Finnish repository concept.

In previous full-scale tests performed by SKB, different plug designs have been tested. The following series of tests has been performed:

- The Stripa mine tunnel plugging experiment in the 1980s.
- The Äspö HRL Backfill and Plug Test in the 1990s.
- The Äspö HRL Prototype Repository in the 2000s.

As a part of the tunnel plugging experiments in the Stripa mine in the 1980s, a simple concrete plug was tested. In the next sets of experiments in Äspö HRL in the 1990s, a ring of bentonite was added in the design along the interface between the concrete and rock. The leakage was found to be too high in this experiment and the design was not deemed satisfactory. The next experiment was also performed at Äspö HRL, where a prototype repository was built. The prototype repository included two identical reinforced concrete dome plugs (Svemar et al. 2016), see Figure 1-2. This was the first time a Swedish full-scale test incorporated self-compacting concrete.

As a part in the development of the KBS-3H method, a low-pH shotcrete plug was developed and tested. Significant leakage was detected during the tests and the concept was replaced by a welded steel plug utilizing contact grouting to achieve a watertight seal. The steel plug has generally been considered a success after low leakage has been observed at two full-scale tests at Äspö HRL.

There are several international programs that has provided valuable knowledge and input to the Swedish repository project. Two projects which are especially relevant to this project are the Tunnel Seal Experiments (TSX) and the Enhanced Sealing Project (ESP), both of which are Canadian projects performed at Atomic Energy of Canada Limited's (AECL's) Underground Research Laboratory (URL). The TSX and ESP projects are summarized in Chandler et al. (2002) and Martino et al. (2011) respectively. The URL and the locations of the two projects are illustrated in Figure 1-3a.

The TSX project sealed a tunnel from two directions to test two bulkheads, one made from concrete and one from bentonite, see Figure 1-3b. The concrete plug was made of unreinforced low-heat, high-performance concrete (LHHPC). The clay plug was made from highly compacted sand and bentonite blocks with a dome-shaped stainless-steel restraint to carry the pressure loads. The filter section between the plugs was loaded with a water head of about 400 m and both bulkheads were successful in reducing the axial water flow. The project proved that building clay bulkheads is a viable method and that the bentonite has a good ability to cut off existing flow-paths and selfheal. It also showed the effectiveness of contact grouting for reducing seepage between the concrete and rock.

The ESP is jointly founded by NWMO (Canada), SKB (Sweden), Posiva Oy (Finland), and ANDRA (France). It is an ongoing project where a permanent plug was installed to seal the access shaft to the URL. The shaft was sealed to block off access to the facility when it was closed and to reduce the mixing of deeper saline groundwater with shallower less saline groundwater on a hydraulically active fracture zone. The plug is continuously monitored to evaluate the performance. Despite the geometrical differences, several concepts are applicable for horizontal tunnel plugs. The plug consisted of two vertical concrete sections filled in-between with bentonite, see Figure 1-3c. The project is a successful example, which further demonstrates the viability of a concrete and bentonite composite plug.

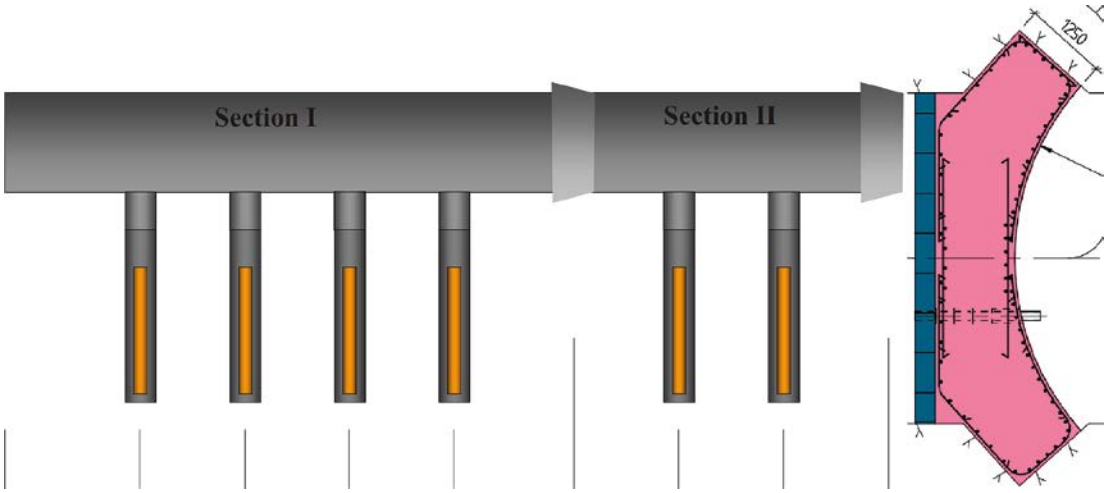

Figure 1-2. *Sections from the prototype repository, Dahlström (2009).*

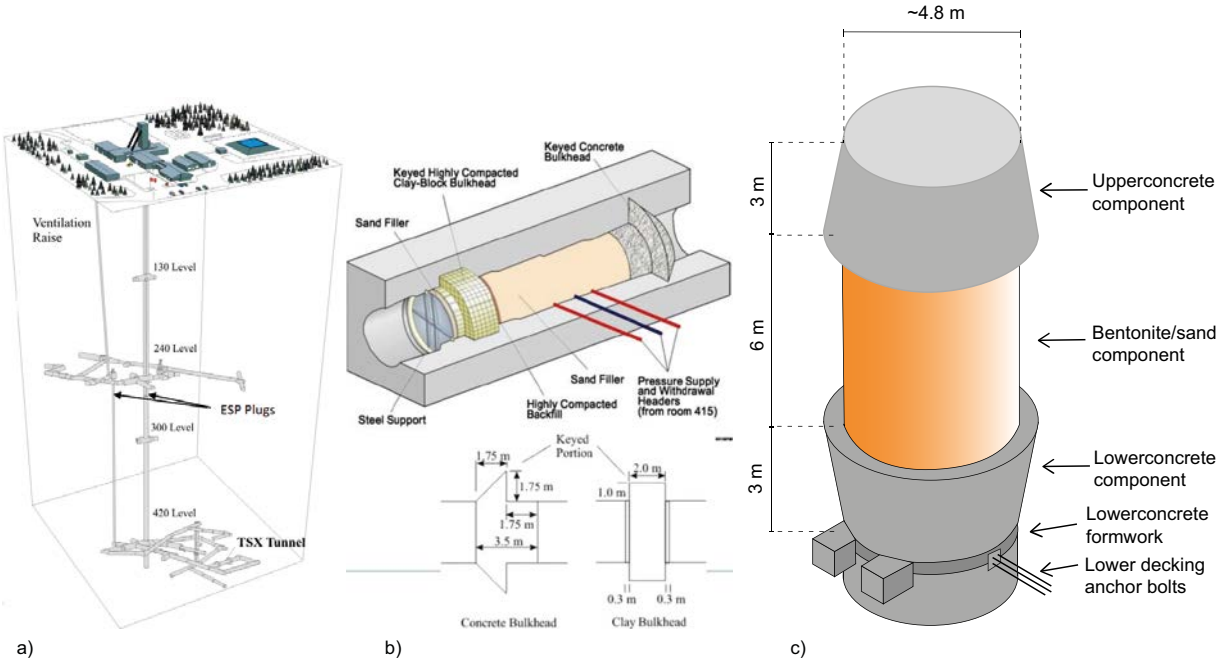

Figure 1-3. *a) AECL's URL facility with the location of the two projects marked. b) Overview of the TSX plug design. c) Overview of the ESP plug design. The Illustrations are taken from Dixon et al. (2016).*

With the experience gathered from previous designs and full-scale tests, a new plugging concept was developed. The new concept includes an unreinforced low-pH concrete dome, see Section 1.1.2. During the period 2012 to 2017, a full-scale test was performed to ensure the viability of the dome plug design. The plug construction was finished by mid-2013 and was subsequently pressurized. The project continued for five years with continuous monitoring and finished by a final gas leakage and strength test before demolition. The design and methodology were first presented in SKB (2010b). The previous reference design of the plug was updated and presented in Malm (2012) and the initial report from the installation of the full-scale test is presented in Grahm et al. (2015). During the execution of the full-scale test, the SKB reference design for plugs have been updated to match the design in the DOMPLU test. The aim of the DOMPLU test was to determine the overall performance of the plug system, its ability to retain water and the validity of the design evaluation methods.

1.1.2 Conceptual design of the deposition tunnel plug

The KBS-3V repository will consist of several kilometres of access tunnels, divided into seven main deposition areas. Each deposition area opens into several deposition tunnels. In total, there will be 150–200 deposition tunnels, and the repository is expected to be in operation for around 100 years. The main purpose of the deposition tunnel plugs is to enable the backfilling of one tunnel while the operation continues in the rest of the repository. The plug also fills the purpose of confining the backfill during the saturation and expansion of the bentonite and preventing erosion before the bentonite is saturated. Another requirement is that the plug must prevent gas and vapor transports to and from the deposition tunnel. Thus, the plug only serves a short-term purpose and the subsequent design life span is 100 years.

The reference design of the studied plug system is presented in SKB (2010b) and includes the following parts:

- Concrete plug
- Watertight seal
- Filter
- Concrete beams
- Drainage pipes
- Grouting pipes

The plug is illustrated in Figure 1-4.

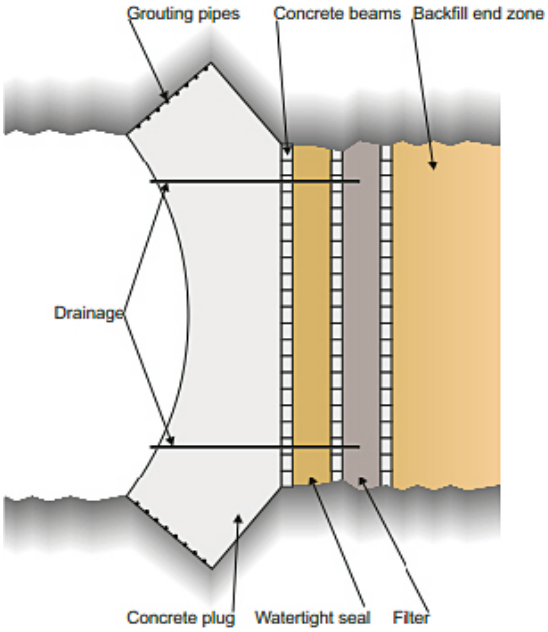

Figure 1-4. *A schematic plan of the reference design, from Grahm et al. (2015).*

1.1.3 Terminology

Some project-specific terminology is used in the projects regarding the DomPlu. A brief list of the abbreviations used in this report is presented in Table 1-1. The structural components included in the reference plug system are illustrated in Figure 1-5.

Table 1-1. Common abbreviations Grahm et al. (2015).

Structural component full name	In abbreviated form
Plug System – or Plug Structure	Plug
Spherical Concrete Dome Structure	Concrete Dome – or dome
Slot excavation	Slot
Material Zone Delimiter	Delimiter
Bentonite Seal	Seal
Filter Zone	Filter – or gravel filter
Backfill Transition Zone – or Backfill end zone	Transition zone – or Backfill TZ

The terms upstream and downstream are used in this report to explain which side of the plug is referred to. The upstream side denotes the side of the plug facing the backfill and the downstream side faces the open tunnel outside of the backfilled area. The term upstream comes from that this area is subjected to water pressure, while the downstream area is subjected to air. This terminology is commonly used in for hydraulic structures such as dams.

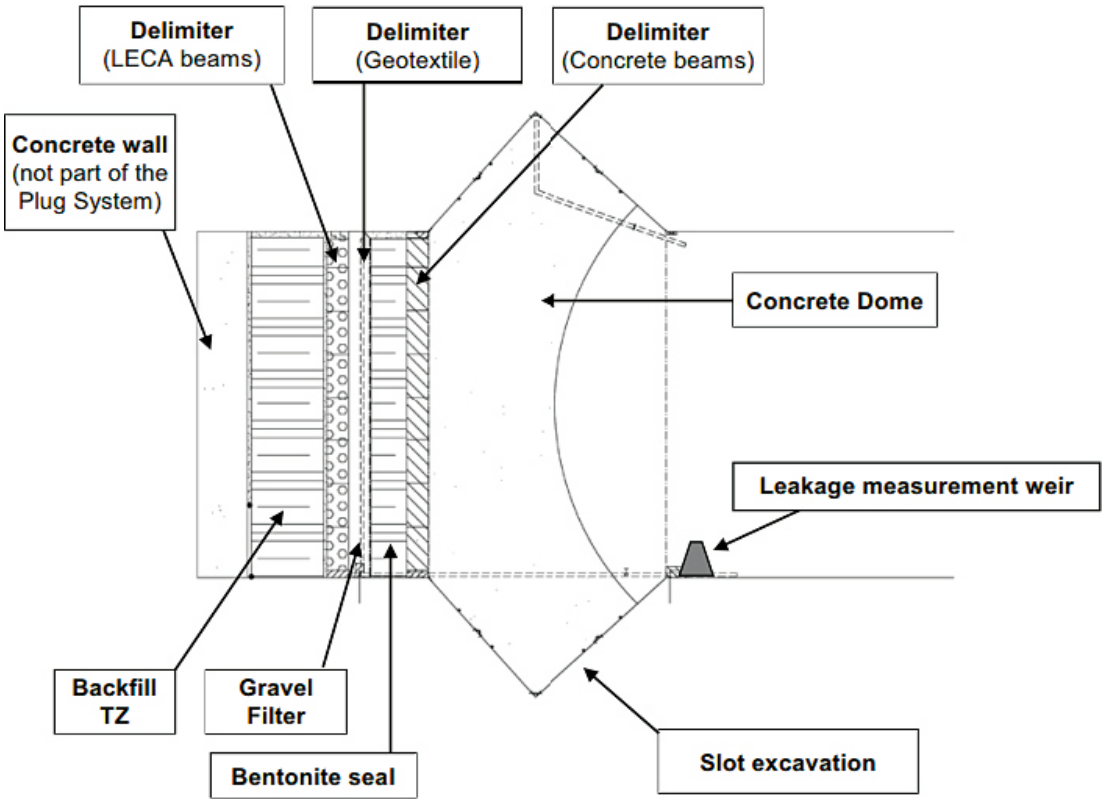

Figure 1-5. *Parts included in the plug system. Note that the concrete wall is a part of the experiment setup and not part of the system design of KBS-3V, Grahm et al. (2015).*

1.2 Purpose of the full-scale test

The purpose of the DomPlu full-scale test was to improve the design basis of the KBS-3V deposition tunnel plugs and to:

- Demonstrate the feasibility of the plug construction.
- Evaluate and improve the construction methods.
- Demonstrate the ability of the DomPlu to withstand the design loads and to verify that it performs as intended under normal operational conditions.
- Evaluate if a sufficiently low leakage could be reached with the proposed design and to develop a method to measure the leakage.
- Improve the control and measurement tools to be used in the final repository.
- Validate the numerical and analytical design tools used in the design process.
- Evaluate if the plug is gas tight.

1.3 Aim and scope of the report

The objectives of this report are to summarize the final findings from the DomPlu full-scale test performed by SKB and Posiva between 2012 and 2017. The report will summarize all results from the final gas leakage and strength tests performed from June to August in 2017, the demolition of the plug, which started in August of 2017, and all subsequent material tests.

2 The DomPlu full-scale test

The construction of the experiment setup and all early results are presented in Grahm et al. (2015), and only a brief summary of the experiment design and the early results will be presented in this section. The experimental setup is illustrated in Figure 2-1. The plug system consists of several material layers (zones) with specific functions. At the end of the tunnel, a concrete wall was casted. The concrete wall is not a part of the repository design but rather the experimental setup. It was placed to obtain a smooth and flat surface for the installation of the backfill blocks and as a support for the swelling pressure and to reduce the leakage in this direction. It was created from the B200 self-compacting low-pH concrete developed by Vogt et al. (2009), which was also used for the concrete dome.

A one meter thick backfill section was installed using compacted bentonite blocks. To fill the gap along the tunnel perimeter, bentonite pellets were used. The backfill was supported on the downstream side with permeable lightweight-aggregate concrete beams (LECA beams). The beams enabled the installation of the filter and separated the materials but did not affect the conductivity of the section. The filter was created with macadam, a coarse crushed rock with good permeability. Drainage pipes were installed in the filter for the ability to drain the plug system and to prevent water pressure from building up during the plug installation and hardening of the concrete dome. The drainage system was also used to artificially saturate the bentonite seal after the installation. The drainage pipe opening in the upper part of the filter was used to let air out of the filter during the artificial saturation and is thus denoted deairing pipe.

The bentonite seal was created to reduce the conductivity of the plug system and reduce the reliance on the concrete and grout injection for the watertight seal. Compacted bentonite blocks were used to build the seal and bentonite pellets were used to fill voids along the perimeter. A geotextile was used to separate the gravel filter and the bentonite seal. Concrete beams were used to support the bentonite seal and the adjacent systems and to provide a surface for the casting of the concrete dome. The downstream side of the beams was draped in a geotextile to prevent bond between the concrete beams and the concrete dome. The concrete dome was casted in place using the low-pH self-compacting concrete B200 mix described in Grahm et al. (2015).

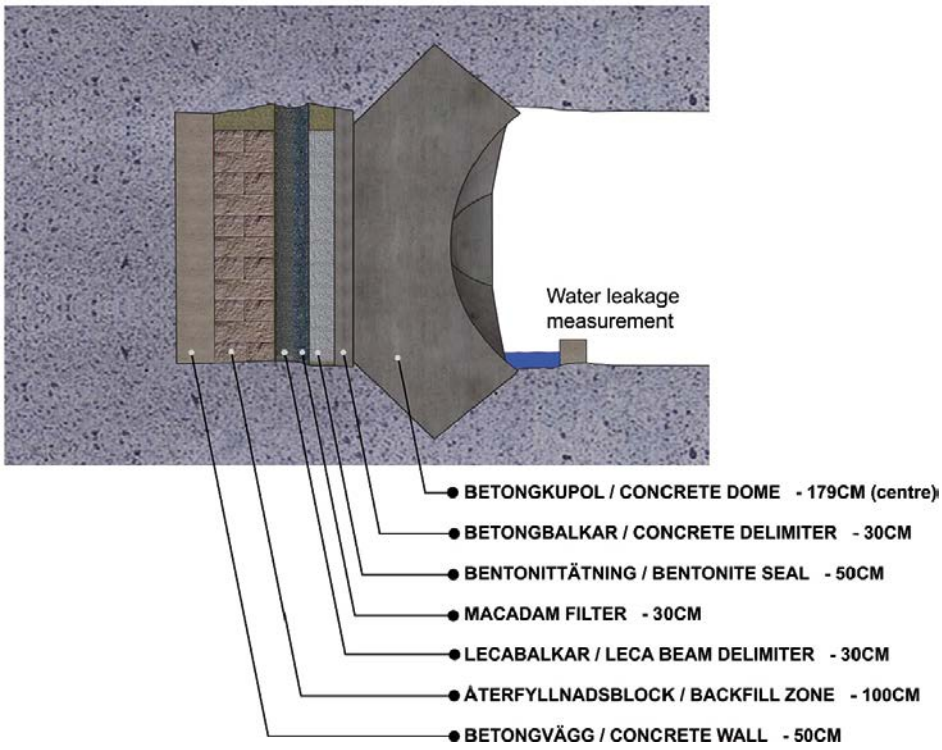

Figure 2-1. *Schematic overview of the experiment design with the approximate length of the different parts (Grahm et al. 2015).*

2.1 Installation of the DomPlu full-scale test

2.1.1 Rock excavation

A brief overview of the rock excavation performed for the DomPlu experiment is described in this section, for a more detailed description see Grahm et al. (2015) and Grahm and Karlzén (2015). The experiment was performed in Äspö HRL, at the –450 m level. The DomPlu project involved large water pressures and sensitive instrumentation, therefore a new tunnel was excavated for the DomPlu project. The location of the DomPlu experiment tunnel is illustrated in Figure 2-2a. The project required a section of tunnel with limited fractures and limited ground water movement. Sufficiently strong rock was also required to transfer the loads from the dome plug.

To find a suitable location, a pilot borehole was drilled and subsequently pressurized with a water jet to test the permeability of the rock. When a suitable location was found the excavation was performed with drilling and smooth blasting techniques to reduce the excavation damage zone (EDZ). The EDZ is the zone around the tunnel perimeter which is damaged by the excavation technique. The EDZ conducts micro cracks that may increase the permeability of the rock and increase the water transport. The theoretical tunnel section is illustrated in Figure 2-2b and the finished tunnel is illustrated in Figure 2-3.

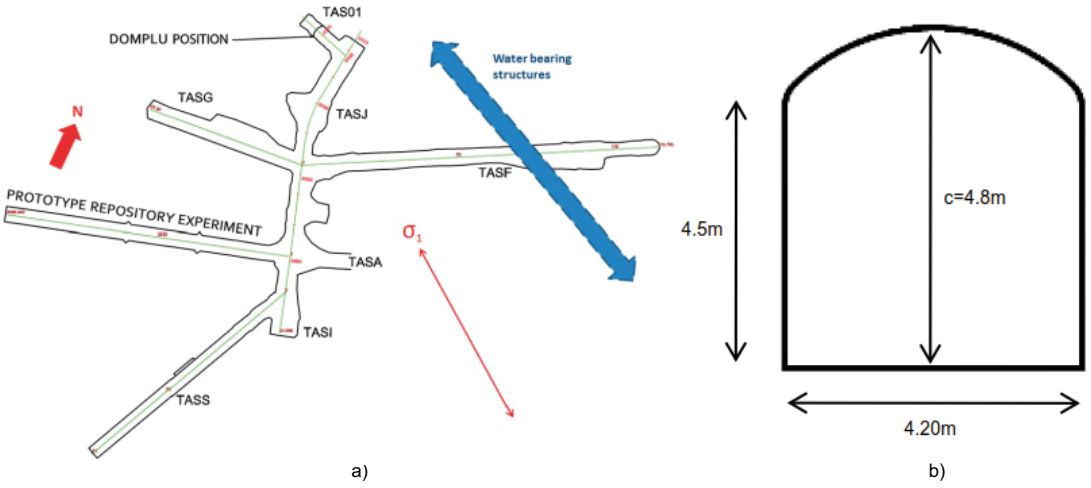

Figure 2-2. *a) Layout of the –450 m level in Äspö HRL, the DomPlu is located in tunnel TAS01 and b) Theoretical tunnel section (Grahm et al. 2015).*

Figure 2-3. *Photo of the finished experiment tunnel (Grahm et al. 2015).*

A niche was also excavated close to the experiment tunnel, as seen in Figure 2-4. The necessary pipes and cables for the pressurization and instrumentation passed through boreholes between the experiment tunnel and the niche. The pressurization system and some of the monitoring systems were placed in the niche.

To provide an abutment for the dome plug and to cut off the EDZ, a slot abutment was wire-sawn into the tunnel perimeter. Wire sawing also provides a smooth surface to cast the concrete against, which is important for the ability of the concrete dome to release from the rock before the contact grouting. The slot was given an octagonal shape and was sawn at about 45 degrees from the upstream and downstream sides, according to Figure 2-5. To guide the wires and provide a fixed point for the pullies, boreholes with a diameter of 250 mm was first drilled along the edges of the octagon. The final abutment is illustrated in Figure 2-6. The remining half-circles from the drill-holes were cast with concrete to even-out slot and thereby reduce the risk of stress concentrations in the concrete dome.

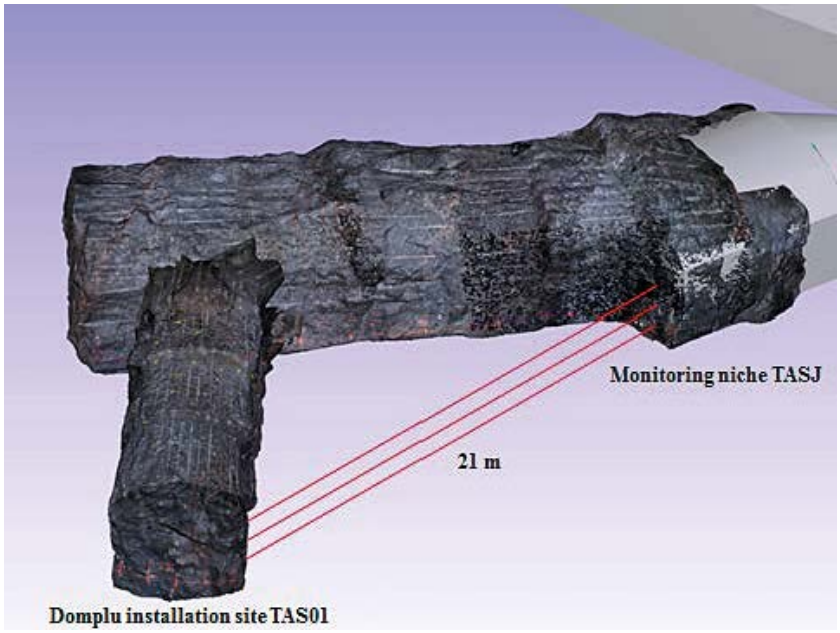

Figure 2-4. *Illustration of the experiment tunnel, the monitoring niche and the connecting boreholes (Grahm et al. 2015).*

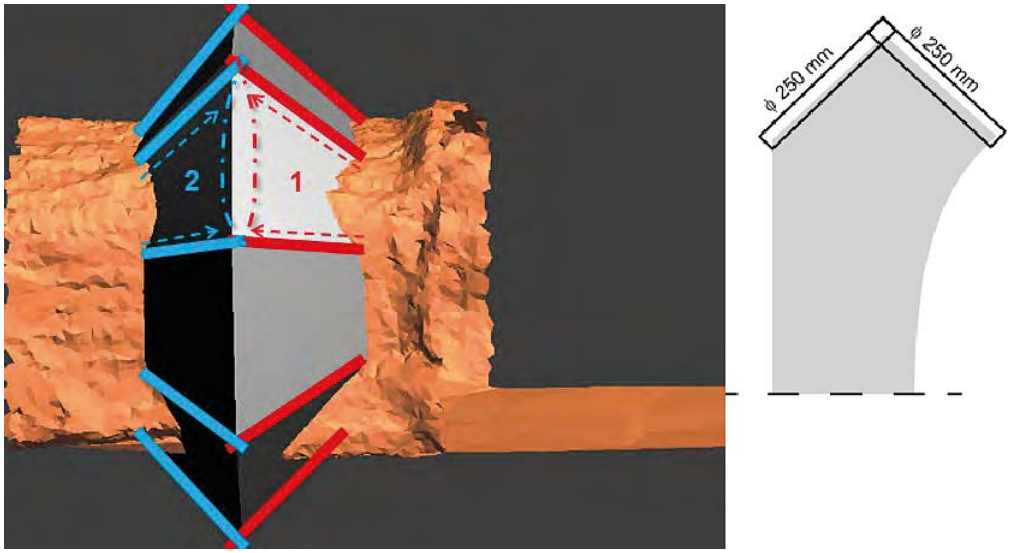

Figure 2-5. *Theoretical sections of the slot abutment (Grahm et al. 2015).*

Figure 2-6. *Final slot abutment (Grahm et al. 2015).*

2.1.2 Installation of backfill and LECA-beams

Underneath the bentonite backfill towards the back wall, a small pocket of gravel was created. The gravel was 50 mm thick and wrapped in a geotextile. This is not a part of the reference design but rather a part of the experiment setup of the full-scale test. Water pipes were led from the monitoring niche to the gravel pocket and were used to pump water and pressurize the system. The pressurization system is presented in Section 2.1.9.

The bentonite was hand stacked along with the LECA-beams and pellets. The total thickness of the backfill was 1 m, whereof 150 mm consisted of bentonite pellets. Pellets were also used to fill the void between the blocks and tunnel perimeter. The bentonite blocks were manufactured of bentonite from Ashapura, India and were representative of the backfill in the spent fuel repository. Figure 2-7 shows the installation of the backfill blocks.

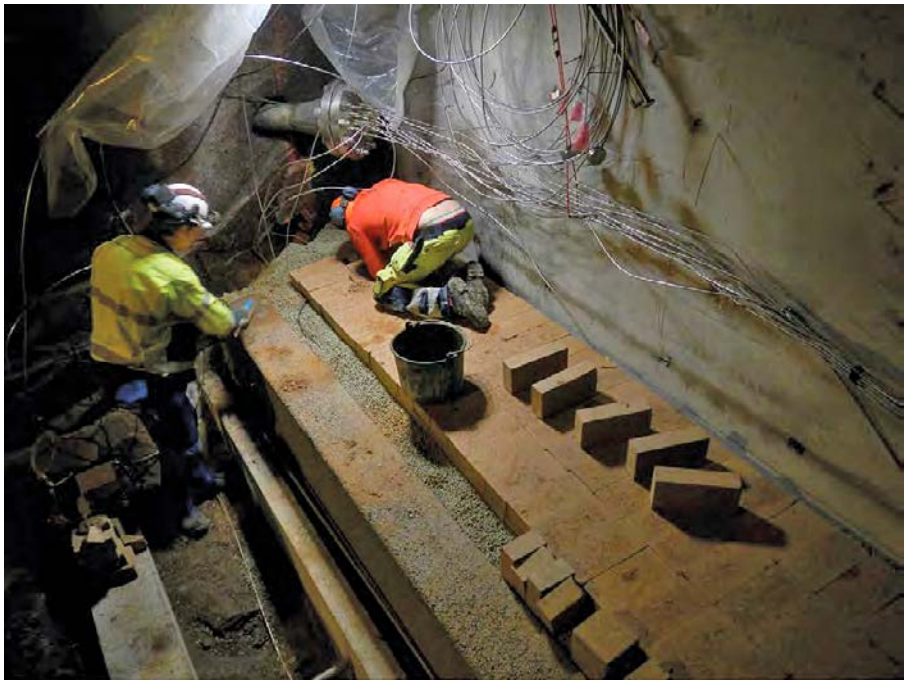

Figure 2-7. *Installation of the backfill blocks, pellets and LECA-beams (Grahm et al. 2015).*

2.1.3 Installation of concrete beams, bentonite seal and gravel filter

The gravel in the filter was installed along with the bentonite seal and the concrete beams. The gravel and the bentonite were separated by a geotextile. A fine coarse macadam with grain sizes of 2–4 mm was used for the gravel filter. The bentonite seal was created with compacted blocks of MX-80 with a dry density of 1 700 kg/m^3. The total width of the bentonite seal was 500 mm. The concrete beams were reinforced and precast from the B200 low-pH concrete, which later also was used in the concrete dome. The development and installation of the bentonite seal and filter is further described in Börgesson et al. (2015) and Grahm et al. (2015).

2.1.4 Concrete material B200

A self-compacting low-pH concrete, denoted B200, has been specifically developed for use in the KBS-3V repository. The concrete was rigorously tested with laboratory experiments to verify the suitability of the material and to increase the validity of the various analyses performed before the construction of the plug. The experiments included tests of the hardened mechanical properties of the concrete, shrinkage, creep, interaction with rock materials and heat development. Detailed descriptions of the performed tests and the concrete mix is presented in Magnusson and Mathern (2015) and Grahm et al. (2015).

2.1.5 Cooling system

To counteract the heat produced by the hydration of the concrete and prevent cracking, cooling pipes were installed. After the hydration was finished, the cooling was increased to force the concrete dome to release from the rock. This was done to ensure that the concrete shrinkage would occur without inducing significant stresses in the dome. After this, the cooling system was turned off for three months. The concrete dome was also cooled during the contact grouting, to force the dome to shrink further before the grouting. The cooling pipes are illustrated in Figure 2-8. The cooling sequence was calculated from the results from the laboratory experiments performed while developing the B200 concrete mix. The cooling pipes were filled with grout after the contact grouting was finished.

The cooling was used in three stages, the sequence is presented seen in Figure 2-9. First, the concrete dome was cooled to counteract the heat released during the hydration of the concrete (A). After the concrete had gained sufficient strength, the concrete dome was cooled to force it to release from the rock (B). The third stage of the cooling was during the contact grouting, when the concrete was cooled to increase the gap in the joint between the rock and concrete in order to introduce a prestress in the structure (C).

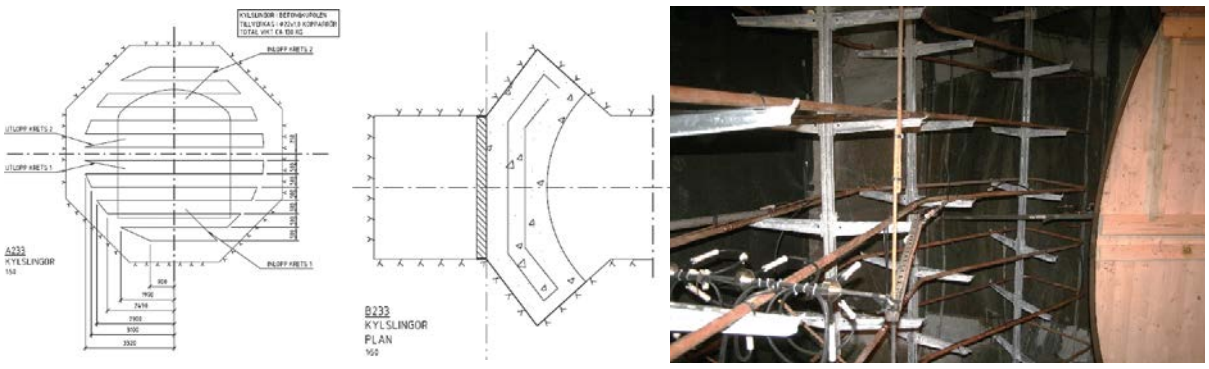

a) b)

Figure 2-8. *a) Theoretical front and plan view of the cooling pipes cut out from the construction drawings (Grahm et al. 2015) and b) The final cooling pipes, including the support frame.*

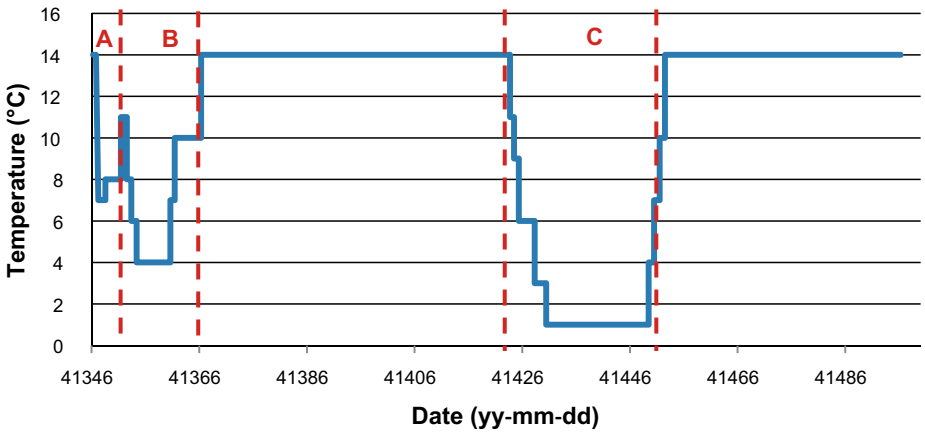

Figure 2-9. *Cooling sequence of the concrete dome (Malm 2018).*

2.1.6 Casting of the concrete dome

The concrete dome was an unreinforced solid body of self-compacting low-pH concrete. The upstream face of the concrete dome was casted against the concrete beams. The concrete beams and the concrete dome were separated by a geotextile. A formwork was built at the downstream side of the concrete dome. Cooling pipes, drainage pipes, grout injection tubes, steel support frames and several types of sensors were casted into the concrete.

The formwork was designed and produced by Doka GmbH. The irregular shape of the plug made it hard to prefabricate the formwork to fit exactly to the abutment walls and the remaining parts were produced on site with plywood and sealing foam. Pressure sensors were fastened to the formwork to monitor the casting of the concrete. The necessary connections for the cooling and grouting pipes, the drains from the filters and cables from sensors were led through the formwork. The final formwork and a theoretical section are illustrated in Figure 2-10. The pouring of the concrete was performed over 10 hours. 13 lorries were used to transport the concrete, which was pumped in through six holes in the formwork at three levels. The formwork was removed three weeks after the casting.

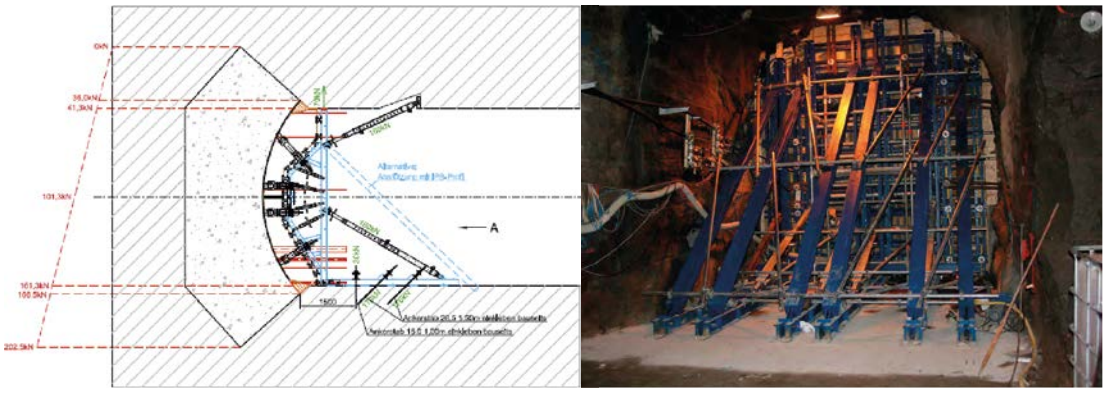

Figure 2-10. *a) Theoretical section of the formwork and b) The final formwork installed in the tunnel. (Grahm et al. 2015).*

2.1.7 Weir and plastic sheet

After the formwork was removed, a weir was constructed downstream from the concrete dome for leakage measurements. The weir was produced by casting of a concrete plinth across the tunnel, with a width and height of 300 mm. A system was installed for continuous leakage measurements. The weir and a hose used for the leakage measurement is illustrated in Figure 2-11.

After the contact grouting was performed, a plastic sheet was installed across the tunnel. The plastic sheet reduced the water evaporation by trapping the moist air and blocking off the tunnel ventilation.

2.1.8 Contact grouting

To create a watertight seal around the concrete dome, at the interface with the rock, contact grouting was performed. Grouting tubes were installed before the casting of the concrete dome. The pipes were mounted at the abutment according to Figure 2-12. The contact grouting was performed about 100 days after the concrete dome was casted.

The concrete dome was cooled down to 1 °C prior to the grout injection to shrink it. The shrinking was performed so that the concrete dome would lose contact with the rock and create a gap, which could be injected with grout. A prestress was also created in the concrete dome due to the shrinkage, which is beneficial for the concrete structure and can reduce cracking.

Figure 2-11. *A photo of the downstream leakage weir.*

Figure 2-12. *Cooling pipes mounted on frame with the grouting tubes visible in the background.*

2.1.9 Pressure system

A system was custom designed from standard components for the full-scale test. The system had a redundant design with two parallel pumps capable of reaching a pressure of 10 MPa each with a flow of 10 l/min. A flowchart of the pressurization system is presented in Figure 2-13. The pumps were placed in the monitoring niche and the water pipes were led through the lowest of the bore holes illustrated in Figure 2-4. Five water pipes with an outer diameter of 20 mm were used for the pressurization. Three pipes opened in the macadam pocket behind the backfill and two in the gravel filter. The two pipes in the filter section were only intended to be used if any of the other pipes malfunctioned. However, during the full-scale test, these pipes were also used to fill up the filter to have better control of the filling of the filter and thereby giving the bentonite seal access to water and to allow it to swell and seal quicker. The pressurization sequence is described more in detail in Grahm et al. (2015) and Åkesson et al. (2019).

After the contact grouting, water was applied to the filter through the drainage pipes to saturate the bentonite seal in a controlled manner. This was done in several steps and went on for about 5 months. After this, the drain pipes were closed, and the plug was only subjected to natural inflow from the rock. When the natural pressure had increased 1 MPa hydrostatic pressure in the filter, the pumps were started to pressurize the filter even further. The initial goal was to pressurize the system at 7 MPa. However, when the pressure reached 3 MPa, large water leakage occurred in the rock. The pressure increase was therefore cut off and maintained at 4 MPa. The pressure was held constant at 4 MPa for about three years, then the gas leakage test was performed. The initial pressurization of the plug is illustrated in Figure 2-14.

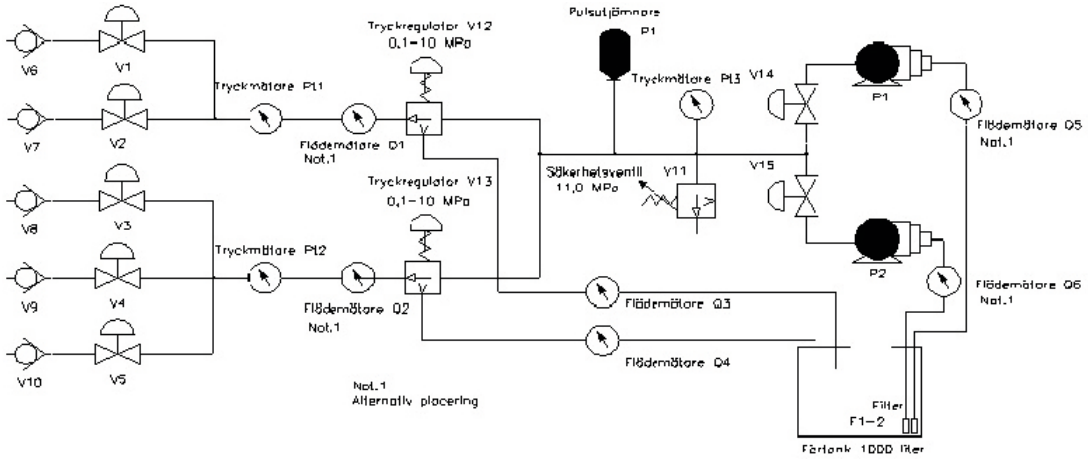

Figure 2-13. *Flowchart of the pressure system (Grahm et al. 2015).*

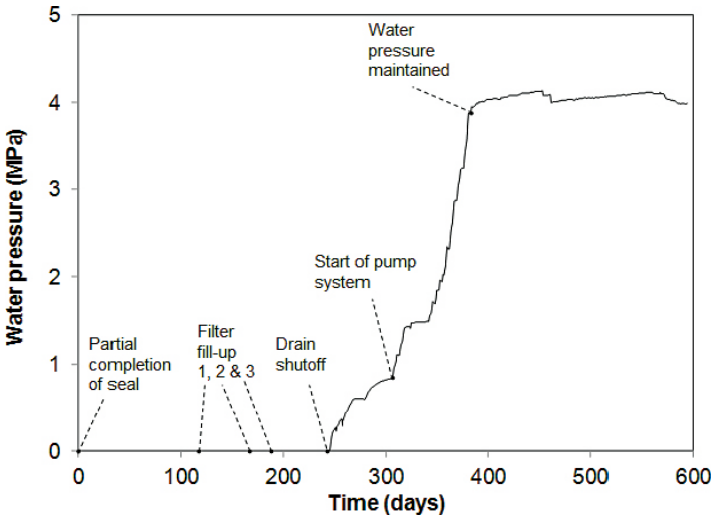

Figure 2-14. *Initial pressurization of the plug system (Grahm et al. 2015).*

2.2 Monitoring system

2.2.1 Leakage monitoring

The leakage water from the plug was collected in a weir downstream of the concrete dome, see Figure 2-15 a. The leakage water was thereafter transported through a steel pipe to a basin as seen in Figure 2-15 b. Measurements were continuously performed to record the weight of the basin, and thereby automatically measuring the amount of leakage water. The leakage measurements were previously reported in Grahm et al. (2015) and are summarized in this report in Section 2.3.1.

2.2.2 Monitoring of backfill, filter and bentonite seal

Sensors were installed in the backfill and bentonite seal to monitor the saturation and swelling of the bentonite, detect displacements in the material zones and to evaluate the sealing function. In total 42 sensors were installed in the bentonite seal and backfill, including:

- 20 total pressure sensors (Geokon 4800-1x-10 MPa).
- 6 pore pressure sensors (Geokon 4500SH-3-10 MPa).
- 16 Relative humidity sensors (Aitemin SHT75 V3).
- 3 Extensometers (Geokon 4435-1X-50).

The sensors were installed in seven layers along the tunnel direction, four layers in the backfill and three in the bentonite seal. Two additional pore pressure sensors were placed in the upstream side of the slot abutment at the interface between the rock and concrete. The placement of the sensors is presented in Figure 2-16.

a) b)

Figure 2-15. *Leakage measurement, a) Weir for collecting water, b) Basin for weighing the leakage water. (Grahm et al. 2015).*

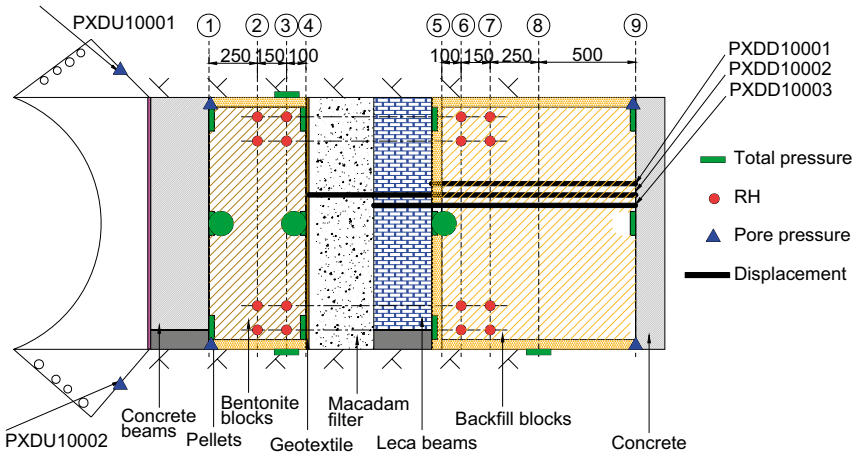

Figure 2-16. *Locations of all the sensors in the backfill and bentonite seal (Grahm et al. 2015).*

To withstand the extreme environment in the backfill, all sensors and cables were designed to withstand a pressure of 10 MPa. The cables from all sensors were led through boreholes to the monitoring niche. Two sensors are illustrated in Figure 2-17.

2.2.3 Sensors in the concrete Dome

To monitor the behaviour of the concrete dome, sensors for continuous monitoring were installed during the construction of the plug. The response of the plug based on the results from the measurements have continuously been reported during the operation of the full-scale test. The monitoring program and the initial results were summarized in Malm (2015a) and Grahm et al. (2015), and continuously in Malm (2015b, 2016, 2017). Some sensors documented the behaviour during the entire operation of the plug, while others were used to monitor the response during the construction of the plug, such as the pressure sensors installed in the formwork.

The installed sensors measure strain in the concrete, temperature in the concrete and the ambient air, the displacement in the joint between the rock and concrete in the downstream face of the abutment, the total downstream displacement of the dome and the pressure on the formwork. In total, 62 sensors were installed, including:

- 5 Pressure sensors (Wika S11) – pressure on the formwork.
- 6 Joint meters (TML type KJA-A) – relative displacement between concrete and rock.
- 3 LVDT (HBM type WA) – total displacement of the concrete dome.
- 14 Strain gauges (TML type KM-AT) – strain and temperature in the concrete dome.
- 10 Strain gauges (TML type KM-A) – strain in the concrete dome.
- Strain gauges (Geokon 4200) – strain and temperature in the concrete dome.
- Temperature sensors (PT 100) – ambient air temperature.

Figure 2-17. *An extensometer and a total pressure sensor during the installation of the backfill.*

The strain gauges were installed on the same rack as the cooling pipes, as illustrated in Figure 2-18a, the positions of all sensors are illustrated in Figure 2-18b. The joint meters were fastened to the rock and casted into the concrete dome, (Figure 2-19) and the LVDT-meters were mounted on a frame downstream of the plug (Figure 2-20a). Before the leakage and strength tests in 2017, four additional LVDT-meters were placed since only one of the three original sensors were functioning correctly (Figure 2-20b). The cables from all sensors casted in the concrete dome were led through the downstream face and connected to a terminal in the monitoring niche.

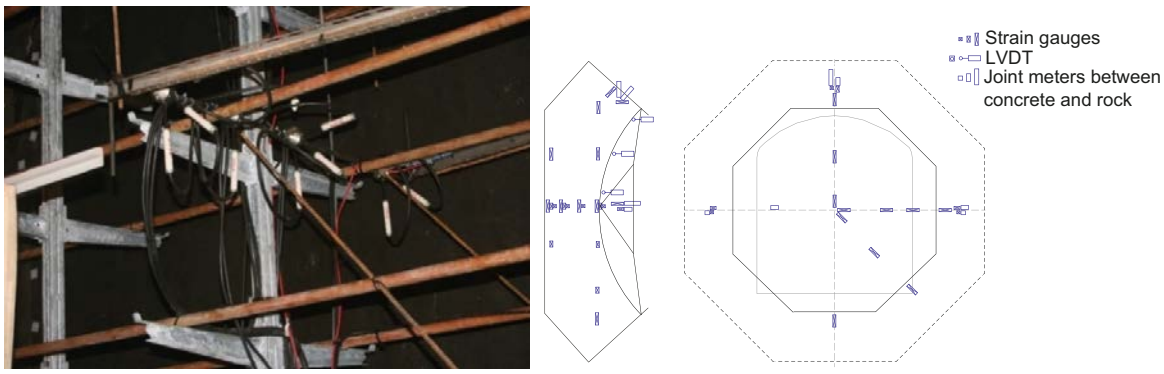

Figure 2-18. *a) Strain gauges installed on the cooling pipe rack at the centre of the concrete dome (Malm 2015a). b) Location of all sensors installed on the concrete dome.*

Figure 2-19. *a) Illustration of two joint meters and two strain gauges mounted on reinforcement bars and b) The sockets used for the joint meters (Malm 2015a).*

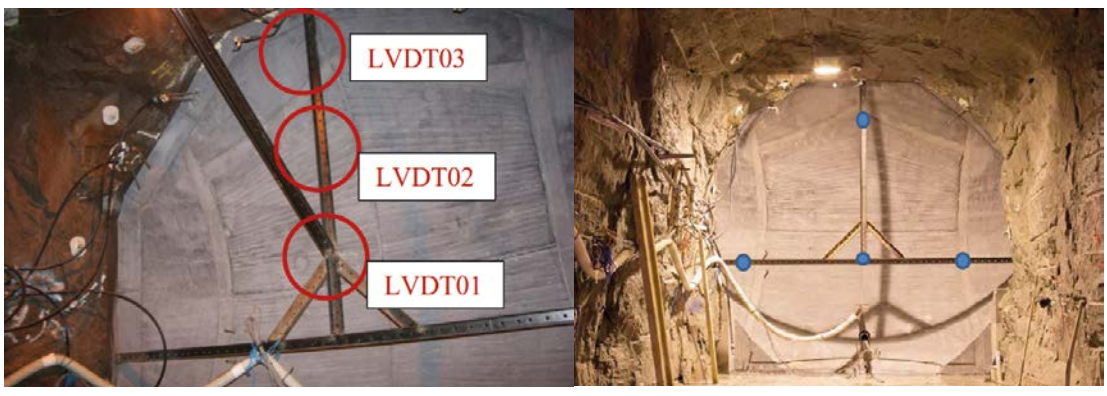

Figure 2-20. *a) Frame used to mount LVDT meters with the original three LVDT-meters mounted (Grahm et al. 2015) and b) The location of the new LVDT-meters (Åkesson et al. 2019).*

2.3 Previous results

2.3.1 Leakage

The original intent of the full-scale test was to pressurize the dome plug at 7 MPa. At the initial pressurization, the water pressure was increased by 0.25 MPa per week. However, when the water pressure reached 3.1 MPa, large leakage occurred. Two major leakage paths were identified, the pipe containing the cables from the instrumentation in the concrete dome and water bearing fractures in the rock surfacing 14 m downstream of the concrete dome. Both water escapes were deemed to be related to the experiment setup rather than the plug design. The leakage from the rock fracture and cable lead through was recorded separately from the water in the weir. The water from the cable feed through was also diverted and measured separately. The leakage and water pressure during the pressurization is illustrated in Figure 2-21.

When the leakage increased, it was decided to pressurize the dome at 4 MPa instead of 7 MPa. This was deemed sufficient since 4 MPa is close to the maximum theoretical hydraulic head of the final repository, see e.g. Malm (2012). When the water pressure was held constant, the leakage steadily decreased. In Figure 2-22, the total pressure, water inflow and leakage to the different outlets is presented. September 30, 2014, the total inflow of water was 399 ml/min, the leakage was distributed to:

- Weir 11 %, 43 ml/min.
- Cable bundle 2 %, 8.5 ml/min.
- Rock fracture 42 %, 169 ml/min.
- Remaining rock mass 45 %, 178.5 ml/min.

Grahm et al. (2015) concludes that the reduced leakage to the weir and through the cable bundle probably is due to the saturation of the bentonite seal. The reduced leakage to the rock could be due to clogging of the cracks by bentonite. However, this cannot be verified since it is unknown where the leakage occurs.

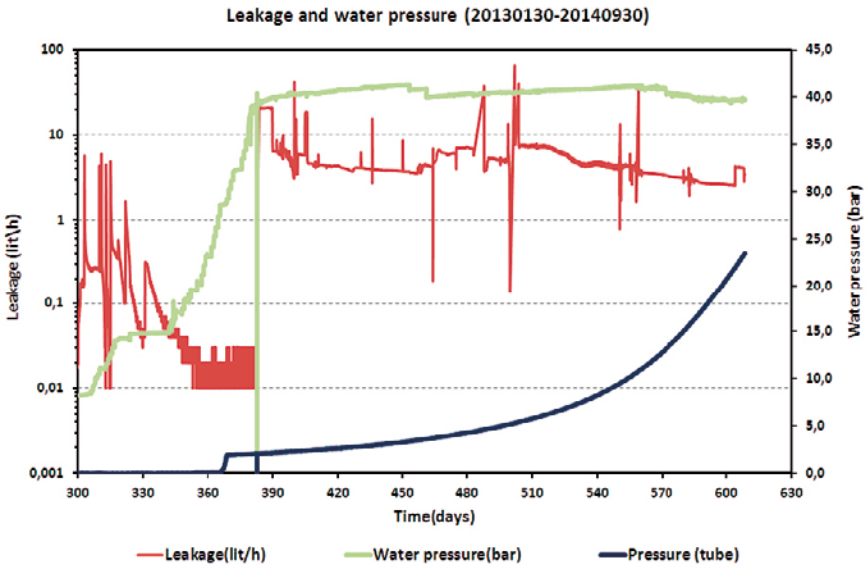

Figure 2-21. *Applied water pressure and leakage measured from the measurement weir.*

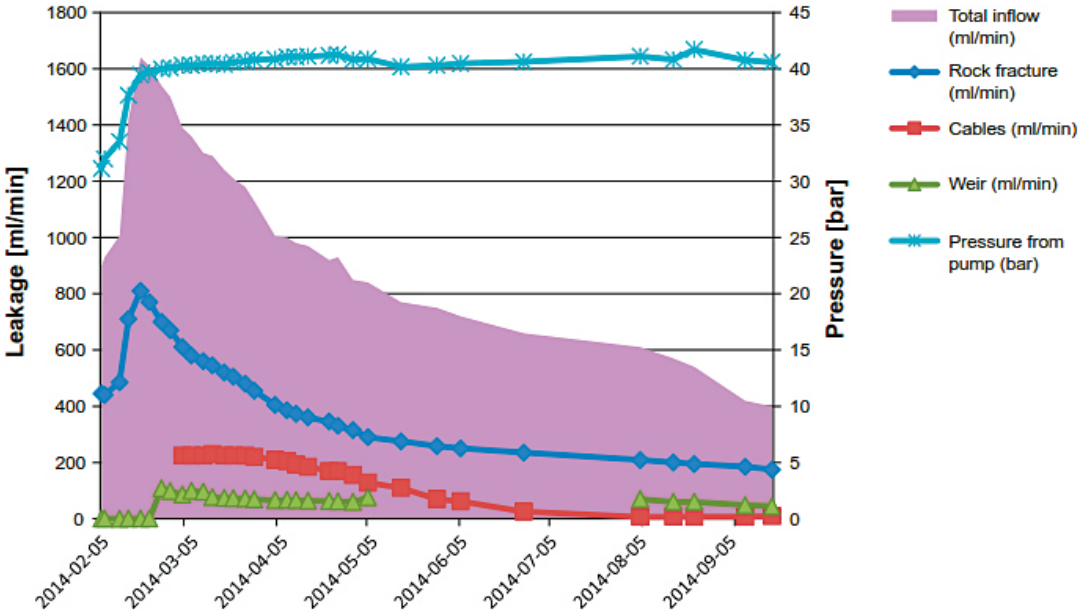

Figure 2-22. *Water pressure from pump, total water inflow and leakage measured in the weir, cable lead-through and the rock fracture for the pressurization to September 30, 2014. The leakage to the weir is low during the pressurization, this is because the filter was clogged.*

2.3.2 Bentonite seal and backfill

Relative humidity and temperature

The relative humidity and temperature was measured in the backfill and bentonite seal. Grahm et al. (2015) reported on the state of the backfill from the initiation of the measurements to September 30, 2014. The initial water content of the bentonite blocks was 17 % and the initial relative humidity after installation was between 72 % and 77 % in the bentonite seal and 63 % and 67 % in the backfill. At the end of the period reported on, the relative humidity was 95–100 % in the bentonite seal and 81–100 % in the backfill. The relative humidity of the bentonite seal is presented in Figure 2-23 and the backfill is presented in Figure 2-24.

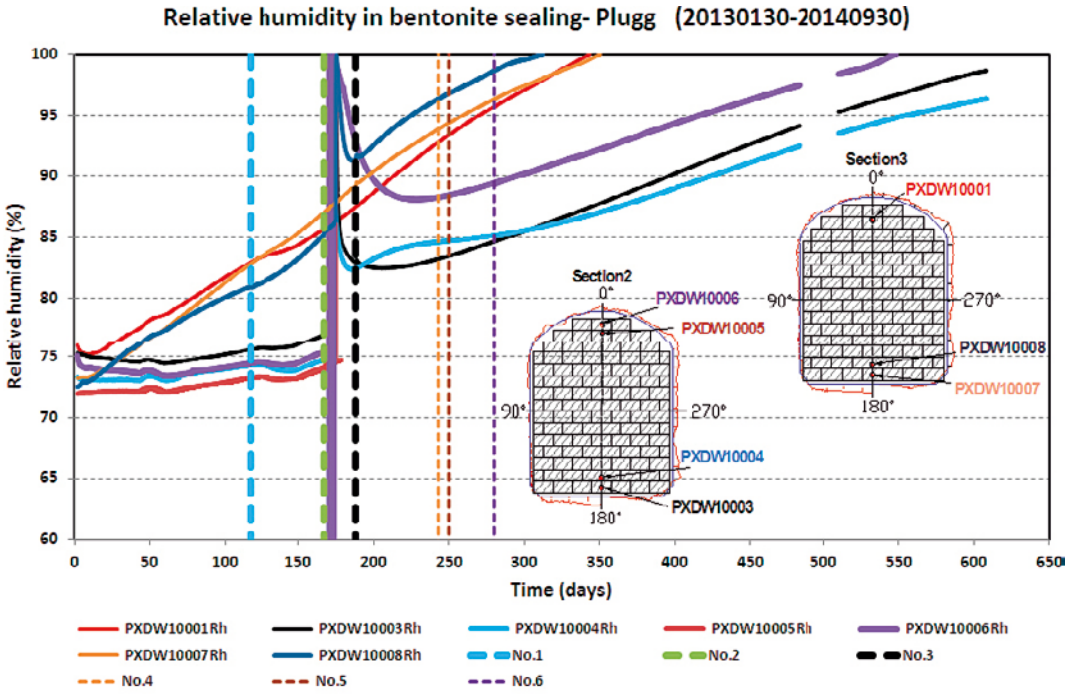

Figure 2-23. *Relative humidity in the bentonite seal from the start of the measurement period to September 30, 2014 (Grahm et al. 2015). The vertical lines represent timepoints used in the reference.*

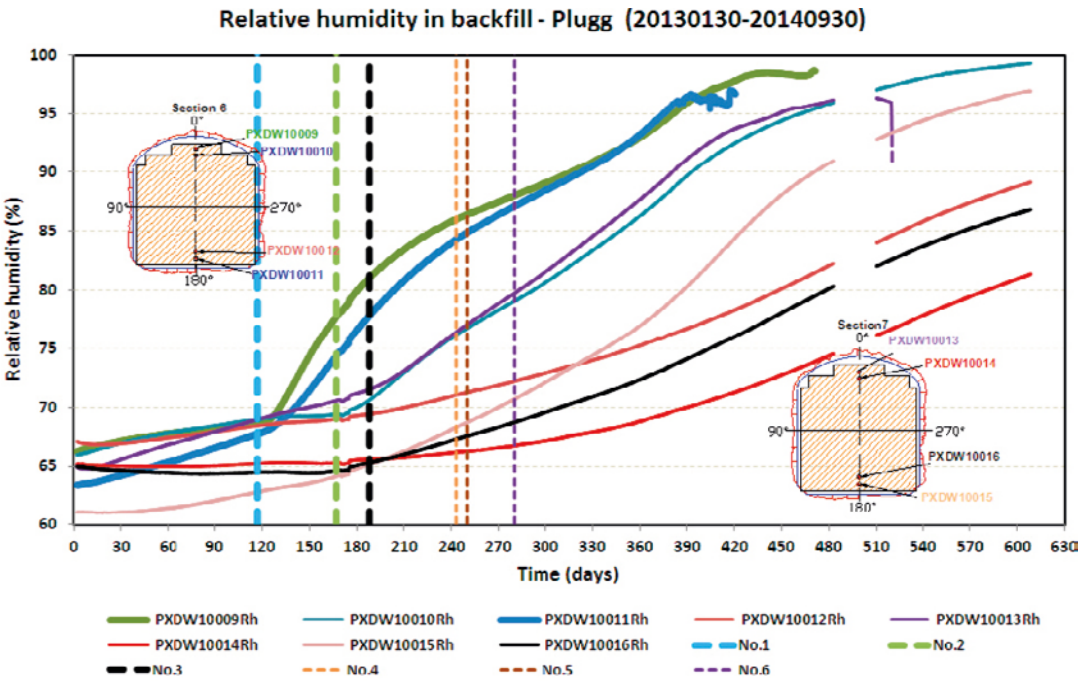

Figure 2-24. *Relative humidity in the backfill from the start of the measurement period to September 30, 2014 (Grahm et al. 2015). The vertical lines represent timepoints used in the reference.*

Total pressure and pore pressure

Sensors for total and pore pressure were installed in the backfill and bentonite seal. Due to technical complications, the total pressure was not recorded for the first 285 days of the test. The initial loading to 4 MPa was however recorded. The total pressure in the bentonite seal is presented in Figure 2-25 and the backfill in Figure 2-26. The pore pressure is presented in Figure 2-27. The pore pressure is constant for the sensors placed in the bentonite sections, but the pressure decreases along the length of the plug, so that the downstream sensors have a lower pore pressure than the upstream sensors. However, in the sensor placed in the top of the slot abutment, the pressure decreases with time. The total pressure increases with time and at the end of the measure period in Grahm et al. (2015), the pressure varies between 4.0 and 4.8 MPa in the backfill and 4.0 and 4.7 MPa in the bentonite seal.

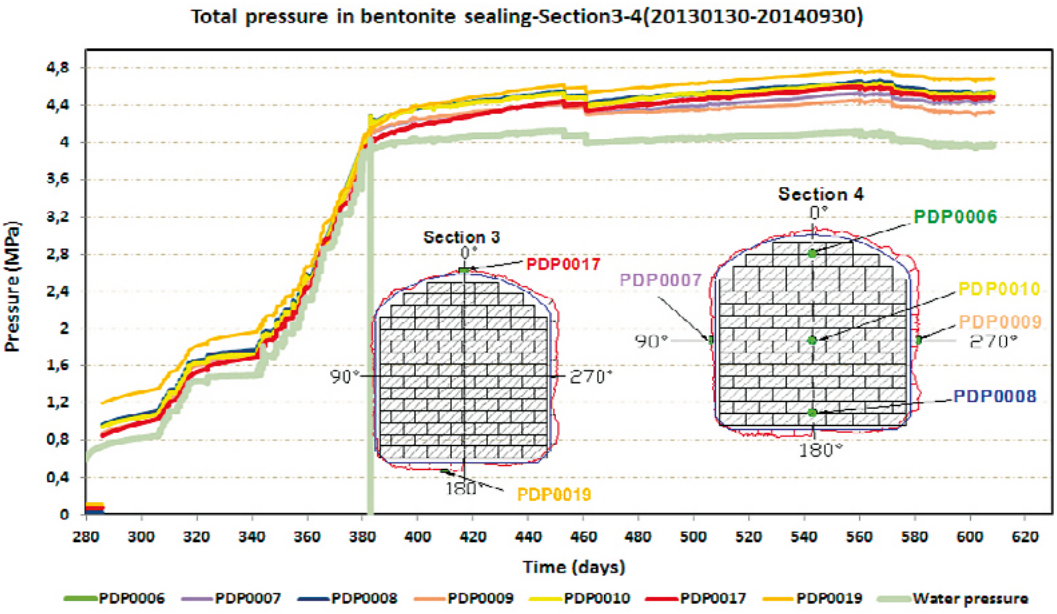

Figure 2-25. *Total pressure in Section 3 and 4 of the bentonite seal from November 11, 2013 to September 30, 2014 (Grahm et al. 2015).*

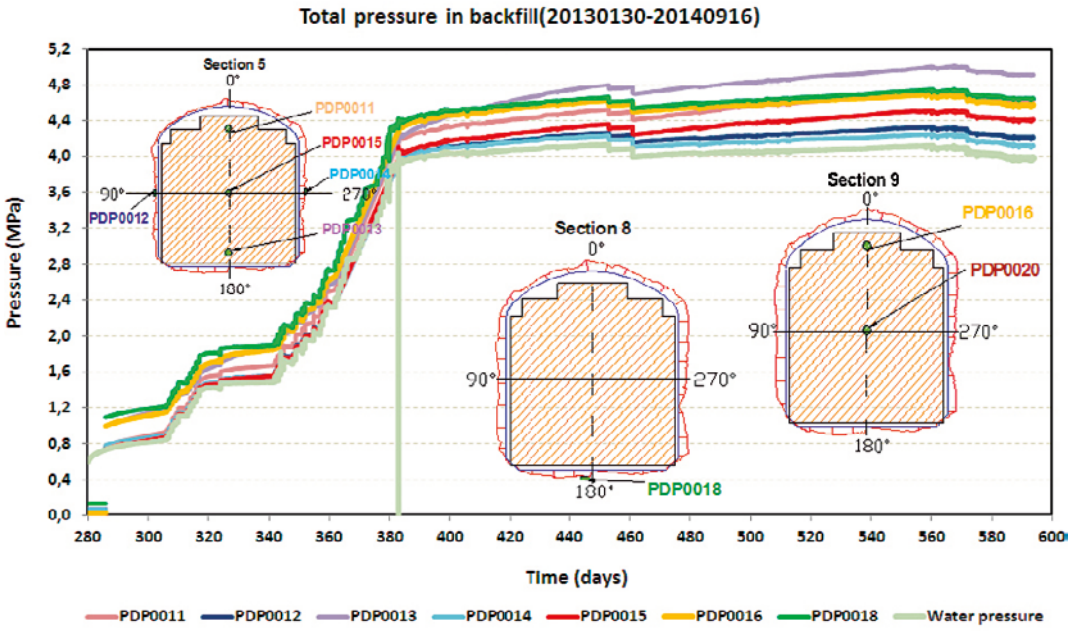

Figure 2-26. *Total pressure in the backfill from November 11, 2013 to September 30, 2014 (Grahm et al. 2015).*

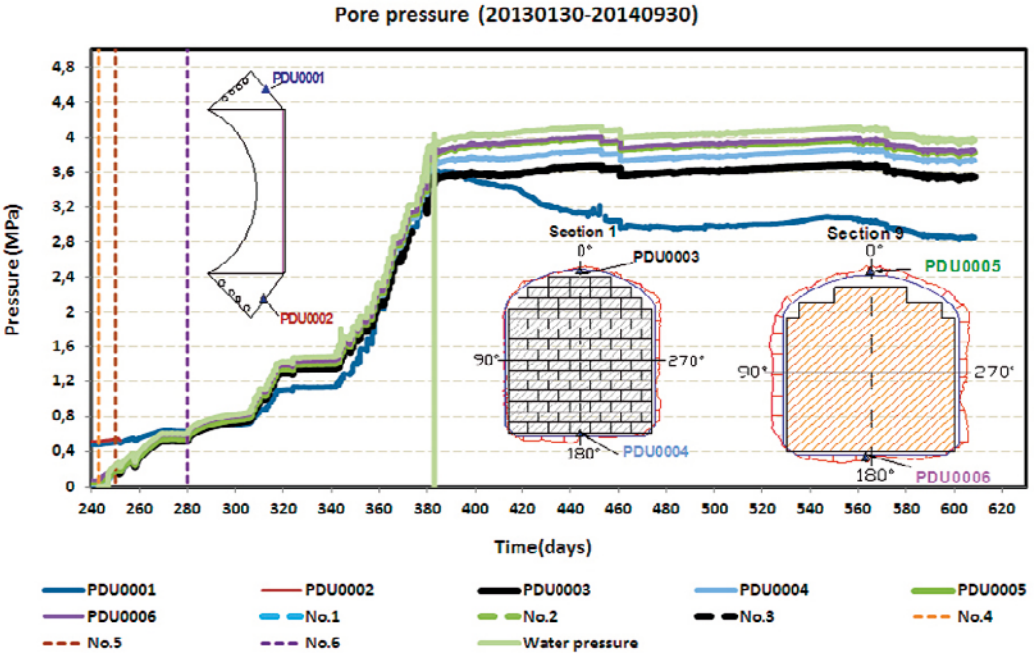

Figure 2-27. *Pore pressure along the plug structure (Grahm et al. 2015). The vertical lines represent timepoints used in the reference.*

Displacements

Three extensometers were installed, which measured the displacement between the concrete back wall and the downstream side of the backfill, LECA-beams and filter section, see Section 2.2.2. The displacements are presented in Figure 2-28. As can be seen in the figure, the sensors failed at a displacement about –30 mm. This is probably because the extensometers were deformed to their limit. The negative sign mean that the relevant sections are compressed i.e. move in the upstream direction due to the expansion of the bentonite seal.

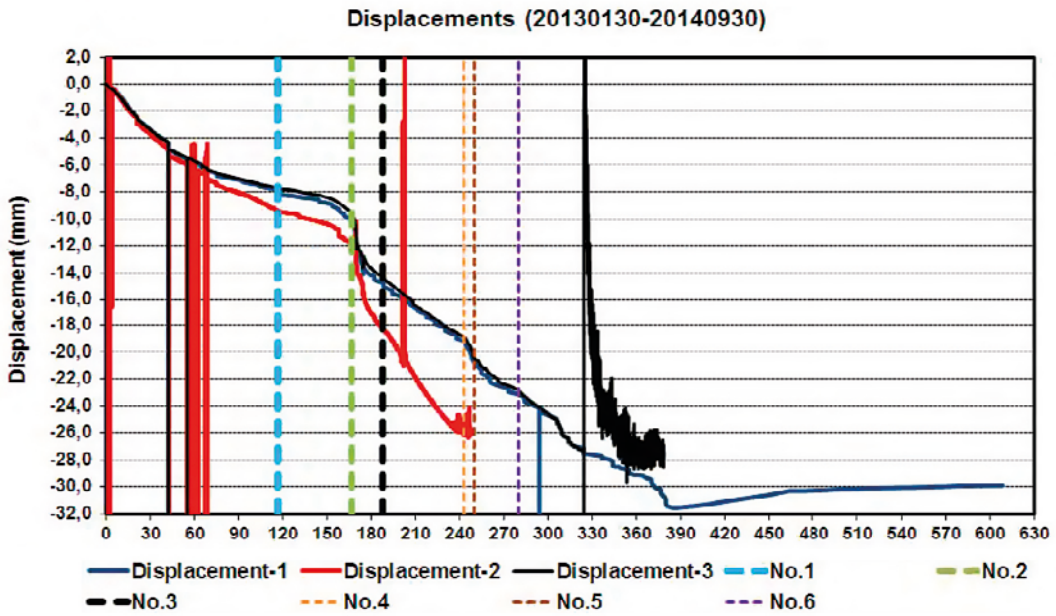

Figure 2-28. *Relative displacements between the concrete back wall and the downstream side of the backfill (1), downstream side of the gravel filter (2) and the downstream side of the LECA-beams (3) (Grahm et al. 2015). The vertical lines represent timepoints used in the reference.*

2.3.3 Concrete dome

Relative displacement between concrete and rock

The joint meters were an important indicator if the concrete dome had released from the rock along the slot abutment. The calculated value of the gap, if the concrete was subjected to unrestrained shrinkage, was 4.1 mm. The results from the joint meters up to the time of the pressurization are presented in Figure 2-29. The largest measured gap was of 0.1 mm, which shows that the concrete dome did not release from the rock, at least not at the location of these sensors. The relative displacements are small in the joint meters and likely corresponds to the strain in the concrete. However, the displacements are larger after the contact grouting, which indicates that the grouting was successful.

During the pressurization of the plug to 4 MPa, two joint meters were rapidly compressed to their maximum. This could indicate cracking or a loss of bond in the upstream face of the slot abutment.

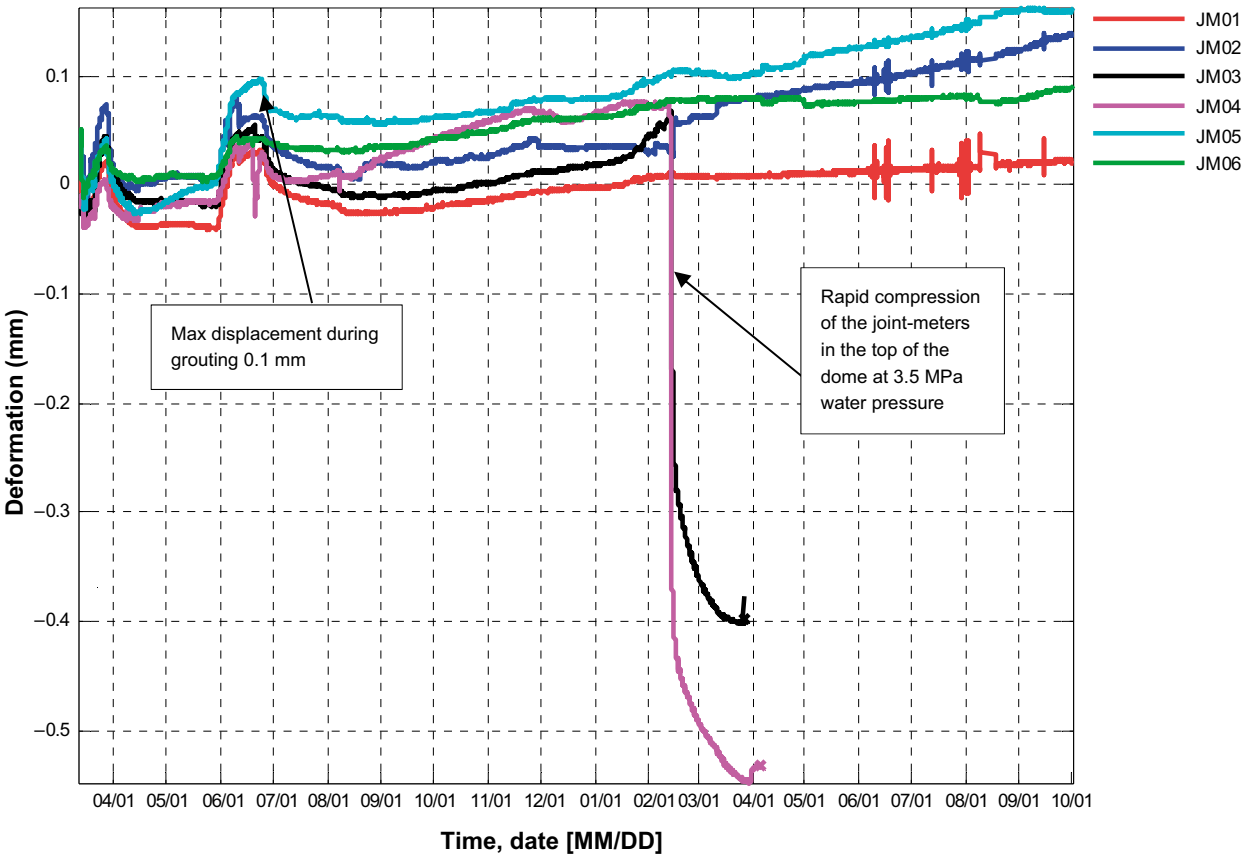

Figure 2-29. *Relative displacements in the interface between the rock and concrete dome.*

Effect of the thermal pre-stress

In addition to making the joint water tight, the contact grouting was intended to induce a prestress in the concrete dome. The strain recorded in the strain gauges is presented in Figure 2-30. To estimate the prestress in the concrete dome, the difference in strain prior to and after the contact grouting was recorded for all strain gauges. The difference in strain is multiplied with the Young's modulus of the concrete (39 GPa) to calculate the compressive prestress. The calculated prestress is presented in Figure 2-31a. As can be seen from the figure, the prestress varied from 0.5 to 3.0 MPa. Two strain gauges, which broke prior to the grouting are presented as zero in the figure. The calculated maximal theoretical prestress is presented in Figure 2-31b and varies between 3 and 4.5 MPa.

The ratio between the measured difference in strain and the theoretical prestress is presented in Figure 2-32. The mean prestress is 53 % and many strain gauges show a quite low prestress. There is a tendency that the prestress is larger in the upstream part of the concrete dome. The sensor ST12, which has a prestress of 100 % is in the centre of the plug toward the upstream face and is oriented in the vertical direction. From this, it can be concluded that the concrete dome released partially from the rock and that the upstream side of the plug released more than the downstream side.

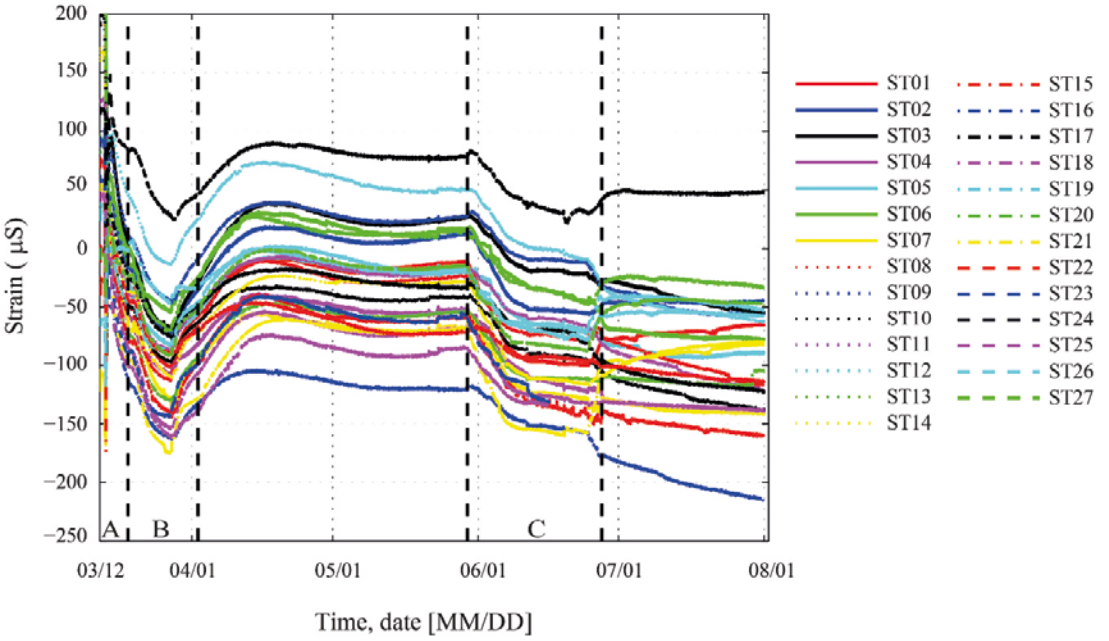

Figure 2-30. *Recorded strain in the concrete dome from the start of the full-scale test to after the contact grouting (Malm 2018).*

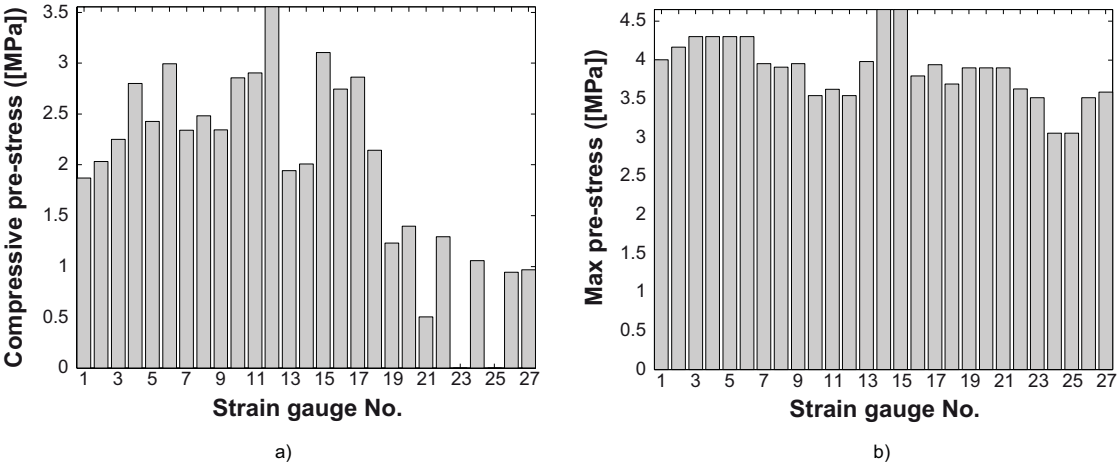

Figure 2-31. *a) Recorded difference in strain in all strain gauges in the concrete dome and b) Theoretical prestress in the concrete dome (Grahm et al. 2015).*

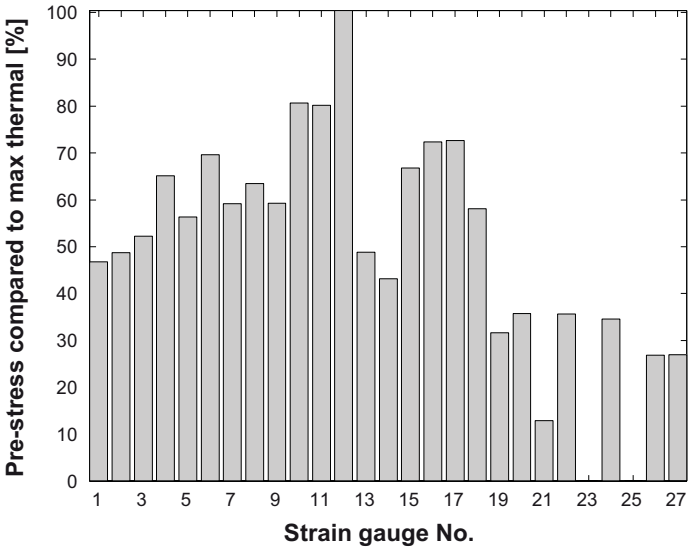

Figure 2-32. *Achieved prestress as a ratio of the theoretical maximum (Grahm et al. 2015).*

3 Gas leakage test

One requirement of the plug is that it should be gas tight in order to stop convection of air during the operation period, Posiva SKB (2017). SKB defines gas tight as a situation where no gas phase is present in the hydraulically sealing part of the plug, SKB (2014). The issue of gas tightness was therefore incorporated in the full-scale test where the aim was to investigate if the test setup can be used to verify the gas tightness requirement of the plug. The gas tightness test was first reported on by Åkesson (2017).

After about 3 years with constant water pressure of 4 MPa, the hydraulic pumps were stopped. This resulted in a decrease in the water pressure which levelled out at approximately 1.5 MPa, which is considered to be the natural hydrostatic pressure in the host rock at the test site. Thereafter the drainage pipes were opened to remove the remaining water and reduce the water pressure to zero. When all available water had been drained from the filter, the gas tightness test started.

3.1 Drainage of the filter and gas pressurization

After the filter had been emptied from water, the drainage pipe was kept open to the atmosphere (through a water hose) while helium gas was pumped into the deairing pipe via a helium gas tube (the drainage pipe opening in the top of the filter is denoted the deairing pipe). This was maintained for approximately three days. The intention for this was to evacuate all water in the filter before the gas tightness test was conducted.

The gas filling was controlled by a gas regulator which was attached to the deairing tube. The volume of water that came out of the drainage pipe was monitored and quantified with a water meter which was connected to the outlet of the water hose. The test set-up for the gas tightness test is illustrated in Figure 3-1.

In Figure 3-2, the recordings from the water meter are shown which shows a relatively rapid increase initially during the first hours but slowed down significantly after this. The final volume of water that escaped from the filter (due to the gas pressure) was about 3.0 m^3. Thereby, this indicates the pore volume in the filter which approximately correspond to slightly more than half of the volume of the filter.

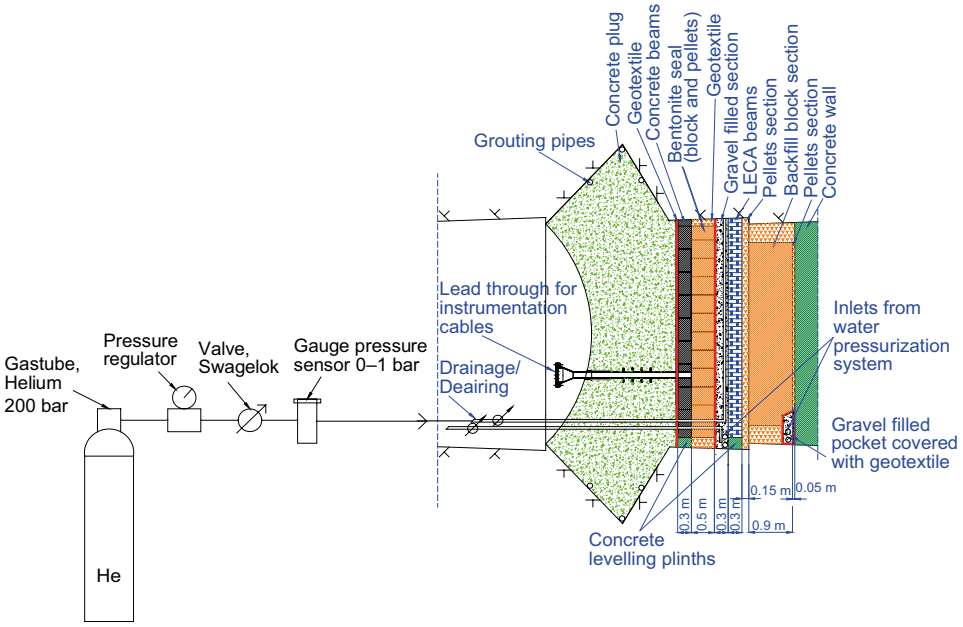

Figure 3-1. *Schematic outline of test set-up (Åkesson 2017).*

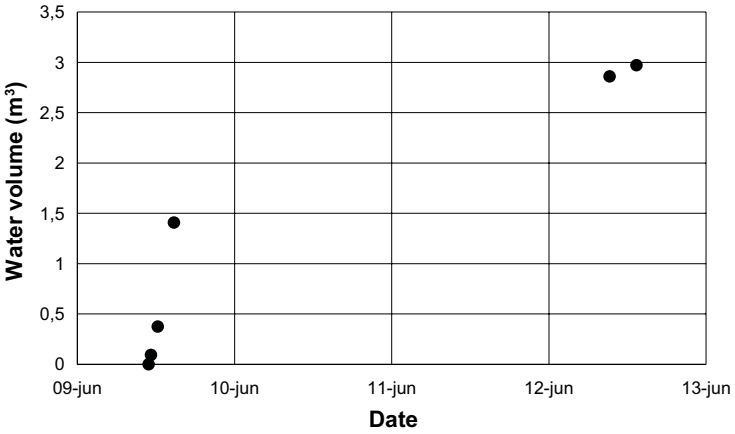

Figure 3-2. *Water meter readings during drainage of filter (Åkesson 2017).*

3.2 Monitoring results of the gas tightness test

The gas tightness test was performed in two steps

- Gas pressurization
- Leakage monitoring

The pressurization was performed through the deairing pipe while keeping the drainage pipe closed. Two 20 litre gas tubes were used for gas filling where the pressure decrease in these two tubes combined was 58 bars. The corresponding pressure increase in the filter was recorded with pressure gauges and was 0.4 bar, as seen in Figure 3-3. Based on these variations in pressure, it is possible to estimate the volume of the filter to 2.9 m^3. This is close to the volume of the evacuated water, presented previously.

The leakage monitoring step lasted for 18 hours and resulted in a small pressure increase of 3 kPa. This shows that noticeable inflow of water occurred into the filter during this test. In addition to the pressure monitoring, a sniffer leak detector was used to detect any leakage of the helium gas. The downstream surface of the concrete dome was systematically investigated as shown in Figure 3-4. However, no findings of helium concentrations could be detected. Considering that the pressure in the filter maintained (or even increased slightly due to the inflow of water) along with no leakage detections with the sniffer, it can be concluded from this test that the plug was gas tight.

To assess the natural water inflow into the filter, both drainage pipes and deairing pipes were open after the leakage monitoring step was finished. The water outflow measured from the drainage pipe showed a decreasing exponential trend where the last recordings was about 0.09 litre per minute after 24 hours. This was considered as the best available assessment of the water inflow, it should however be noted that the outflow rate likely would decrease even further with time.

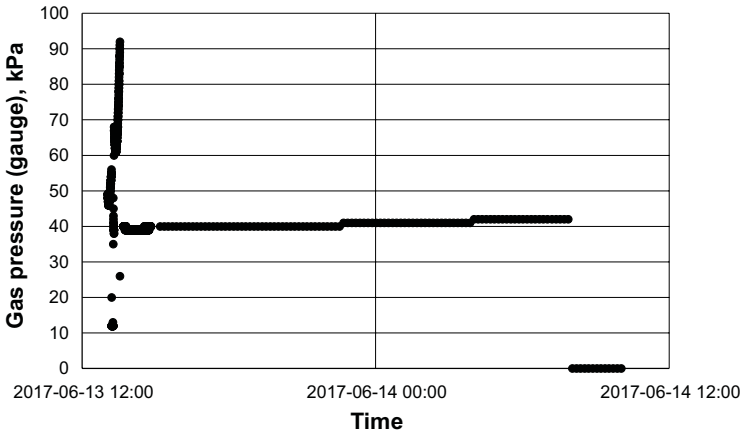

Figure 3-3. *Recorded gas pressure during gas tightness tests.*

a) b)

Figure 3-4. *Photographs from sniffer leak search; a) Equipment and b) Investigation from scaffold (Åkesson 2017).*

3.3 Numerical results

The recorded increase in gas pressure during the leakage monitoring step showed that a noticeable inflow of water had occurred during the measurement. As mentioned in the previous section, the estimated inflow was 0.09 litre per minute. The following hypothesis was developed:

- The bentonite was gas tight and the water inflow was the sole process governing the increase in gas pressure.

It should be mentioned that if the measured water inflow rate was higher than the flow rate corresponding to the measured pressure increase, then this could indicate evaporation of gas in to the rock, through the concrete dome or dissolved in the water phase.

To test this hypothesis, numerical investigations were presented by Åkesson (2017) where a differential equation was defined that described the connectivity between inflow of water, gas pressure and gas leakage. This is illustrated in Figure 3-5, where the inflow of water is denoted (Q_w), the pore volume of the filter (V_f), the gas pressure (p_f), ambient pressure (p_a) and the permeable section with an area (A) and length (L) and permeability (k).

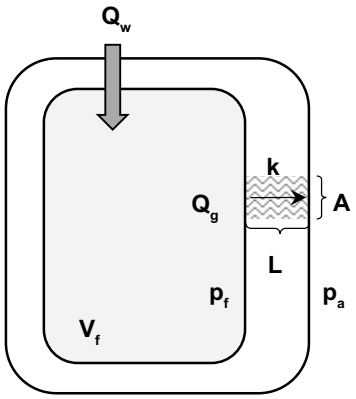

Figure 3-5. *Schematic illustration of filter and relation between water inflow, gas pressure and potential gas leakage.*

In Åkesson (2017), the following differential equation was derived, which express the relation between these parameters.

$$\frac{dp_f}{dt} = \frac{p_f \cdot Q_w}{V_f} - \frac{\kappa}{V_f} \cdot (p_f{}^2 - p_a{}^2) \tag{3-1}$$

In the equation, the parameter κ has been introduced which denotes

$$\kappa = \frac{A \cdot k}{2 \cdot L \cdot \mu_g} \tag{3-2}$$

where,

μ_g is the viscosity of the gas.

The differential Equation (3-1) was solved numerically with the MathCad software based on the following conditions:

- $p_f(0)$ = 1.39 bar (absolute)
- p_a = 1 bar (absolute)
- $V_f(0)$ = 3 m^3

In addition, a base case water flow rate (denoted Q_b) was defined equal to the quantified value of 0.09 litres per minute. Based on this a base case κ-value (denoted κ_b) was calibrated so that the gas pressure increased to 1.42 bar after 18 hours and was found to be 7.5×10^{-12} ($m^3 \cdot Pa^{-1} \cdot s^{-1}$), see Figure 3-6. This would imply that a gas leakage of 2 litres per hour (at 1.4 bar absolute) occurred.

Two sensitivity analyses were performed, where the κ parameter varied with a factor 2 and 0.5, respectively. It was found that the κ parameter had a considerable influence on the pressure evolution. Finally, a simplified case with a pressure evolution similar to the base case could be modelled with a zero κ-value if the water flow rate was reduced to 0.06 litres per minute. This evaluation thus demonstrates that inflowing water would be the sole process governing the gas pressure evolution if the inflow rate would be one third lower than the measured value.

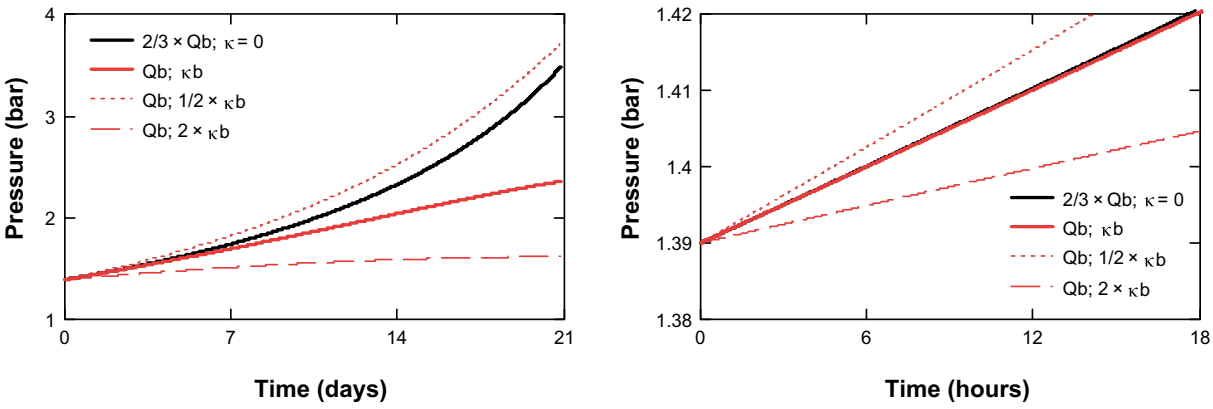

Figure 3-6. *Modelled absolute pressure evolution for the base case (Q_b = 0.09 l/min; $\kappa_b = 7.5 \times 10{-}12$ $m^3 \cdot Pa^{-1} \cdot s^{-1}$) with two sensitivity cases ($\kappa_b/2$ and $2 \cdot \kappa_b$), and one simplified case (2/3 Q0 and κ = 0). Figures and caption are taken from Åkesson (2017).*

3.4 Evaluation

The measurement result in the bentonite seal showed that the relative humidity was close to water saturation, which in turn would imply that the seal was gas tight. This could be verified by the results from the gas tightness test, based on the two following observations:

- Increasing gas pressure in the filter after the helium gas had been pumped into the filter.
- No concentration of helium could be detected with the sniffer leak search.

The increasing pressure was, as previously mentioned, most likely caused by inflow of water into the filter. This was supported by the measured inflow of water preformed after the gas tightness test. The quantity of the inflow was approximately 50 % higher than the flow rate required to cause the measured increase in gas pressure. This level of precision can be regarded as fairly high considering the uncertainties in pore volume and the drainage capacity of the filter. Other potential sources of uncertainty that could explain the pressure increase are, dissolution of gas in the water phase, gas escape into the rock or as leakage past the concrete dome.

3.5 Comparisons with requirements

Posiva SKB (2017) states that the plug must be reasonably gas tight during the operation phase of the spent fuel repository. Åkesson (2017) concludes that the plug fulfils the requirement based on the results from the gas tightness test. The actual rate of oxygen transfer through the plug is thus governed by the diffusion of oxygen dissolved in water through the water filled pore-spaces in the filter as well as in the bentonite seal. This is a slow process and the risk of oxygen transport into the closed off tunnel is deemed low.

4 Structural response to the gas leakage and strength tests

4.1 Pressurization scheme

After the initial pressurization of the plug, the pressure was held constant slightly above 4 MPa for about three years. As previously mentioned, the pressurization pipes in the gravel pocket was mainly used for the pressurization. Before the gas leakage test, the filter was drained so that the water pressure was reduced to zero. The pumps were turned off June 2nd, 2017 and the drainage pipes were opened 10 days after this. Before the drainage pipes were opened, the pressure stabilized at 1.5 MPa, which is considered the natural water head of the host rock at the test site. After the gas leakage test was performed, and the water pressure was returned to 4 MPa, which was reached on July 21st. The pressure was held constant for one week until July 27th.

During the strength test, the goal was to reach a water pressure of 9 MPa. The water pressure was increased in increments over a period of 20 days, but the maximum water pressure reached was 8.1 MPa, due to large leakage in the host rock. As mentioned in Section 4.3.1, the swelling pressure in the bentonite seal varied between 0.2 and 1.9 MPa, implying a total pressure between 8.3 and 10.0 MPa. The maximum pressure was reached at 15th of August and was held constant for three days before the water pressure was reduced to 4 MPa again. The plug was depressurized shortly thereafter, and core drilling and demolition commenced. Figure 4-1 depicts the pressurization scheme during the gas leakage and strength tests.

Figure 4-1. *Water pressure in the backfill during the period June 1st to August 20th 2017, during which time the gas leakage and strength tests were performed (Malm et al. 2019).*

4.2 Concrete dome

This section describes measurements and numerical results from the concrete dome during drainage for the gas leakage and pressurization to 8 MPa in water pressure for the strength tests. The results described in this chapter were first reported on in Malm (2017). The monitoring system of the concrete dome is presented Section 2.2.3.

4.2.1 Monitoring results

Temperature sensors

In Figure 4-2, all temperature sensors in the concrete dome are presented for the entire operation of the full-scale test. In Figure 4-3, the ambient temperature is presented for the same duration. As can be seen in the figures, the concrete temperature follows the annual temperature variations in the ambient air. The temperature in the tunnel varies between +12 °C and +16 °C with highest temperatures reached during August and September and the coldest period is in February and March. The magnitude of the temperature change is smaller in the concrete dome and slightly delayed, so that the peaks occur in October and April.

During the studied period between July 1st and August 20th, 2017, no shift in the ambient temperature was recorded and no other activities occurred that would affect the temperature in the concrete. However, while studying the zoomed in recordings of the concrete temperature in Figure 4-4, some unexpected behaviours can be seen starting from August 1st.

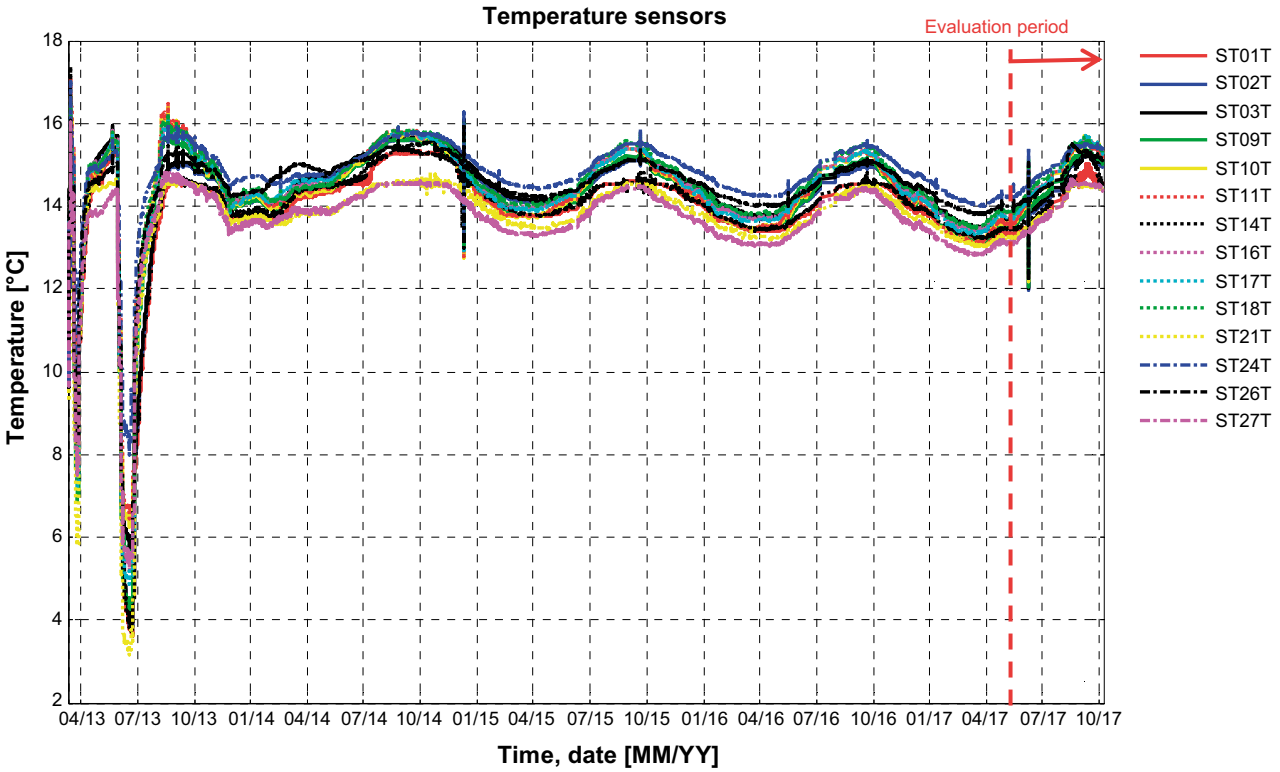

Figure 4-2. *Measured temperature from all temperature sensors in the concrete dome during the entire operation of the full-scale test (Malm et al. 2019).*

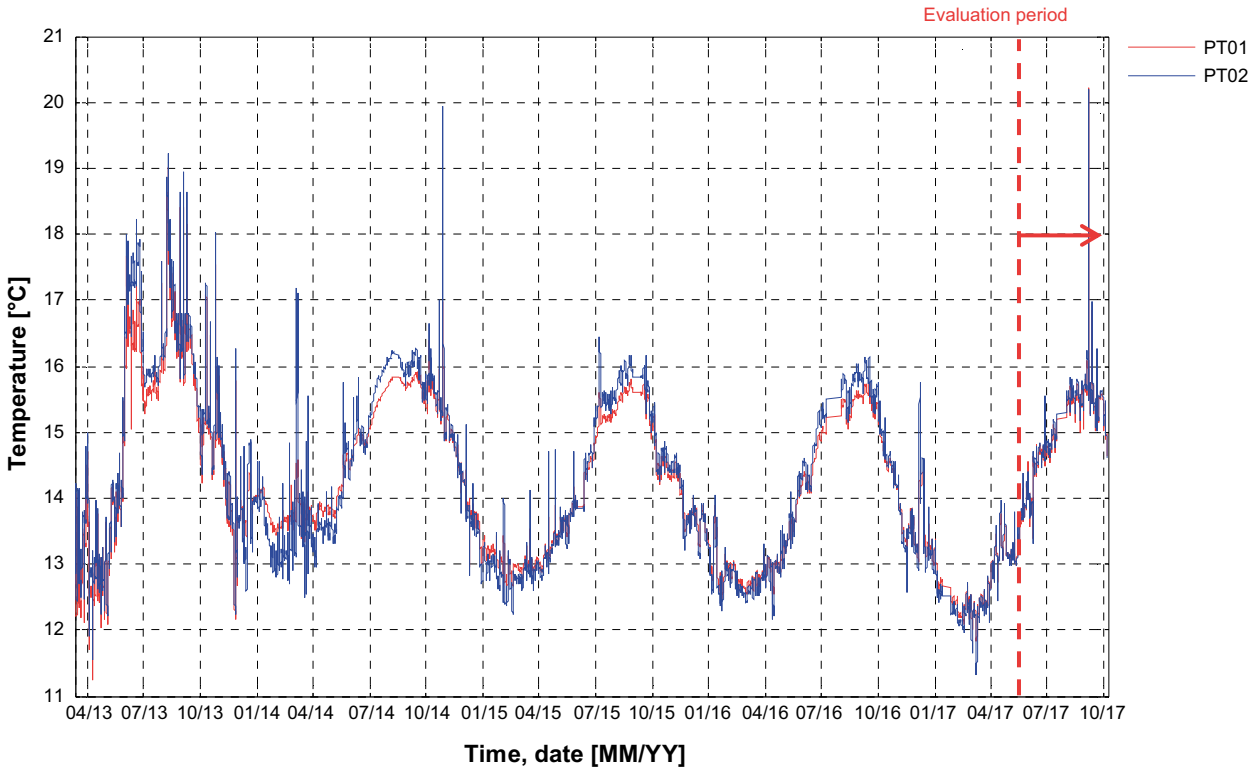

Figure 4-3. *Ambient temperature variation during the entire operation of the full-scale test (Malm et al. 2019).*

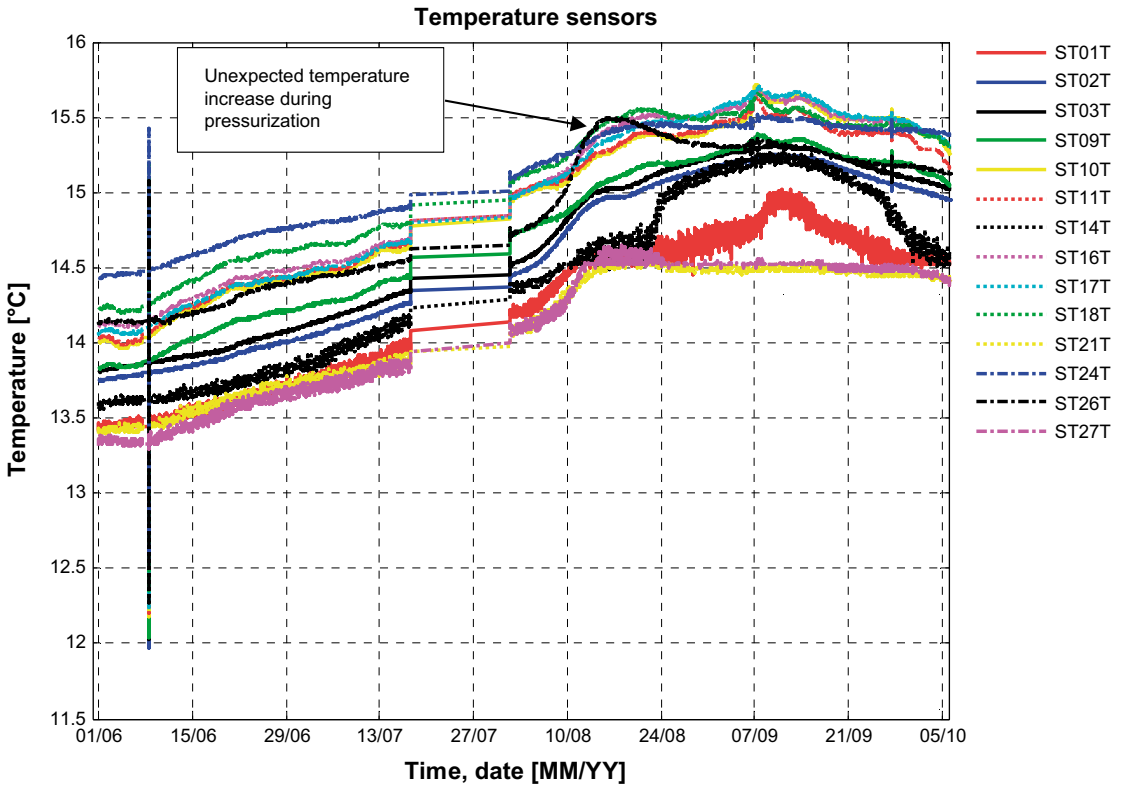

Figure 4-4. *Measured temperature from all temperature sensors in the concrete dome during the gas leakage and strength tests (Malm et al. 2019).*

The behaviour is most obvious in sensor ST27T, which gives a significantly larger temperature peak than expected. The peak also occurs earlier than expected. This sensor is placed close to the downstream side of the abutment at the right-hand side as seen in Figure 4-8. The temperature is 0.5 °C higher than expected at August 15th, the day when the pressure reached 8 MPa.

The rising temperature could occur for two reasons: leakage or confined pressure. If leakage occurred at the interface between the rock and the concrete in this region, the temperature of the flowing water would affect the surrounding structure. The temperature of the water used for pressurization was not recorded, since all temperature sensors in the backfill and bentonite seal had malfunctioned at the time of the strength test. However, it seems unlikely that the temperature would be higher than the ambient temperature since it was stored in a tank in the monitoring niche. Leakage is therefore not considered a probable cause to the rise in temperature. In a confined space, however, the temperature can rise due to an increased pressure if the pressure rises rapidly and the temperature does not have time to distribute in the surrounding structure.

Displacements

Only one of the original LVDT-meters (which measures displacements) was still giving a reliable signal at the time when the gas leakage test started. Four additional LVDT meters were therefore added to the frame downstream of the plug to record the effect of the varying loads during the pressure tests. The remaining original sensor was denoted LVDT002 and was placed approximately at the quarter-point above the centre of the concrete dome. Figure 4-5 shows the downstream displacement of the plug recorded by LVDT002 for the entire operation of the full-scale test. The initial deflection when the water pressure of 4 MPa is first applied was 1 mm.

During the period with constant water pressure, before drainage during the gas leakage test, the deflection increased to 1.6 mm. This time dependent increase in deflection is caused by the increased swelling pressure from the bentonite and concrete creep caused from the sustained water pressure. In addition, it is possible to detect a small influence from the seasonal temperature variation in the measurements.

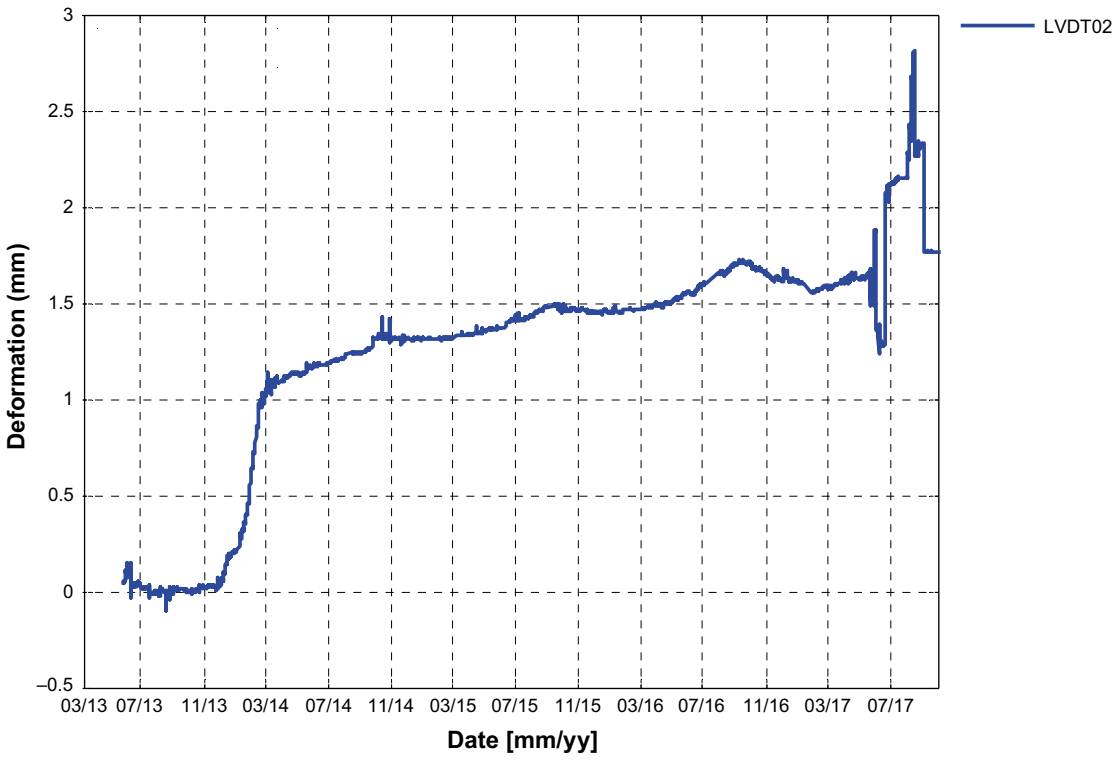

Figure 4-5. *Measured displacements in the downstream direction in LVDT002, placed at the quarter point above the centre of the plug for the entire duration of the full-scale test (Malm et al. 2019).*

When the concrete dome was unloaded for the gas leakage test, the deflection decreased about 0.3 mm (to 1.3 mm). The decreased deflection is significantly less than the initial 1 mm, which was measured during the loading in 2013/2014. The reason for this is to some extent creep. If the concrete dome would have been unloaded for a longer time, the deflection would decrease further but not return to the initial sate. The irreversible effects are caused by cracking in the concrete and the increased swelling pressure of the bentonite.

After the gas leakage test, when the pressure was resumed to 4 MPa, the deflection increased to 2.1 mm. The difference in deflection before and after the gas leakage test can be seen in Figure 4-6. It is likely caused by cracking in the concrete dome or loss of bond in the interface between the rock and concrete. As later shown in Section 4.2.2, reduced water pressure leads to increased risk for cracking, especially in the region close to the upstream end of the slot abutment.

During the strength test, the deflection increased by 0.7 mm as the water pressure increased from 4 to 8 MPa. The displacement was also larger after the strength test than before, both when the water pressure was 4 MPa and when the pressure was released. This indicates that further cracking and permanent deformations. The final deflection of the unloaded plug was 1.8 mm at location of the sensor LVDT002.

The LVDT-meters installed before the gas leakage and strength tests gave equivalent results as LVDT002, even though some of these sensors did not give a reliable signal throughout the entire test. The measurements from all LVDT sensors are presented in Figure 4-7.

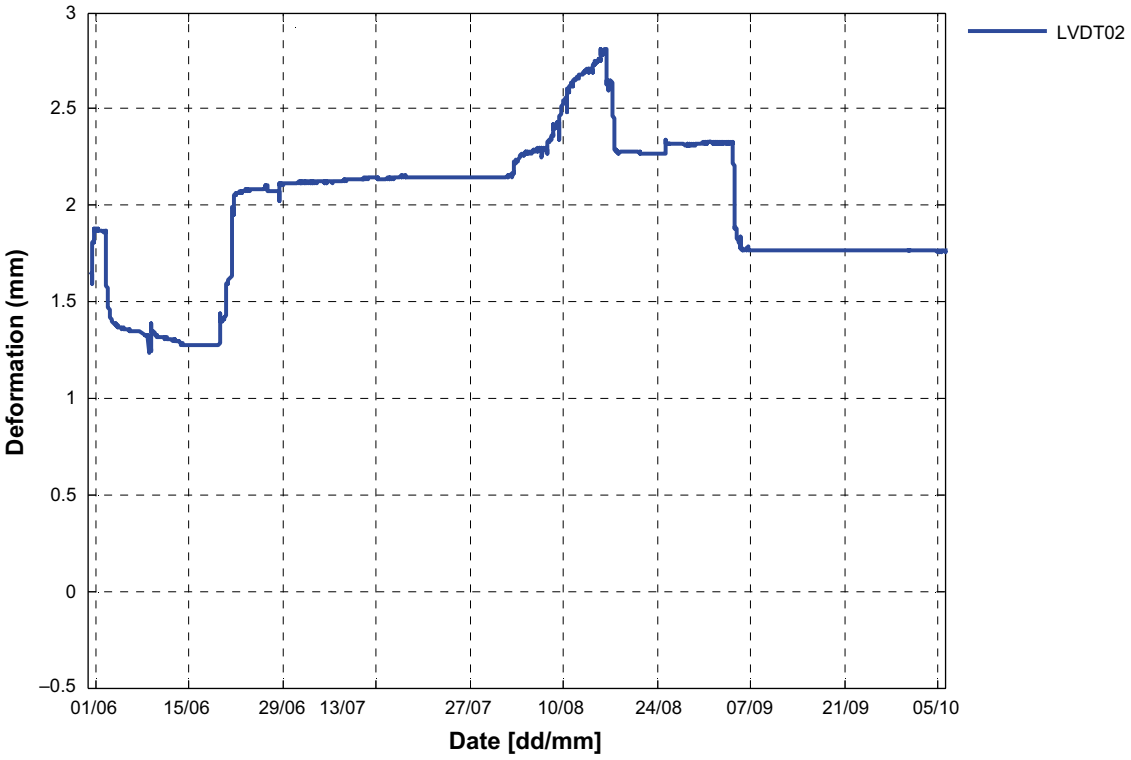

Figure 4-6. *Measured displacements in the downstream direction in LVDT002, placed at the quarter point above the centre of the plug for the duration of the gas leakage and strength tests (Malm et al. 2019).*

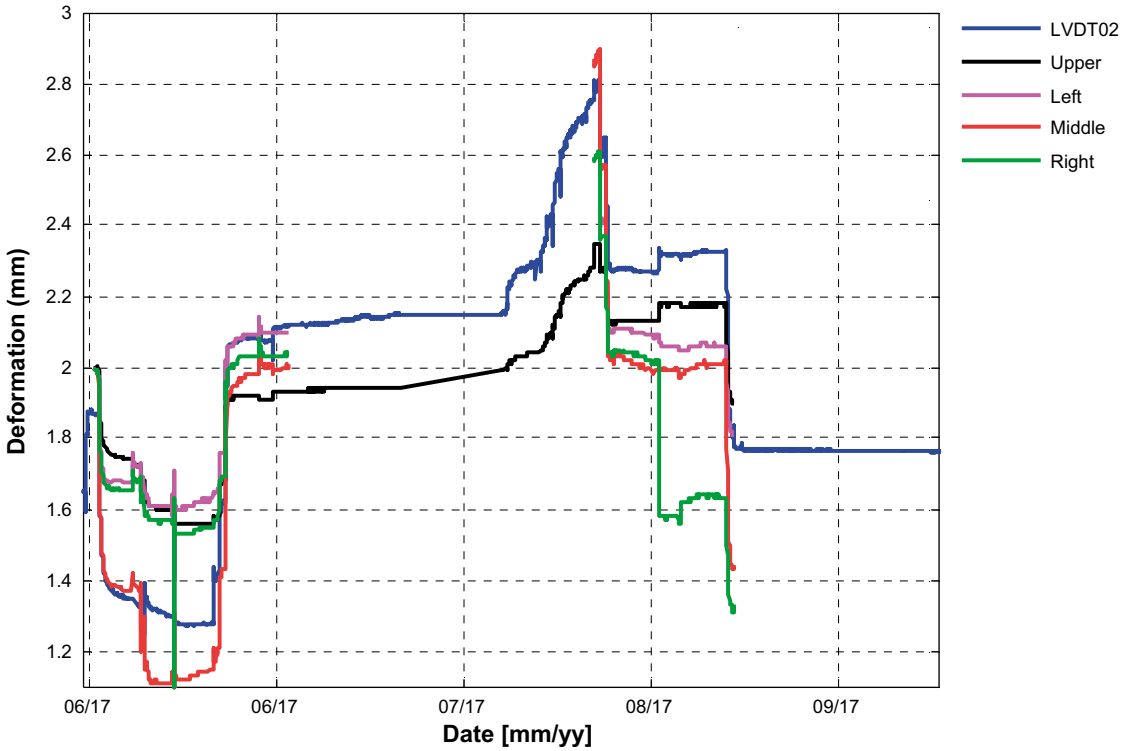

Figure 4-7. *Measured displacements in the downstream direction in all LVDT-sensors during the gas leakage and strength tests (Malm et al. 2019).*

Strain gauges

Figure 4-8 presents the locations of all strain gauges in the concrete dome, in total, 27 strain gauges were installed. At the time of the gas leakage test, 15 strain gauges were still functioning.

During the gas leakage and strength tests, the strain varied with the changes in water pressure. During the gas leakage test, when the pressure was released, the strain increased about 100–120 µS (see Figure 4-9). If the elastic modulus of concrete of 33.9 GPa is assumed, according to Vogt et al. (2009), the reduced strain corresponds to a reduction of the compressive stress by 3.3 to 4.4 MPa. During the strength test when the water pressure was increased from 4 MPa to 8 MPa, the strain decreased by 100–150 µS. This corresponds to increased compressive stress of 3.3 to 5.1 MPa.

It can be noted that the strain level remains the same before and after the tests. Which means that the concrete dome mainly behaves linear elastically, in the areas where the strain gauges are placed, based on the recordings from the strain gauges.

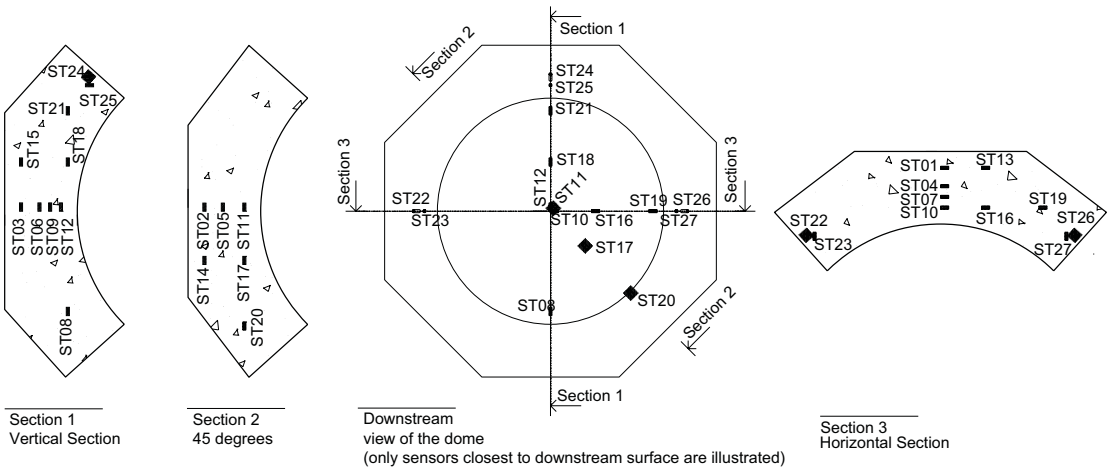

Figure 4-8. *Placement of strain gauges in the concrete dome (Malm 2017).*

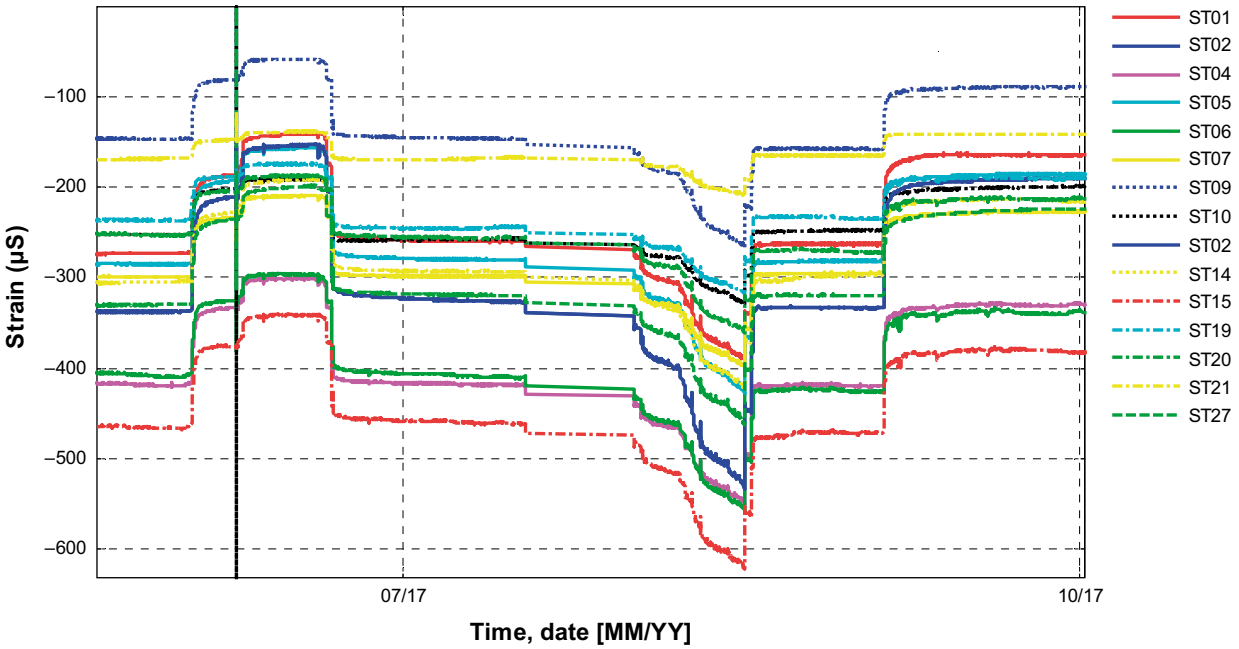

Figure 4-9. *Recorded strain from the strain gauges embedded in the concrete during the gas leakage and strength tests (Malm et al. 2019).*

Joint meters

The relative displacements in the joint between the rock and concrete in the slot abutment was measured with six extensometers, denoted joint-meters. The placement of the joint-meters is presented in Figure 4-10.

At the start of the gas pressure test, four joint-meters was still functioning. The relative displacement is presented in Figure 4-11. For three of the four of the joint-meters, the variation in displacement is small. This indicates that the bond between the rock and concrete is intact in these regions. However, the fourth joint-meter, JM06, compresses rapidly during the strength test. The compression indicates cracking or loss of bond that leads to increased compressive stress and movement in the joint. This behaviour is similar to JM03 and JM04, which failed during the initial loading, see Figure 4-12.

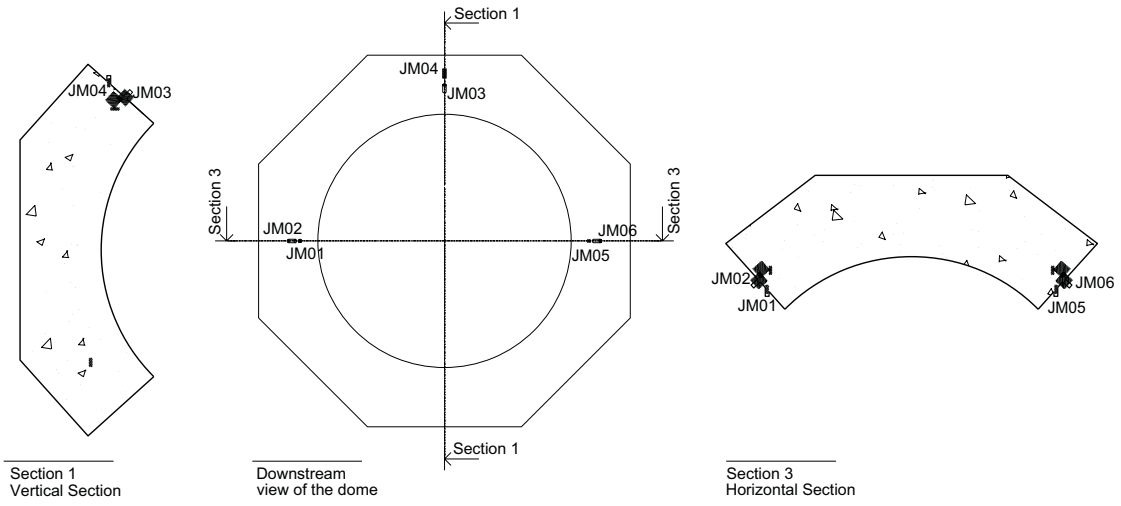

Figure 4-10. *Placement of joint-meters (Malm 2017).*

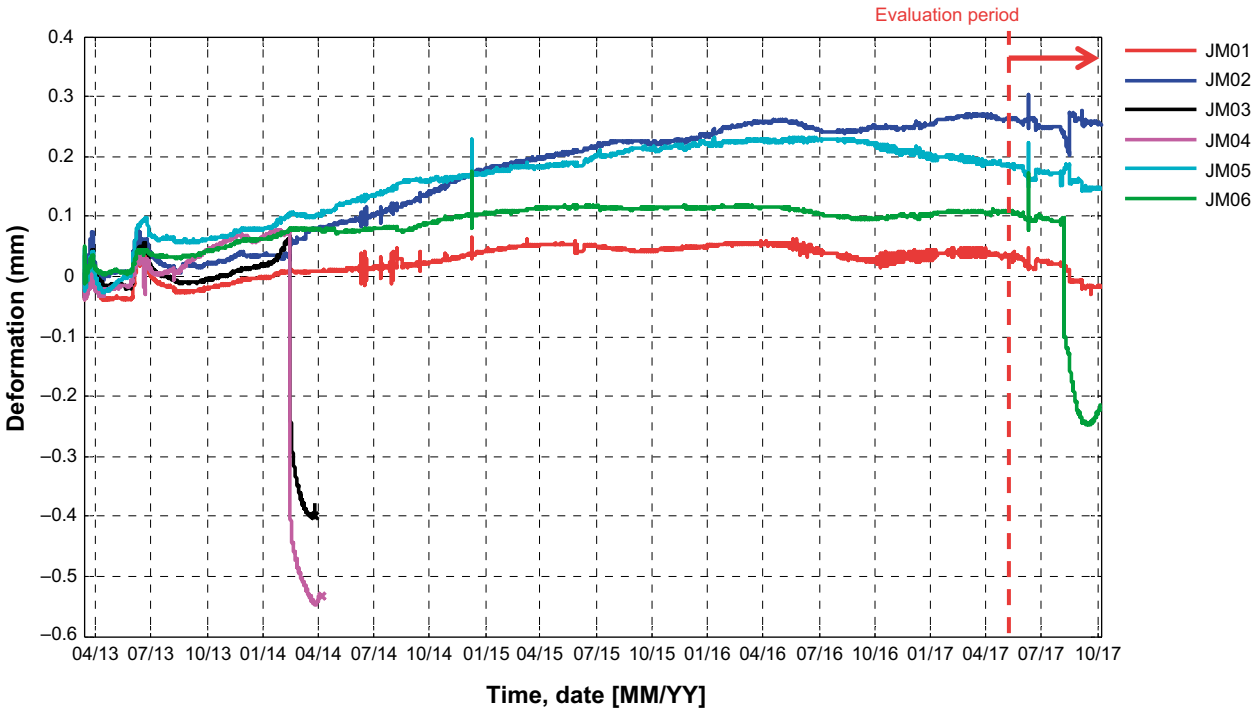

Figure 4-11. *Relative displacement in all joint-meters during the entire full-scale test (Malm et al. 2019).*

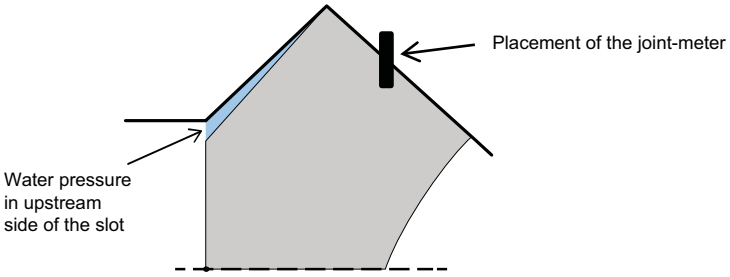

Figure 4-12. *Illustration of the top of the dome with release of bond on the upstream surface of the slot abutment.*

Conclusions

Based on the results from the leakage and strength test, it could be seen that the sensors that measure the global behaviour, i.e. LVDT-sensors show differences before and after the leakage or strength tests which indicates cracking in the dome or loss of bond in the slot. Some of the strain gauges and one joint meter also shows that nonlinear behaviour has occurred. The rest of the sensors measuring local performance showed a linear elastic behaviour, where the displacements returned to the original values after the tests were performed. In conclusion, local cracking or loss of bond occurred in the concrete dome. The pressure test was successful in proving that the dome concrete dome can withstand its theoretical design loads.

4.2.2 Numerical results

Numerical model

Before the gas leakage and strength tests, FE-simulations were performed to predict the behaviour of the concrete dome. The simulations were updated after the tests to represent the actual water pressure sequence, rather than the theoretical. The full analyses are presented in Malm et al. (2019), only some meaningful results are presented here. The FE-model used was the same as used in Grahm et al. (2015) and it is presented in Figure 4-13.

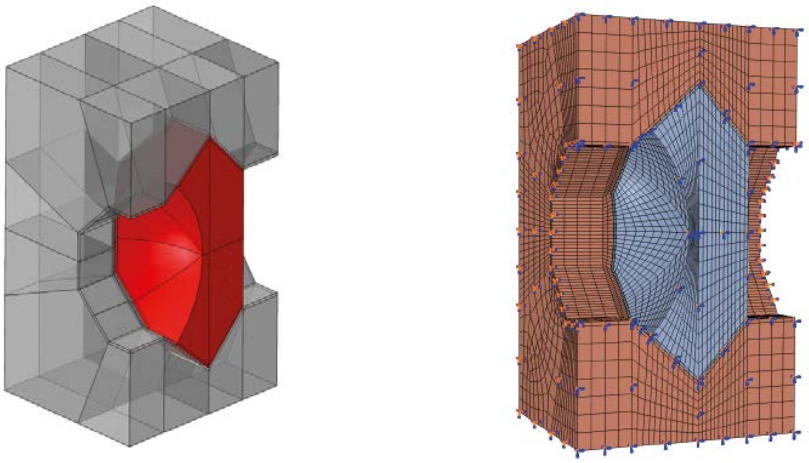

Figure 4-13. *FE-model used for analyses of the concrete dome (Grahm et al. 2015).*

The three simulations were performed with different assumptions for the interaction between the rock and concrete. The difference was when, after the casting, the concrete dome released from the rock. After the contact grouting, full contact was assumed along the downstream face of the slot abutment for all simulations.

In one simulation, no initial bond was assumed, and the contact was modelled with an interaction. In the other two simulations, full initial contact was assumed, which released during the cooling respectively just before water pressure was applied. The last two simulations performed very similar during the application of the water pressure and during the gas leakage and strength tests.

The simulations showed that there would be an increased risk for cracking or loss of bond between the rock and concrete during the gas leakage test. The cracking would occur in the top and centre of the concrete dome, primarily near the downstream side. However, no cracking except micro-cracking (see Section 6.3.2) was observed in this area after the tests were performed. The stresses in the simulation during the gas leakage test is presented in Figure 4-14.

During the strength test, the stresses decreased in the entire concrete body for all simulations but not enough to cause crushing in any part of the concrete dome. The stresses for the three simulations are presented in Figure 4-15.

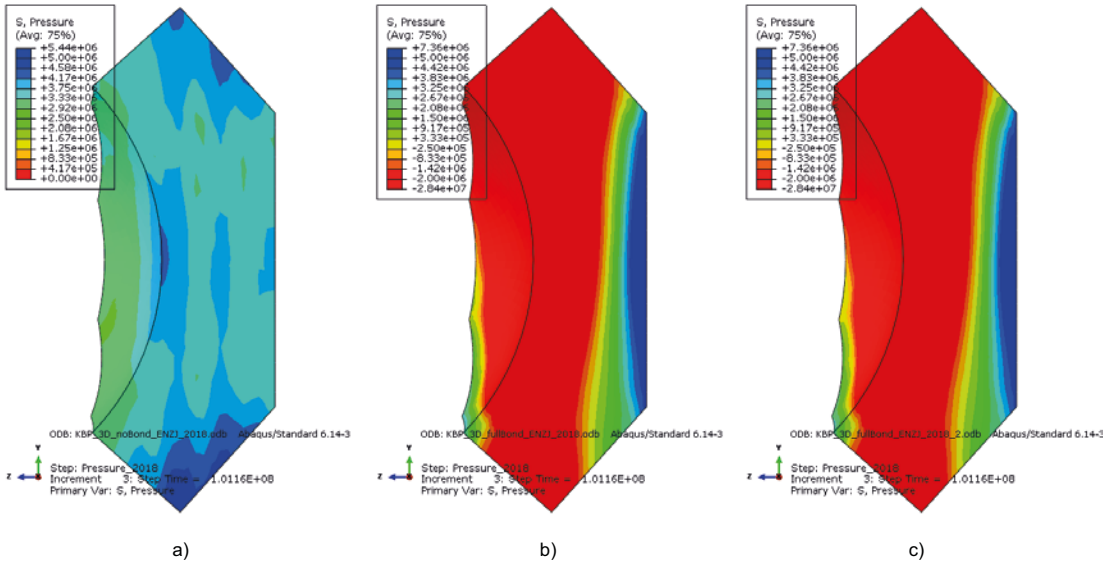

Figure 4-14. *Stress distribution during drainage, before gas leakage test, a) No bond before contact grouting, b) Initial full bond with release during the cooling before contact grouting, c) Initial full bond with release when the water pressure is applied (Malm et al. 2019), Unit: Pa.*

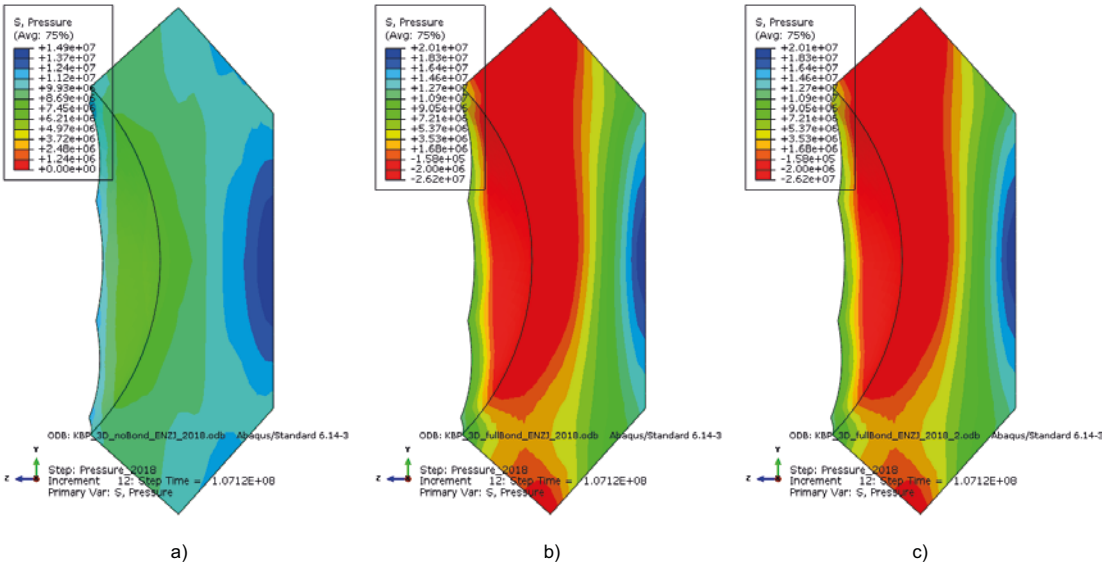

Figure 4-15. *Stress distribution at a hydrostatic pressure of 8.1 MPa, a) No bond before contact grouting, b) Initial full bond with release during cooling before contact grouting, c) Initial full bond with release when the water pressure is applied (Malm et al. 2019), Unit: Pa.*

Comparison to measurements

In Malm et al. (2019), results were extracted from the FE-models and compared to the different measurements during the gas leakage and strength tests. For the sake of comparison, all signals were normalized to conform to the measurements on June 1st.

Comparisons with strain gauge ST12 and ST21 are presented in Figure 4-16 and Figure 4-17 respectively. ST12 is placed in the centre of the concrete dome and ST21 is placed closer towards the top of the dome near the upstream surface. At the centre of the concrete dome, the measurements correlates better with the full bond-simulations during the leakage test. However, the correlation is better with the no bond-simulation during the strength test. This could indicate that cracking has occurred. Toward the upstream surface of the concrete dome, the measurements correlates better with the no bond-simulations for both the leakage and strength tests.

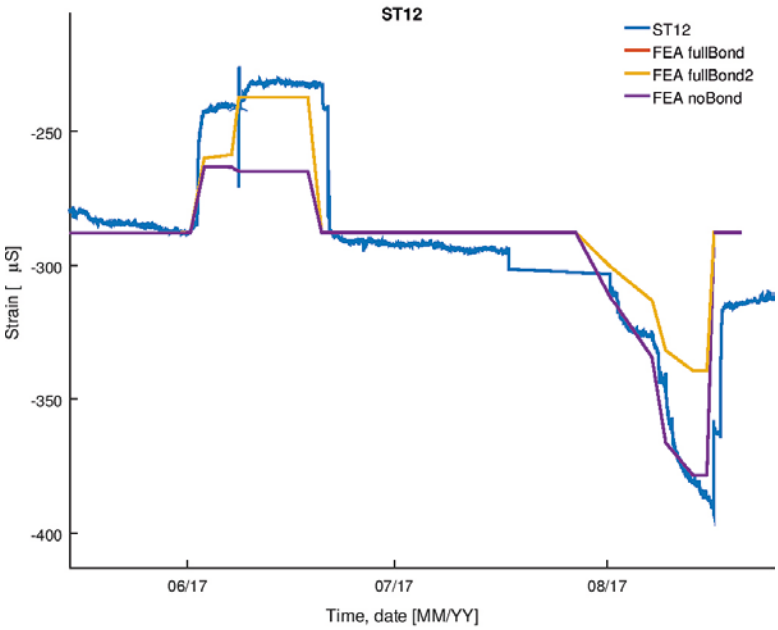

Figure 4-16. *Strain gauge ST12 compared with FE-simulations (Malm et al. 2019).*

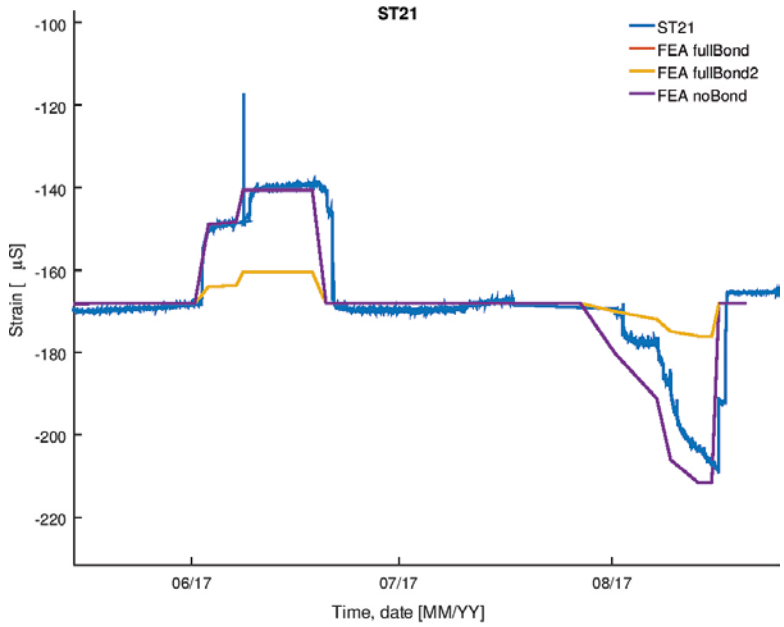

Figure 4-17. *Strain gauge ST21 compared with FE-simulations (Malm et al. 2019).*

A comparison between the simulated downstream displacements and the LVDT-meter LVDT002 is presented in Figure 4-18. The measurements correlates better with the FE-simulations with initial bond between the rock and concrete. The LVDT-sensors shows increased displacements after the leakage and strength tests, which indicates cracking. The FE-simulations were performed with a linear elastic material model and therefore, it cannot capture this nonlinear behaviour.

4.2.3 Evaluation

The measurements show that the concrete dome behaves overall elastic, during both gas tightness test and the strength test, since the strain is about the same before and after a load event. However, the global sensors such as displacements (LVDT and joint-meters) shows that some non-linear effects had occurred during these tests. The most likely reason for these is that the bond between concrete and rock had been lost in, especially the upstream side of the slot.

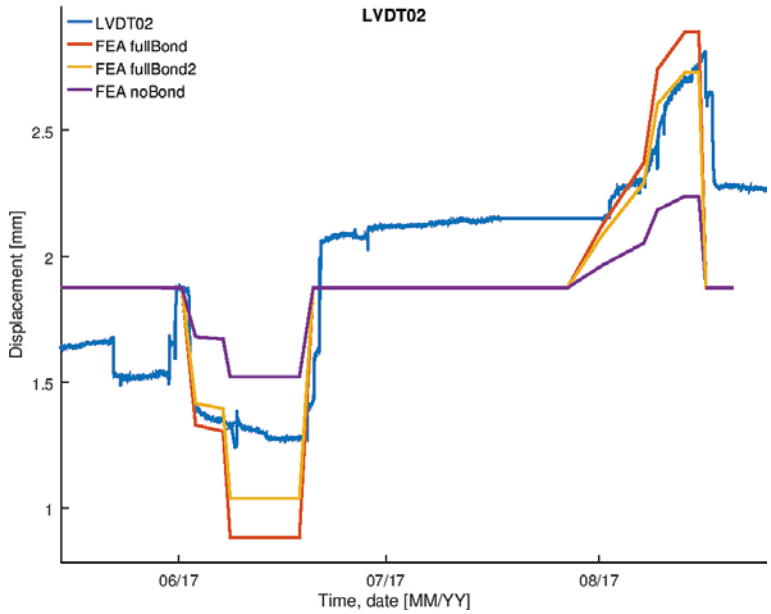

Figure 4-18. *LVTD002 compared with displacements from the FE-simulations (Malm et al. 2019).*

The FE-simulations do not incorporate nonlinear material behaviour such as cracking or the swelling pressure from the bentonite. Despite these simplifications, the FE-simulation gives good predictions of the behaviour of the concrete dome regarding all measured behaviours, e.g. temperatures, strains and deformations. The simulations showed that there would be an increased risk for loss of bond or cracking in the top part of the concrete dome during the unloading for the gas leakage test. No cracking was observed during the material tests and the demolition, but tests of bond strength in the slot showed that the strength was low or zero, which further validates the model.

4.3 Bentonite and filter

4.3.1 Monitoring results

As previously mentioned in Section 2.2.2, several sensors were installed to monitor the bentonite seal, filter and backfill. The previous results were presented by Grahm et al. (2015) and were summarized in Section 2.3. In the following section, the monitoring of the plug (except the concrete dome) will be presented for the time period during the gas leakage and strength tests that includes the pressure decrease during the gas tightness test and the pressure increase during the strength test. The monitoring of these components has included sensors measuring:

- Relative humidity
- Temperature
- Total pressure
- Pore pressure
- Displacement

In addition, the applied water pressure and inflow to the filter section have been registered together with the leakages past/through the plug.

Relative humidity

As mentioned in Section 2.3.2, the relative humidity (RH) in the bentonite seal was between 72–76 % prior to the installation. The gas leakage test started 2017-06-02 (day 1 583). Prior to the gas leakage test, i.e. after been subjected to a constant water pressure of 4 MPa for three years, almost all sensors had reached 100 % or failed. Only one RH sensor in the backfill was working at this point and recorded a relative humidity of 96 %, see Figure 4-19 and Figure 4-20.

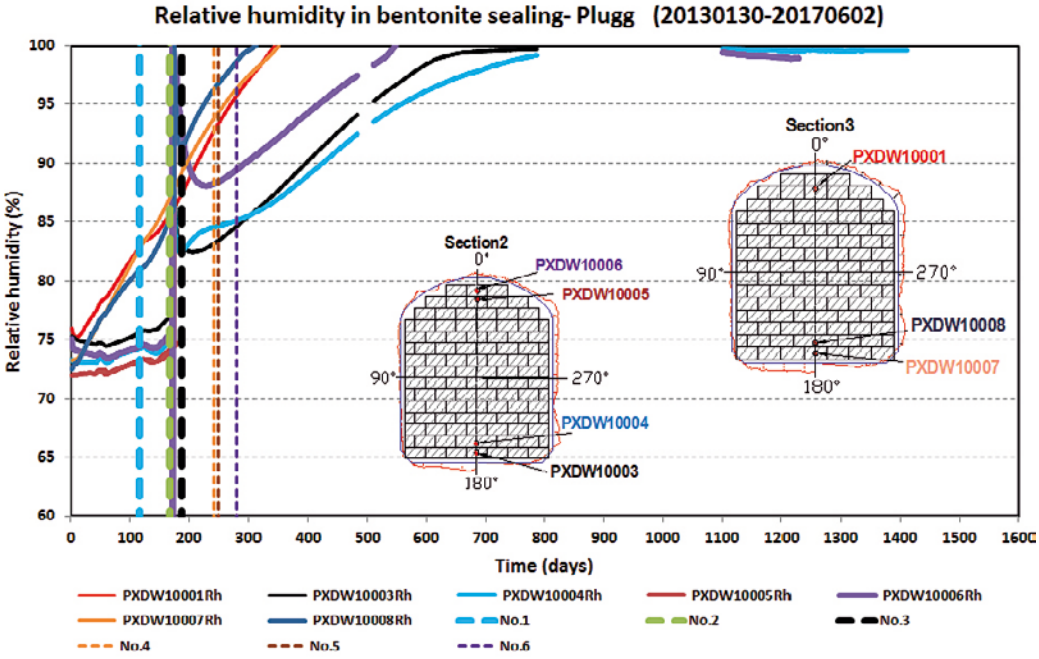

Figure 4-19. *Measured relative humidity in the bentonite seal, from Åkesson et al. (2019).*

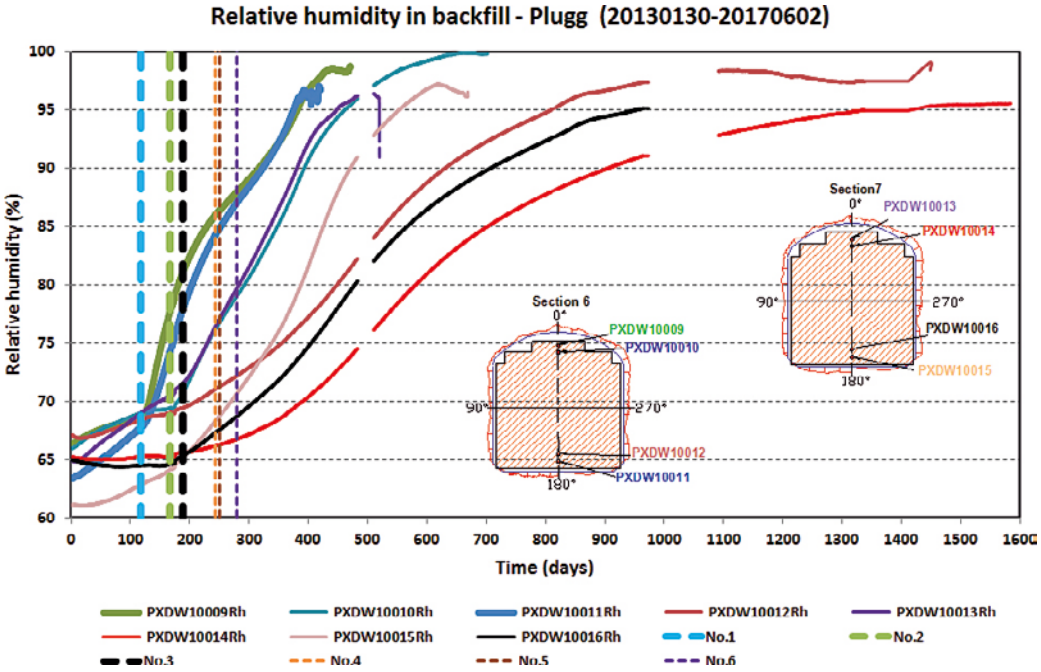

Figure 4-20. *Measured relative humidity in the backfill, from Åkesson et al. (2019).*

Temperature

As mentioned previously in Section 4.2.1, the ambient temperature in the tunnel varied between 12 and 16 °C annually. The temperature in the plug was slightly higher than this and varied typically between 14 and 16 °C. Unfortunately, all the temperature sensors had stopped recording when the gas leakage test started except one temperature sensor in the backfill that still was in operation, see Figure 4-19. As mentioned in Section 4.2.1, the temperature in the concrete dome increased slightly during the pressurization. Unfortunately, no results are available in Åkesson et al. (2019) that could show if this also occurred in the bentonite seal.

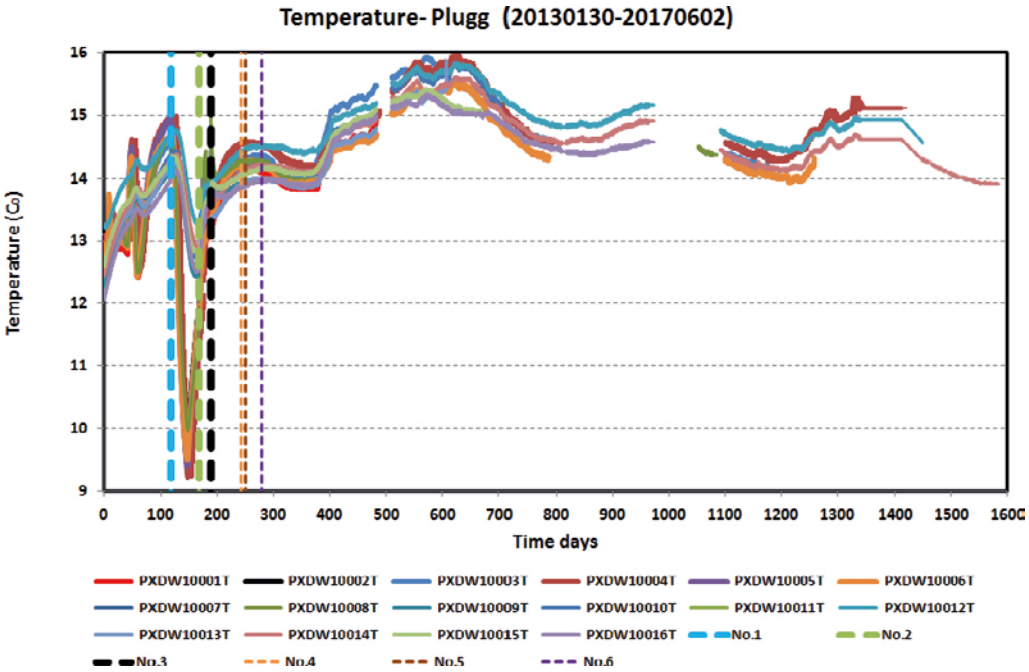

Figure 4-21. *Temperature variation in the plug, from Åkesson et al. (2019).*

Total pressure

Total pressure sensors were placed in the bentonite seal and backfill to monitor the sum of water pressure and swelling pressure. The results from these sensors are presented in Figure 4-22 and Figure 4-23, and show slight increase after the constant water pressure of 4 MPa was reached in 2013/2014. This is caused by the development of the swelling pressure in the bentonite. As can be seen in Figure 4-22, the swelling pressure in the bentonite seal varies significantly, and is between 0.2 and 1.9 MPa.

The results for the backfill are similar to the bentonite seal except for one sensor which increased up to 15 MPa in total pressure (i.e. 11 MPa in swelling pressure). The result from this sensor was judged unrealistic according to Grahm et al. (2015). However, the results have shown that the pressure recorded by this sensor has successively decreased to about 9 MPa after about two years. It can also be seen that this sensor behaves in a similar manner as the other sensors during the drainage of the filter during the gas tightness test, where it decreases with a level corresponding to the water pressure. This implies that the sensor is still working. When the filter was drained, the remaining pressure in the backfill was 5.2 MPa at this location. It is not possible to find the reason for the significant increase up to 15 MPa in total pressure in the backfill. It is however, believed to have been caused by local effects and possibly that the water pressure in the filter was transmitted over a smaller sectional area in the backfill at this location.

Pore pressure

The pore pressure sensors show the hydrostatic water pressure in the upstream side of the slot, in the bentonite seal closest to the concrete dome and in the end of the tunnel in the backfill. In addition, the pressure in the lead-through tube in the concrete dome was also monitored (PDU0002).

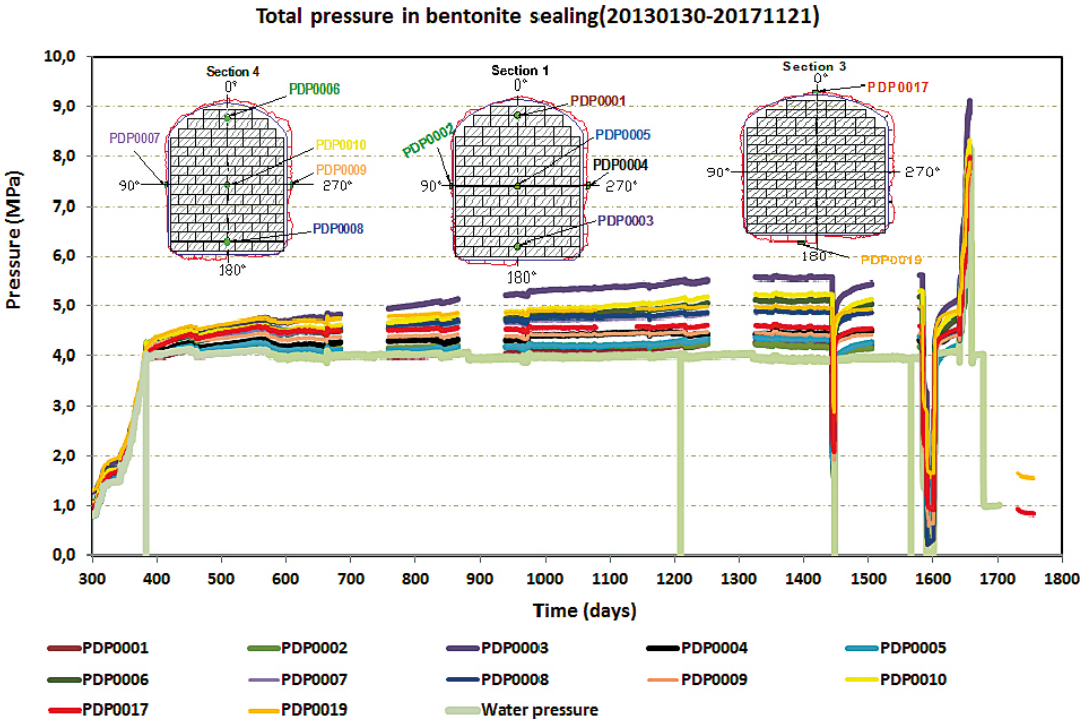

Figure 4-22. *Development of total pressure in the bentonite seal, from Åkesson et al. (2019).*

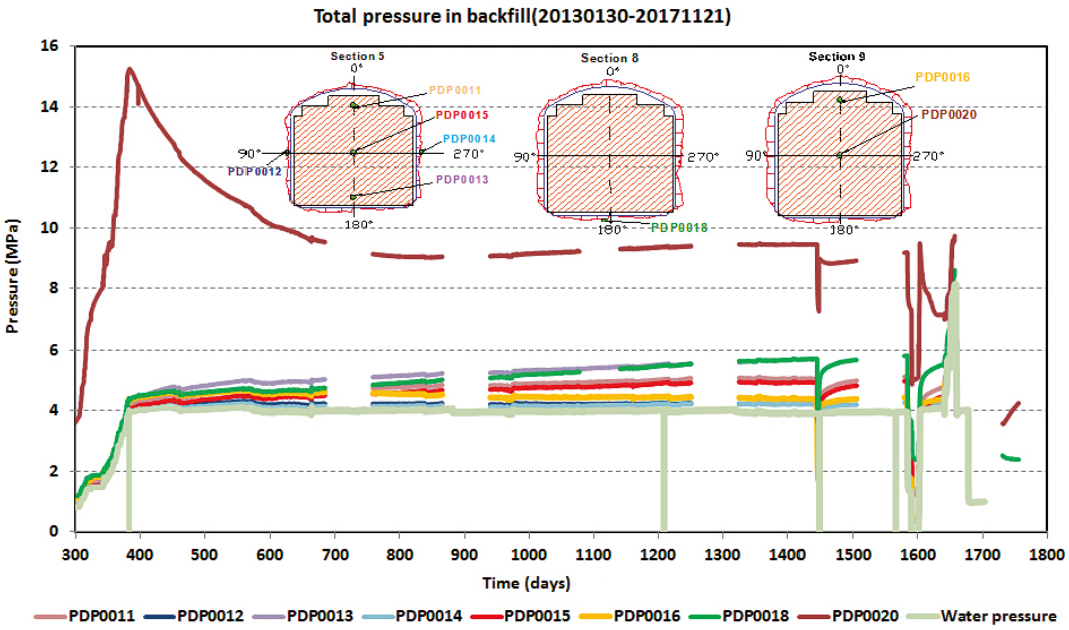

Figure 4-23. *Development of total pressure in the backfill, from Åkesson et al. (2019).*

The monitored pore pressure is presented in Figure 4-24. As can be seen in the figure, the pore pressure is close to (slightly below) the water pressure in all monitoring points except the sensor mounted in the top of the slot (PDU0001). This sensor showed increasing pressure of the same magnitude as all other sensors during the initial pressure increase to 4 MPa of water pressure in 2013/2014. This shows that the bentonite seal was not water tight initially. As the water pressure in the filter was maintained constant at 4 MPa, the pore pressure in the slot successively decreased to about 3 MPa and was constant at this level until the filter was drained during the gas tightness test. This showed that the bentonite seal started to seal and to some extent started to restrict access of water to this location. However, considering that a significant water pressure was present, this shows that the concrete dome was subjected to water pressure and that the concrete dome constituted an important part of the water tightness of the plug system.

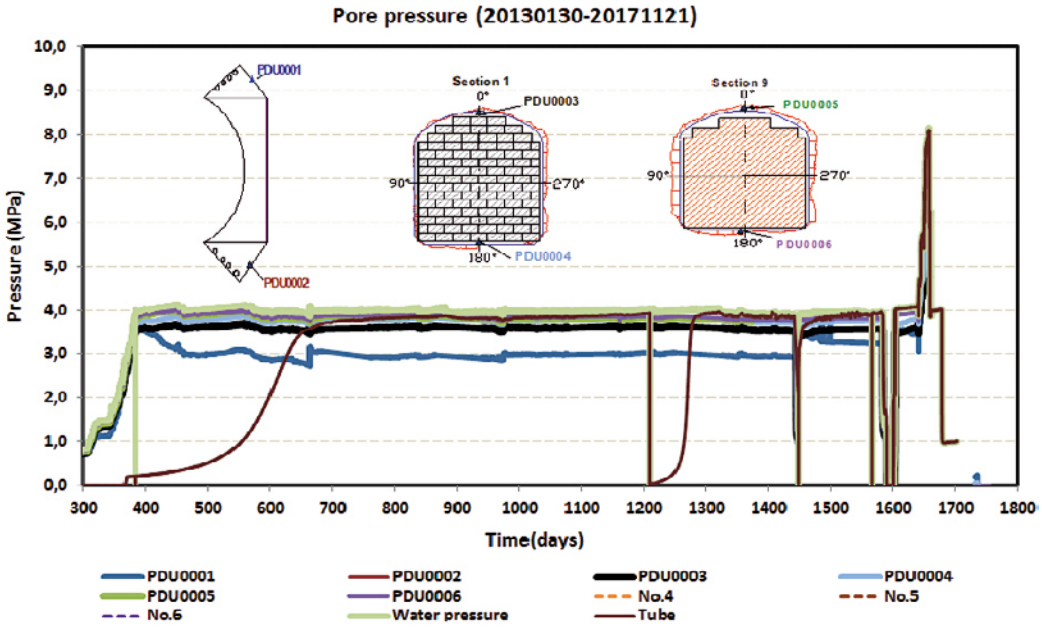

Figure 4-24. *Development of the pore pressure in the plug, from Åkesson et al. (2019).*

These results show that the bentonite seal was by-passed to a great extent in the full-scale test, where the water in the filter was transported in the rock due to fractures and micro-fractures. These conclusions are further supported by the measurements of the water content in the bentonite seal, presented in Section 8.3.1.

It seems likely that the water leakage had by-passed the bentonite seal and resulted in a pressure distribution in the rock as shown in Figure 4-25.

Displacement

Three extensometers were installed in the bentonite, filter and backfill. Unfortunately, only one of the sensors was in operation during the gas leakage and strength test (i.e. drainage during gas tightness test and pressure build up during strength test). In Figure 4-26, the measured displacement and the corresponding pressure development is shown for the displacement sensor monitoring the displacement of the LECA beams. Negative displacements mean that the LECA beams moves in the upstream direction, i.e. towards the backfill. The results show a marginal change in downstream displacement (< 0.5 mm) during the drainage of the filter. The corresponding re-pressurization up to 4 MPa, however, shows quite significant upstream displacement (> 2.5 mm). This means that non-linear effects occur within the plug. It can also be seen that increasing the pressure from 4 MPa to 8 MPa results in a displacement of about 7 mm, which shows the non-linear behaviour even more clearly. The nonlinear displacements are believed to be caused by compaction of the filter due to swelling of the bentonite seal and backfill.

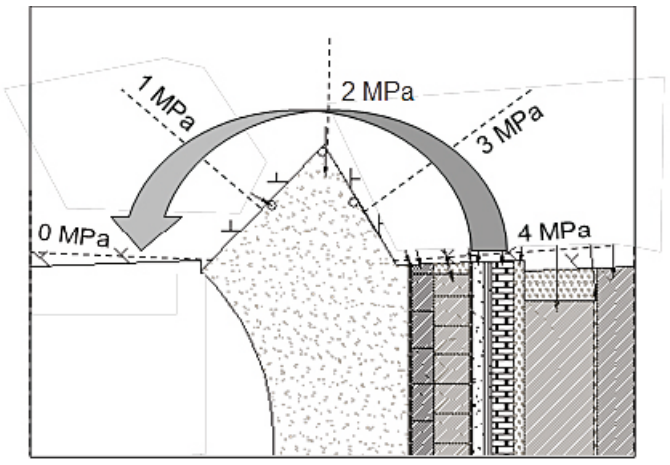

Figure 4-25. *Illustration of assumed distribution of pore pressure in the rock.*

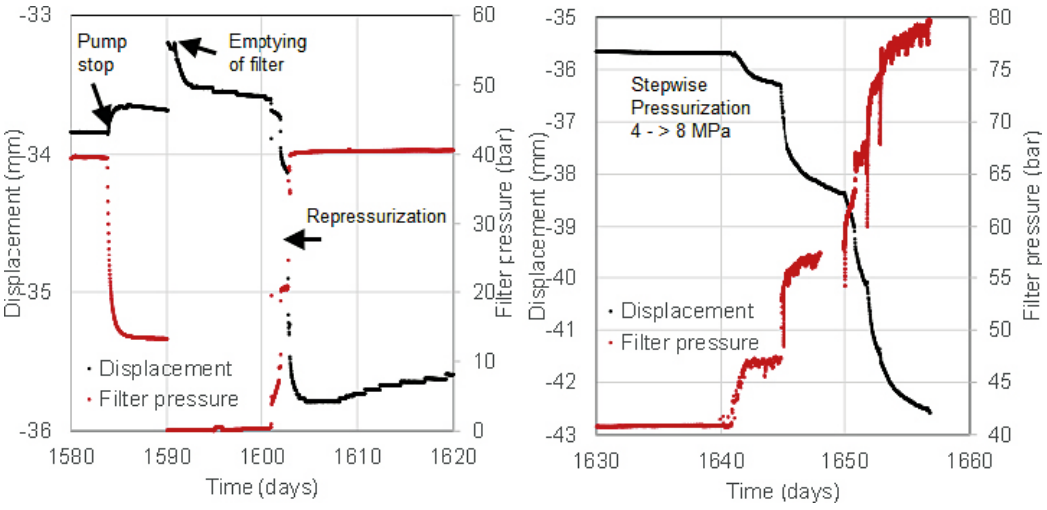

Figure 4-26. *Displacement and filter pressure evolution during drainage (gas tightness test) and strength test, from Åkesson et al. (2019).*

4.3.2 Numerical results

Numerical finite element analyses have been performed by Åkesson et al. (2019) to analyse the behaviour of the plug with focus of the bentonite seal and backfill. In these analyses, an axisymmetric model has been developed that considers the hydro-mechanical effects in order to calculate the saturation of bentonite, swelling pressure and displacements within the plug. The developed numerical model is illustrated in Figure 4-27. The model contains the following material layers:

- Bentonite seal blocks
- Macadam filter
- LECA beams
- Backfill blocks

In addition, the pellet filled slots were also considered in the model. The model does not consider the concrete beams or the concrete dome, instead the downstream surface of the bentonite seal is assumed to be restrained from movement. The same assumption is done in the end of the tunnel where the backfill does not experience deformation.

Numerical analyses have only been performed for the initial saturation up to 4 MPa which in was maintained constant until the time of demolition in hydraulic models. However, in models that combine the hydraulic and mechanical behaviour, i.e. also calculates the deformations, it was only possible to increase the pressure up to atmospheric pressure. No specific results have been obtained for the gas tightness test and the strength test in any of the models. Only, a short description of the results from the numerical modelling are presented in this report, but further information can be found in Åkesson et al. (2019) and Grahm et al. (2015).

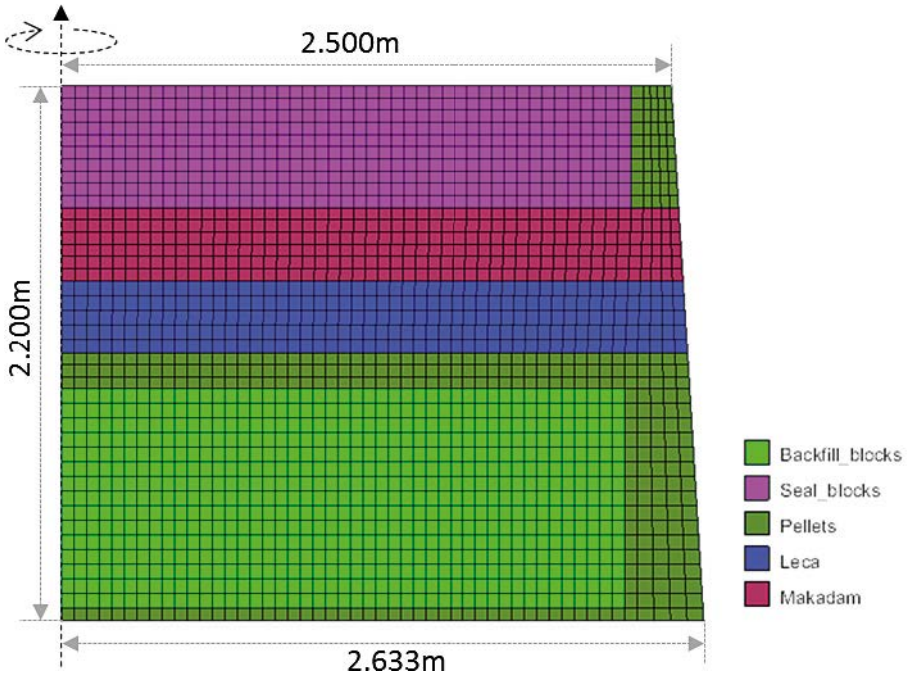

Figure 4-27. *Geometry, material assignment and mesh used in the numerical model to predict the hydro-mechanical behaviour of the plug.*

Due to the restraints in the numerical framework with convergence problems, two hydraulic models (i.e. without mechanical behaviour such as stress, strain and deformation) were performed that considered the pressure increase of the water pressure up to 4 MPa. In these two models, one was performed with all material considered in their initial state and the other started where all material were considered to be in a fully homogenised state. In Figure 4-28 a comparison between the two models and the measured results are presented. There degree of saturation in the seal blocks is rather similar in the two models. In Figure 4-29 a similar comparison is shown for the backfill section. In the backfill, larger difference between the models where the model based on an assumption where homogenised properties shows lower relative humidity. This is also illustrated in Figure 4-30 where a comparison of the degree of saturation between these two models at the time of dismantling is shown.

Åkesson et al. (2019) summarized that the hydraulic numerical models were fairly good at predicting how far the hydration and the homogenization of the bentonite seal and the backfill had developed until the time of demolition.

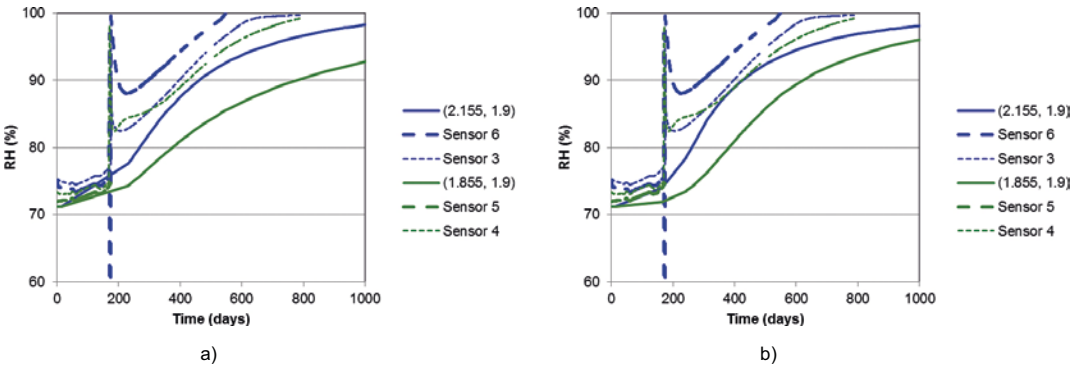

Figure 4-28. *Comparison of evolution of relative humidity in the centre of the bentonite seal from hydraulic analyses (solid lines) and measured (dashed lines, a) Model based on initial state, b) Model based on fully homogenised state. From Åkesson et al. (2019).*

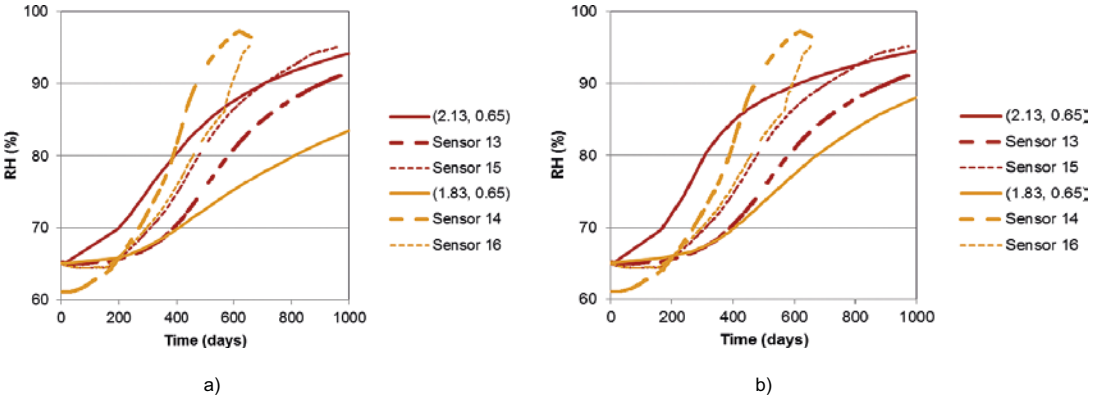

Figure 4-29. *Comparison of evolution of relative humidity in the of the backfill section (350 mm from the LECA beams) from hydraulic analyses (solid lines) and measured (dashed lines, a) Model based on initial state, b) Model based on fully homogenised state. From Åkesson et al. (2019).*

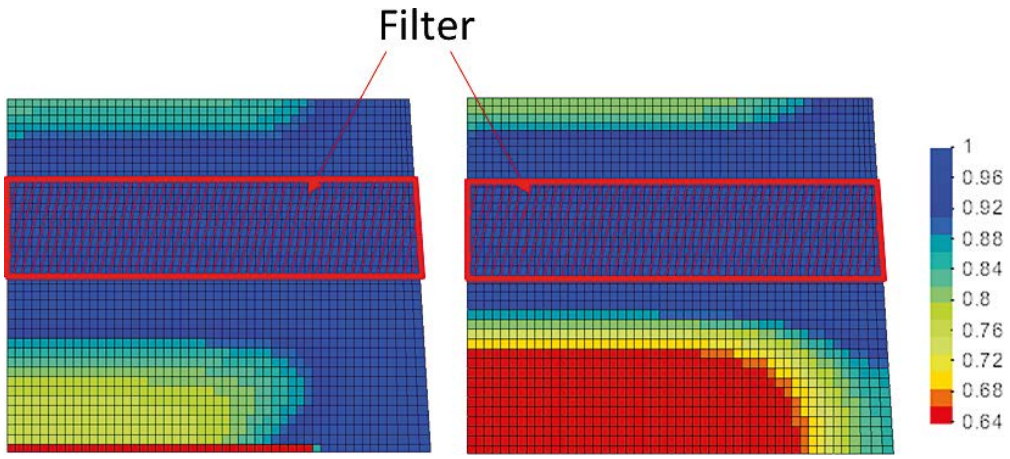

Figure 4-30. *Obtained degree of saturation at the time of dismantling according to the two hydraulic models with different assumption on the initial properties of the material state; materials are assumed in initial state (left) and in a fully homogenised state (right). From Åkesson et al. (2019).*

As mentioned previously, only the initial increase in pressure up to atmospheric pressure (0.1 MPa) was simulated in the hydro-mechanical model. A comparison for the calculated and measured swelling pressure is shown in Figure 4-31. According to Åkesson et al. (2019), the hydro-mechanical model showed fairly good ability to predict the overall evolution of the relative humidity, swelling pressures and displacements during simulation of pressure increase up to atmospheric pressure. The main reason why the numerical models gave lower rate of homogenization is due to the fact that the simulations were performed with lower water pressure. Åkesson et al. (2019) also states that the extent of the homogenization was in fairly good agreement with the experimental data. The low values of dry densities found in the experiments could not be captured in the numerical modelling.

4.3.3 Evaluation

The performed measurements have shown that both the bentonite seal and backfill started to take up water almost directly after installation. The saturation of the bentonite increased successively starting from the period with only natural inflow but increased more rapidly during the pressurization of the filter. After about two years with constant water pressure, all sensors in the bentonite seal showed 100 % relative humidity or had failed. In the backfill, all sensors showed above 95 % in relative humidity after two years. Overall, the measurements showed that the bentonite had saturated to a great extent after two years. The corresponding swelling pressure in both bentonite seal and backfill have been typically between 0.2 to 1.9 MPa. The highest obtained value from the measurements is close to the expected values from the simulation, but the low swelling pressure obtained at the other sensors are lower than expected, according to Åkesson et al. (2019).

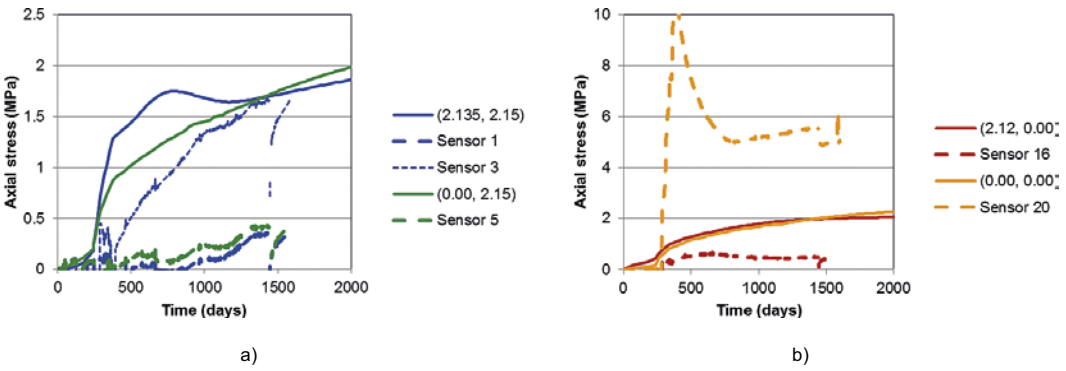

Figure 4-31. *Comparison of evolution of swelling pressure (axial stress) between hydro-mechanical analyses (solid lines) and measured (dashed lines, a) Bentonite seal (section closest to the concrete beams), b) Backfill (section closest to the concrete back wall). From Åkesson et al. (2019).*

4.4 Water inflow and leakage

The development of required water inflow and the leakage from the plug has been measured for about 4 years as seen in Figure 4-32 and Figure 4-33. After the water pressure of 4 MPa was reached, both the required net inflow of water and the leakage has successively decreased. About 200 days after the pressure had been reached, the required inflow of water to maintain the 4 MPa water pressure was about 20–25 litres per hour. The leakage from the plug have been divided into four separate sources:

- Leakage from a rock fracture in the main tunnel, perpendicular to the experiment tunnel.
- Leakage from the cable lead-through from sensors embedded in the concrete dome.
- Leakage through the plug and the rock about 1 m downstream from the plug which is collected in the weir.
- Leakage to the surrounding rock mass, which cannot be measured.

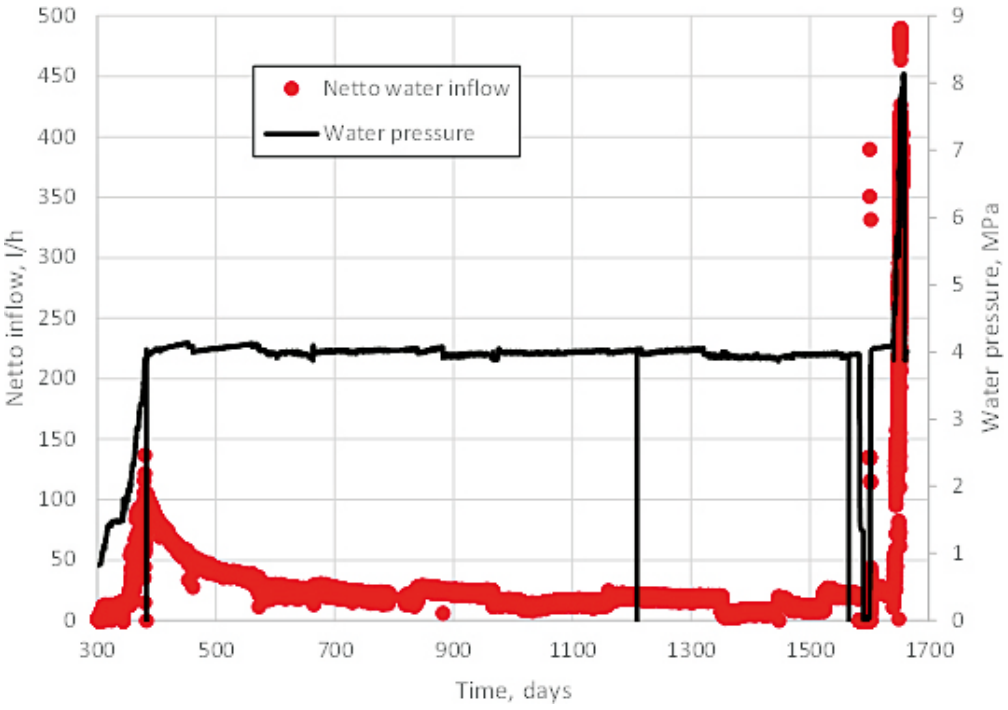

Figure 4-32. *Net water inflow to the filter section and water pressure plotted versus time (Åkesson et al. 2019).*

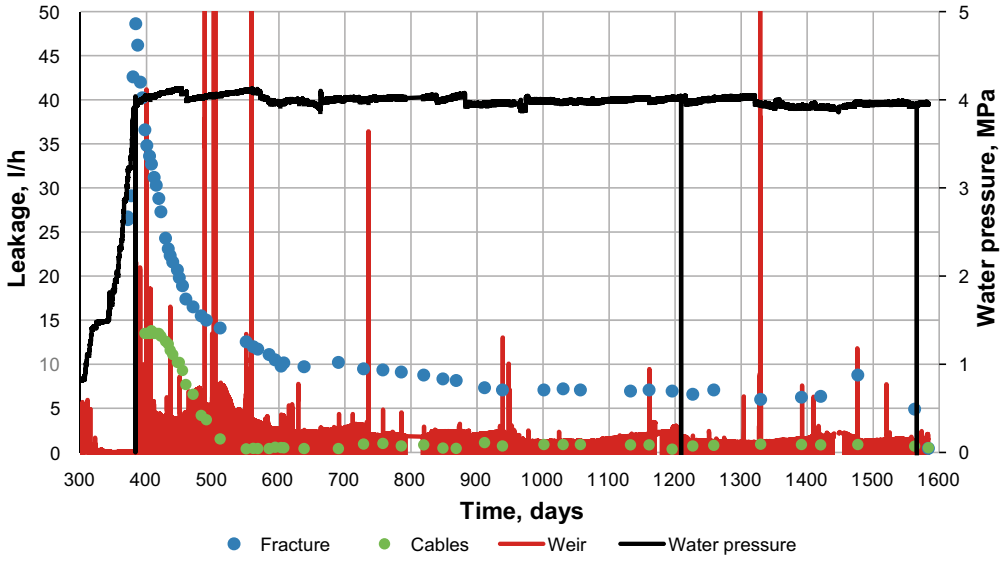

Figure 4-33. *Determined leakages and water pressure plotted versus time, from Åkesson et al. (2019).*

As mentioned in Grahm et al. (2015), the first two sources are experimentally related escapes of water and therefore separated from the leakage through the plug. During the initial pressurization to 4 MPa, a fracture mapped as small and dry before the test started to have significant leakage when the pressure increased up to 3.1 MPa. The water escape from this rock fracture is located about 14 m from the plug. The other source of experimentally related leakage is from the cable bundle of embedded sensors in the concrete. These sensors were not designed to be subjected to significant water pressures, since it was believed that there should be no direct water pressure in these regions. The leakage through the surrounding rock mass is considerable but can also be regarded as a part of the experiment setup.

The results are also presented as zoomed in for the time-period corresponding to the gas leakage and strength test with drainage during the gas tightness test and pressure increase to 8.1 MPa during the strength test, as seen in Figure 4-34 and Figure 4-35.

The inflow of water had to be increased significantly to be able to increase the pressure up to 8.1 MPa during the strength test. Prior to the pressure increase, an inflow of 20 to 25 l/h was required while an inflow of more than 400 l/h was needed to keep the water pressure at 8.1 MPa, as seen in Figure 4-34.

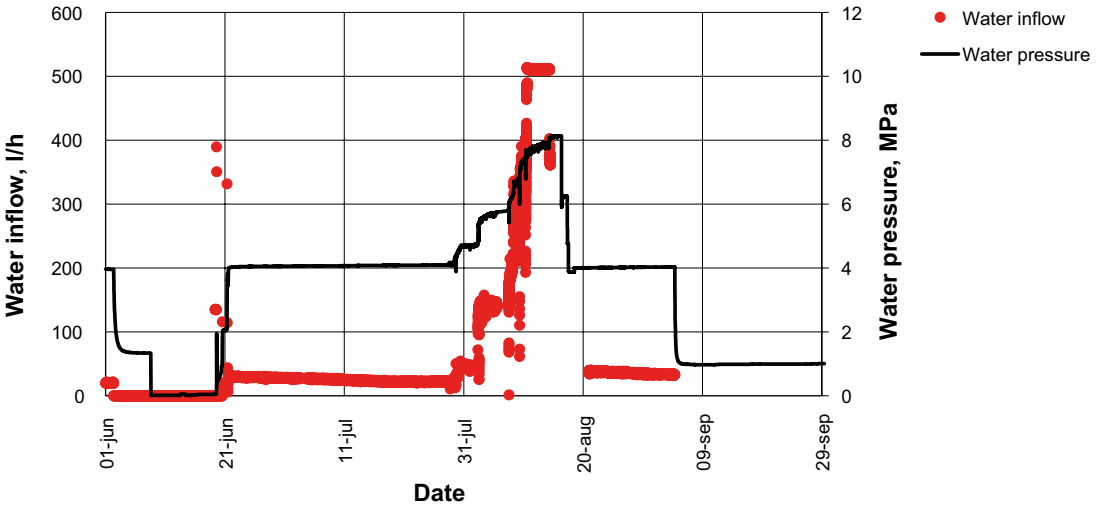

Figure 4-34. *Applied water pressure and water inflow to filter plotted versus time, from Åkesson et al. (2019).*

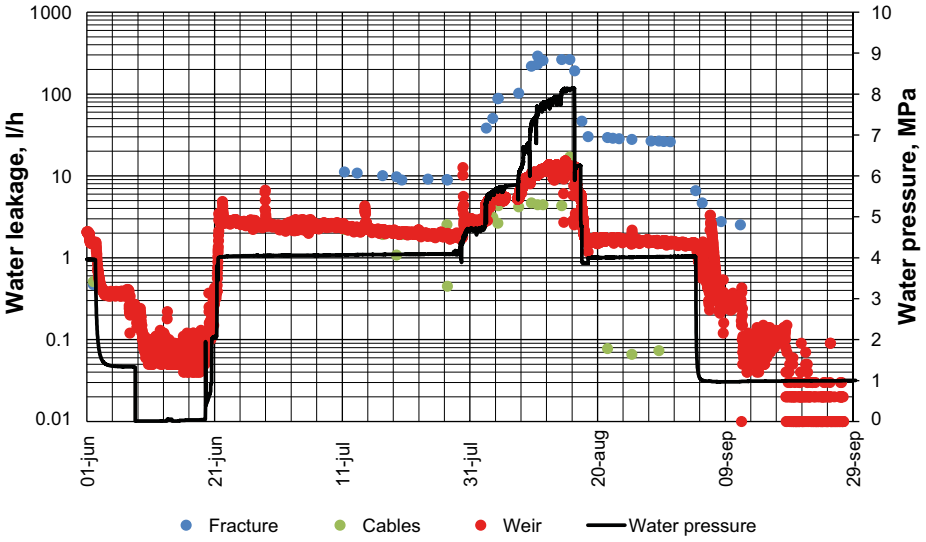

Figure 4-35. *Applied water pressure and measured leakages from weir, rock fracture and from cables plotted versus time (Åkesson et al. 2019).*

The measurements showed that all observed leakages decreased to zero during the gas tightness test. The measured leakage through the plug and the cables increased to the same level as before the test only a few weeks after the pressure had been increased up to 4 MPa again.

During the strength test significant increase in leakage was observed. The leakage in the rock fracture reached about 257 l/h (compared to 7–8 l/h before the test). The leakage though the cables increased to 15 l/h compared to 1 l/h when the pressure was 4 MPa. The leakage collected in the weir increased to about 13 l/h compared to 1–2 l/h prior to the pressure increase.

4.4.1 Evaluation

The measurements showed high pore pressure on the upstream side of the slot that acts as an abutment for the concrete dome. This means that the water likely bypassed the bentonite seal to a large extent. The water was likely transmitted through fractures in the rock. Even though the weir was built close to the downstream surface of the concrete dome, some leakage going through the rock will be collected. In addition, some of the leakage can also short-circuit the bentonite seal if water bearing fractures are located in the filter section, and connected with the section of the concrete dome. This shows that the surrounding rock has significant influence of the water tightness of the plug and that water bearing fractures at the plug location can result in that the bentonite seal is by-passed.

During the strength test, leakages increased significantly as expected. It was especially the fracture in the rock that surfaced the adjacent main tunnel that showed extremely large leakages. The leakage measurements also showed that the leakage came back to about the same level before and after the gas tightness test and the strength test.

4.5 Comparisons with requirements

The main relevant requirements of the plug are related to leakage. When the concrete dome was built, no specific leakage requirement was defined, see Grahm et al. (2015). Therefore, the aim was to test how leak tight the developed plug design was. The long-term test of the plug showed that the leakage collected in the weir was about 1–2 l/h (17–33 ml/min) with a water pressure of 4 MPa prior to the gas tightness test. The evaluation presented in this report has shown that the water in the filter by-passed the bentonite seal and was transmitted in the rock adjacent to the plug and thereafter collected in the weir. This shows the importance of having a rock that is free of fractures at the plug location that could transport water.

The rock quality at Äspö, and at the test-site was highly fractured as shown in the mapping of the cracks after dismantling. This became apparent, when some fractures opened due to the water pressure and created a conductive channel, which contributed to a large part of the total water transport during the test. In Figure 4-36, the mapping of fractures after the test are illustrated with the following colours to indicate their status:

- Blue fractures – open fractures that transmit water.
- Red fractures – open fractures that does not transmit water.
- Green fractures – fracture that has self-healed.

The full-scale test had a requirement that the test site should not contain any water bearing fractures. However, before the concrete plug was built, water bearing fractures was observed in the slot abutment, Grahm et al. (2015). The risk of increased leakage through the rock was thus recognized before the full-scale test started.

The test results show that a leakage of 1–2 l/h should be considered as an upper limit of the expected leakage of a plug. It can be considered the upper limit because the rock at plug location in the Äspö is more fractured than the expected conditions in Forsmark. The plug was also artificially pressurized with a higher water pressure than the natural hydraulic head of the ground water.

Finally, the test results showed that the even though the leakage increased significantly during the strength test, the leakage came down to the same level when the test was done. Thereby, no irreversible damages that had an effect on the leakage seems to have occurred in the plug or the adjacent rock.

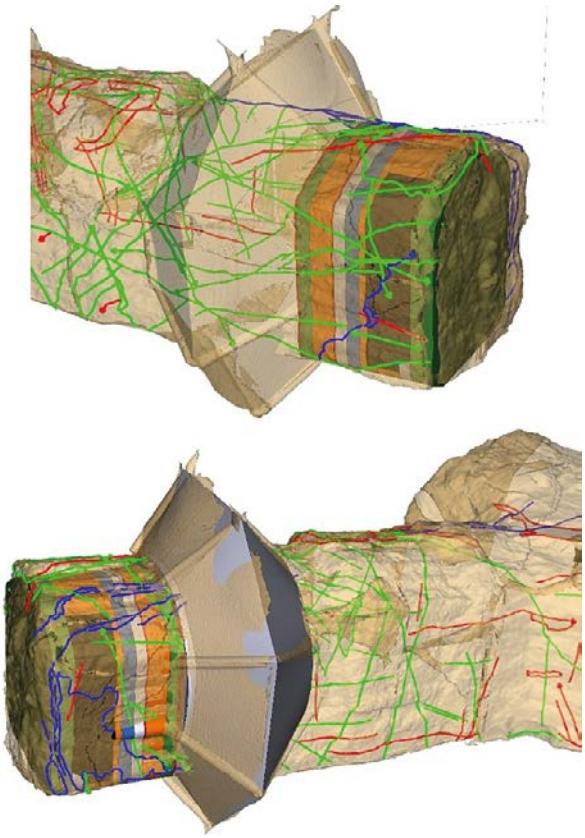

Figure 4-36. *Illustrations of rock fractures at the plug location.*

5 Non-destructive testing of the concrete dome plug

After the unloading of the plug, before the demolition was commenced, a series om non-destructive tests (NDT) were performed on the concrete dome. The aim of the NDT was to look for manufacturing defects in the concrete dome, such as cavities, honeycombing and material segregation that may occur during casting. The tests were also performed to evaluate the suitability of the studied methods for usage in the final repository. The implementation of the NDT was reported on by Kristensen (2018). A discussion of the used methods and their suitability for the concrete dome was further presented in Malm et al. (2019).

5.1 Methods

Four categories of NDT methods were used:

- Ultra-sonic pulse-echo concrete tomography, MIRA
- Ground Penetrating Radar, GPR
- Impact Echo, IE
- Impulse Response, IR

The NDT-methods will be presented briefly below.

5.1.1 Ultra-sonic pulse-echo concrete tomography, MIRA

Ultra-sonic pulse-echo concrete tomography works by introducing shear and pressure waves in the medium and interprets the echo with a software. The concrete dome was scanned with the instrument A1040 MIRA, which operates with shear waves within a nominal centre frequency of 20 kHz to 85 kHz. The pulse is composed of waves with different frequencies. The centre frequency is the main wave, which has the highest amplitude. For instance, a pulse with the centre frequency of 50 kHz may be composed of waves with frequencies ranging from a few kHz up to 100 kHz. At a given amplitude, waves with a lower frequency penetrate deeper than waves with higher frequencies, but the resolution of the instrument decreases with decreasing frequency (Germann Instruments 2018).

The A1040 MIRA has 48 individual transducers organized into a 4×12 matrix. All transducers are capable to transmit and receive signals and are spring loaded to conform to irregular surfaces. The transducers do not need any coupling medium and can be operated in dry conditions, Kristensen (2018). The surface of a structure can be scanned along a grid pattern to capture the entire geometry and the software automatically constructs a 3D-model. In this case, a 0.5×0.5 m grid was used.

5.1.2 Ground Penetrating Radar, GPR

Ground Penetrating Radar (GPR) applies similar principles as MIRA. The major differences between MIRA and GPR are that GPR uses a high frequency radio signal (electro-magnetic waves) and that the GPR antenna do not need to be in contact with the surface of the object. The antenna unit includes both transmitting and receiving devices. When the radio waves penetrate a material, they continue to travel inside the material until they meet areas, surfaces or details with dielectric constants differing from the mass material. The greater the difference between the dielectric constants the greater the reflection of the waves.

GPR is good for detecting reinforcement and transitions to other materials in concrete. However, it is hard to detect cracks, delamination and honeycombing unless these are waterfilled because of the low difference in dielectric constants between air and concrete. If the back of the structure is in contact with water or a material with a different dielectric constant, the thickness of the concrete structure can be detected by GPR.

Using a GPR with a higher frequency gives a higher resolution, however the range decreases with increased frequency. In practice, different frequencies are used when analysing a structure to improve the results. In this project, antennas with frequencies of 400 MHz, 900 MHz and 1 600 MHz was used. Like with the MIRA, the surface of a structure is scanned along horizontal and vertical lines and the individual scans are combined into a 3D image.

5.1.3 Impact Echo

Like MIRA, Impact Echo utilises the echo from stress waves to determine the state of a structure. An elastic impact, usually produced with a handheld hammer, produces a mechanical pulse. The stress waves from the mechanical pulse reflects of cracks and imperfections in the concrete and the echo is recorded by a transducer.

The range of the impact echo depends on the size and diameter of the instrument used to introduce the elastic impact. In this project, a hammer with a weight of 1 kg and a diameter of 50 mm, which gave a theoretical scan depth of 430 mm at a frequency of 4.7 kHz. The test was performed in a 0.5 m grid over the downstream surface of the concrete dome and was presented as a contour plot of the dominant frequencies.

5.1.4 Impulse Response

Impulse Response is carried out in the same manner as the Impact Echo, but the force of the impact is recorded and the displacement at the surface is recorded by a velocity transducer (geophone). The from the recorded force and velocity, the mobility is calculated. The mobility is the ratio of the velocity at the surface to the applied force. The mobility is plotted against the frequency and the average mobility is calculated according to Figure 5-1. The IR was performed at a 0.5 m grid over the downstream surface of the concrete dome and the average mobility was presented in a contour plot.

According to Kristensen (2018), no conclusions can be drawn from the IR alone. Along with other measurements it can, however, be used to cover large surfaces cheaply in a brief period of time to locate damaged areas of a structure.

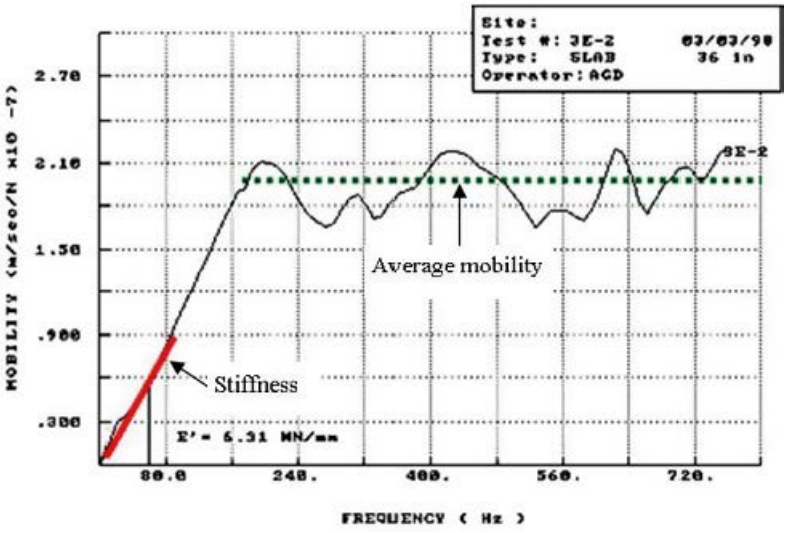

Figure 5-1. *Example of mobility plot from an IR test, from Kristensen (2018).*

5.2 Results

All results from the scans were presented in Kristensen (2018). They were further discussed and interpreted in Malm et al. (2019).

5.2.1 Ultra-sonic pulse-echo concrete tomography, MIRA

In Figure 5-2, a plot from the MIRA-scan is presented. The red line in the figure shows the transition between the concrete dome and the material behind; the dotted line shows the cooling pipes. The scan did not reveal any imperfections in the concrete.

The waves did penetrate far enough to cover the entire thickness of the concrete dome. However, it was not possible to scan the entire concrete dome because of the dome shape and the design of the scanning equipment. The main body of the concrete dome was covered by the scan, but the entire abutments could not be scanned.

5.2.2 Ground Penetrating Radar, GPR

Figure 5-3 depicts the three scans with the 400 MHz, 900 MHz and 1 600 MHz antennas. As expected, the 400 MHz antenna was able to scan through the entire thickness and detected details behind the concrete structure. The 900 MHz scan was also able to penetrate through the thickness of the concrete dome, while the 1 600 MHz scan penetrated about 1 m into the concrete. However, the resolution of the scans increased with the frequency. The 400 MHz scan gave a quite course resolution while the 900 MHz and 1 600 MHz scans were finer.

Both the 400 MHz an 900 MHz scans were able to detect the geotextile at the upstream face of the concrete dome, located at a dept of 180–220 cm. The 400 MHz was also able to detect the second geotextile at a dept of 250–300 cm. All the scans located the cooling pipes, but no imperfections were detected in the concrete.

The scans were hard to perform because of the geometry of the plug, and the heavy equipment. In addition, the software used for interpreting the data was not able to interpret a curved surface. The resulting geometrical models were therefore somewhat deformed e.g. the straight cooling pipes were curved.

5.2.3 Impact Echo

It was not possible to use an automated Impact Echo-scanner, the test was therefore performed with a hand-held sledgehammer. No imperfections were found in the concrete. However, Kristensen (2018) notes that the defects must be quite large to be discernible with the IE. It was also hard to get a clear reflection from the backside of the concrete dome. Malm et al. (2019) concluded that the tests did not prove the applicability of the IE-method on structures such as the concrete dome.

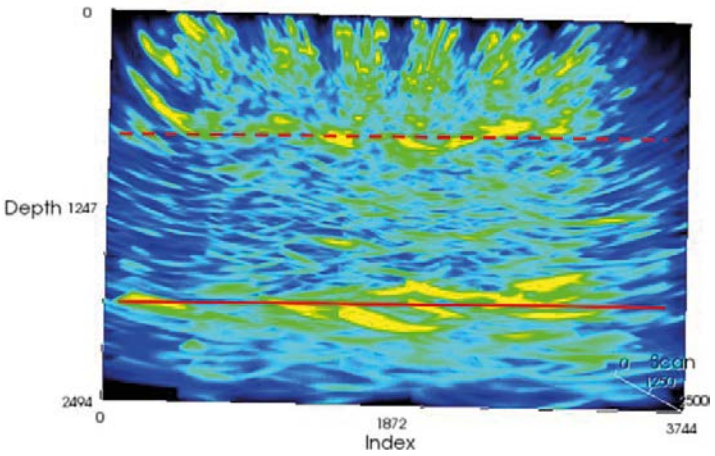

Figure 5-2. *Results from the MIRA-scan. The red line shows the transition between the concrete dome and the materials behind, the dotted line shows the cooling pipes (Kristensen 2018).*

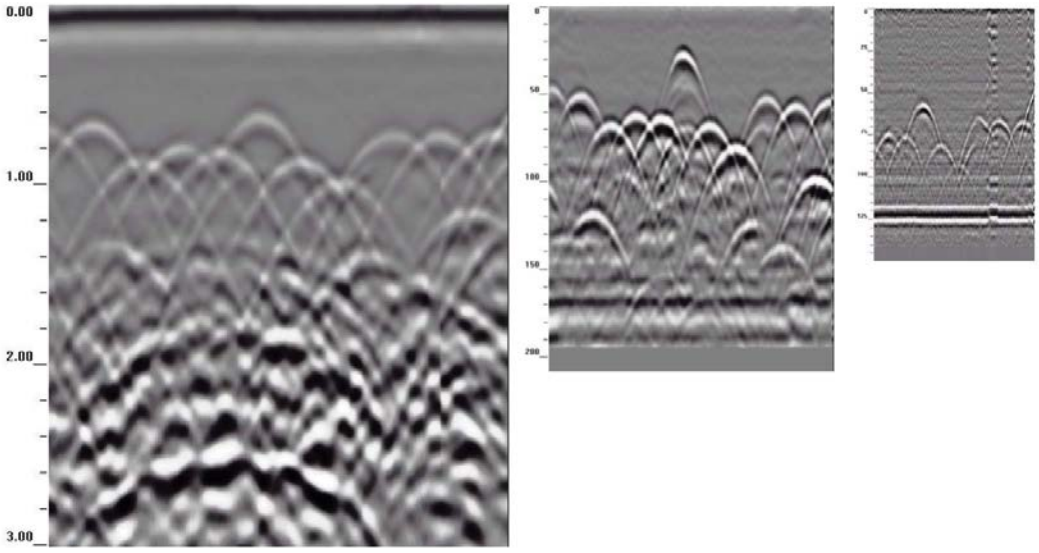

Figure 5-3. *Results from the GPR-scans with different frequencies a) 400 MHz b) 900 MHz and c) 1 600 MHz (Kristensen 2018).*

5.2.4 Impulse Response

The IR-test gave good results for all studied parameters and did not reveal any diverging areas of the concrete dome. The data was hard to interpret, since no reference structures were available for comparison. The available literature suggests that any damage would have to be quite large to impact the mobility of a thick concrete structure, especially if the imperfection is located deep into the cross section. Malm et al. (2019) concluded that the tests did not prove the applicability of the IR-method on structures such as the concrete dome.

5.2.5 Large void in the top of the concrete dome

The NDT was performed when the plug was depressurized but before the core drilling commenced. During the core drilling, a large waterfilled void was found in the top of the concrete dome. This is further presented in Section 7.2, but the implications for the non-destructive testing will be discussed in this section.

The aim of the NDT was to detect manufacturing defects in the concrete dome. Therefore, the contractor did not target the abutments of the structure or the affected area. According to Malm et al. (2019), the contractor claimed that the void would be impossible to detect even if it was targeted. The void was located deep into the plug. When NDT is used at depths of more than 2 meters, the resolution is very coarse. The results from this depth could at best indicate that an anomality exists in an area. If the cavity was detected, only the front surface would be seen in the scan. The dept or the shape of the cavity could not be scanned, since the waves reflects and does not travel through the void. In addition, the location of the void is problematic since it borders to the edge of the concrete dome. Since the inspection waves spreads out in a slightly circular pattern, they will reflect of the abutments. This creates interference, which is common while scanning close to the edge of a slab. This is illustrated in Figure 5-4, where the top of the dome is illustrated with the void in the top and the gap on the upstream surface of the slot abutment. The wave from the NDT scan is illustrated with the red line. If the scan is performed on a case where a void exists in the top, then the wave will be reflected at the intersection between concrete and air (solid line) compared to a case without the void where it is reflected at the interface between concrete and rock (dotted line). The difference in length between the solid and the dotted line is quite small and considering the uncertainties when scanning at such great depths, this type of defect will likely not be easy to detect.

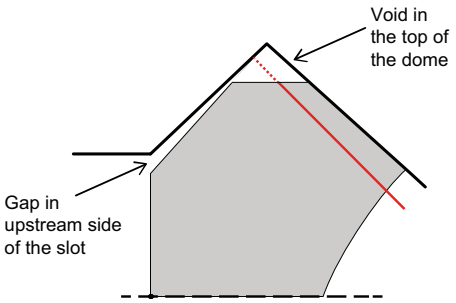

Figure 5-4. *Illustration of the top of the dome, with the void in the top and a gap on the upstream surface of the slot. The wave from the NDT scan is illustrated with a red line.*

5.3 Evaluation

In this report, the possibilities and limitation of several different NDT-methods have been evaluated to find possible defects in the concrete dome. The conclusions from these tests was that none of the methods could detect any defect in the dome. With that said, the only defect that was detected during demolition was the void in the top and none of the NDT-methods targeted this region. As previously discussed it could be difficult to find this void even if the NDT-methods target this region due to the geometry of the slot.

However, if NDT-tests are used in the final repository, the test program should aim to detect defects and damages which can occur during the manufacturing of the plug. Continuous monitoring could also be performed at a certain time interval, where the plugs are controlled for continuous damage or deterioration.

Malm et al. (2019) summarizes the following series of parts which a NDT-program should contain as shown in Figure 5-5:

A. Characterization of the gap between the concrete dome and the rock. The aim should be
- *to detect areas with poor contact between the concrete dome and the rock,*
- *to detect areas with insufficiently filled gaps and*
- *distinguish between water-filled (leaking parts) and dry parts of the gap.*

B. Calculations indicate that a crack plane occurs at relatively high pressures inside the dome. The approximate location of the crack is shown in Figure 5-5. In cases where the bearing capacity and tightness of the dome is tested, the existence of such a crack should be verified by NDT.

C. At the abutment surface, the concrete dome presses against the rock. The pressure can cause stresses and cracks in the both concrete dome and the rock. The cracks may be formed both parallel and perpendicular to the transition zone between the concrete dome and the rock. In cases where the concrete dome's bearing capacity and tightness is tested, the existence of the cracks should be verified by NDT.

D. Manufacturing defects such as cavities, honeycombing and material segregation that may occur during production. The existence of the manufacturing defects should be verified by NDT.

E. Location of cooling pipes and the quality of the concrete around the pipes should be determined by means of NDT.

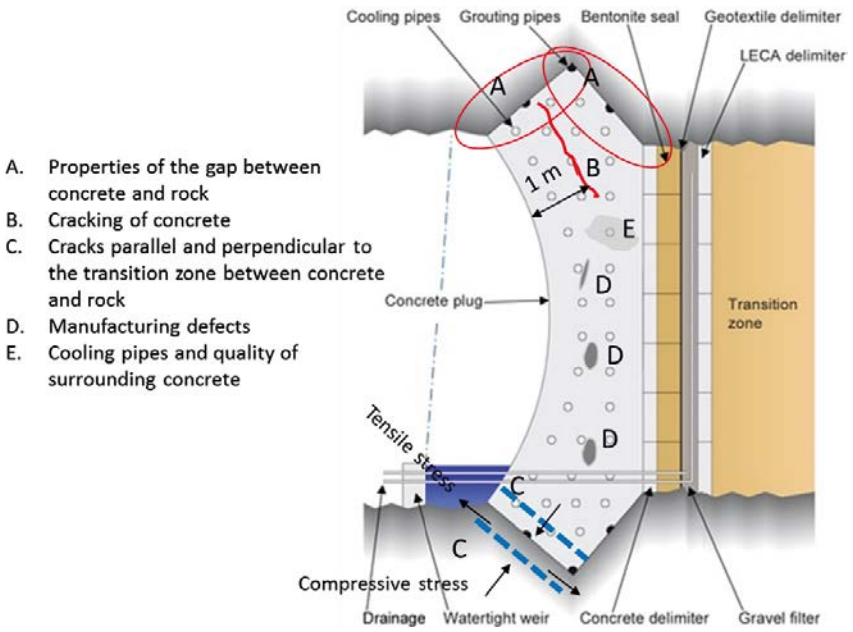

Figure 5-5. *Location of defects which should be examined by NDT (Malm et al. 2019).*

5.9 Comparisons with requirements

The dome is a thick structure of massive concrete. Most NDT equipment is not designed for massive concrete and thick section, which lead to some issues during the test, especially for the IE and IR methods.

Further evaluation would have to be carried out if it is decided to use the tested methods in the final repository. Some testing equipment might also have to be modified e.g. mounted on a truck with a robot arm automated to be more useful in the final repository.

The testing focused on detecting issues such as cavities, honeycombing and material segregation i.e. Category D in Figure 5-5. No such manufacturing defects were found during the testing. The casting of the concrete dome was carefully planned and monitored, and no manufacturing defects was expected. However, the lack of response does not constitute definite proof that such defects does not exist, since it has not been proven that the defects can be found in structures as the concrete dome. Nonetheless, there are indications that MIRA and GPR could detect anomalies in the concrete dome.

6 Core samples of the concrete dome

In the project performed by Vogt et al. (2009), a low-pH concrete mix was developed which is denoted B200. The low-pH concrete consists of large amounts of silica in the cementitious binder to reduce the pH from the cement paste. To use the concrete mix in the design of the concrete dome, several material tests had to be performed. These were primarily performed in small-scale laboratory tests. It was therefore of great interest to determine the material properties of the concrete dome in the full-scale test to verify that it had the properties as assumed in the design. Thereby, ensuring that it is possible to produce a concrete according to this mix on a large scale, but also to verify that the development of the properties has progressed as expected under realistic environmental conditions for concrete dome used in the future repository.

From the concrete dome, several core drillings were made to obtain test samples. In addition, during casting of the concrete dome in 2012 a reference monolith was also cast in the tunnel. This monolith constitutes the basis for undisturbed samples, where it was subjected to similar conditions as the dome but not subjected to high water pressures.

All the test results from concrete material tests are presented in the report by Vogt (2019). Several mechanical properties and some durability related properties of the low-pH concrete are compared to the design values. The properties obtained from the core sampling has been subjected to severe loading conditions for about five years and thereby gives an indication of expected properties and the risk of durability problems for exposure conditions similar to a future repository.

In addition to testing of cores taken from the dome plug, other long-term material tests such as creep and shrinkage tests are also presented in Vogt (2019). These tests results were already described in Grahm et al. (2015) but have now been updated with the last measurement points. The main conclusions have however not changed and are therefore not presented in this report.

6.1 Core sample plan

Several different material properties were planned to be measured from the concrete dome. The purpose was also to determine if these properties varied over the geometry of the dome, both between different batches, i.e. over the height of the dome, but also in the thickness direction. In addition to determine the properties in the concrete dome, it is also of great interest to determine properties of the concrete-rock interface, i.e. the bond strength.

Drill cores were taken from along the vertical centre line of the dome close to the base, mid-height and near the top. Besides these, cores were also taken at critical regions where internal damages are most likely to occur due to the pressure loading, see Section 5.3. All these cores were 95 mm in diameter and were used for all material testing except the tests of bond strength. The drill plan for these cores are shown in Figure 6-1.

Core samples were also taken from the upstream side of the slot that were drilled along the interface of concrete and rock to determine the bond strength. These cores were drilled with a 150 mm diameter and drilled to correspond to 50/50 of concrete and rock. Several cores were taken prior to demolition of the concrete dome. After the demolition, some additional cores were taken to measure the in-situ bond strength. The drill cores intended for test of bond strength are illustrated in Figure 6-2.

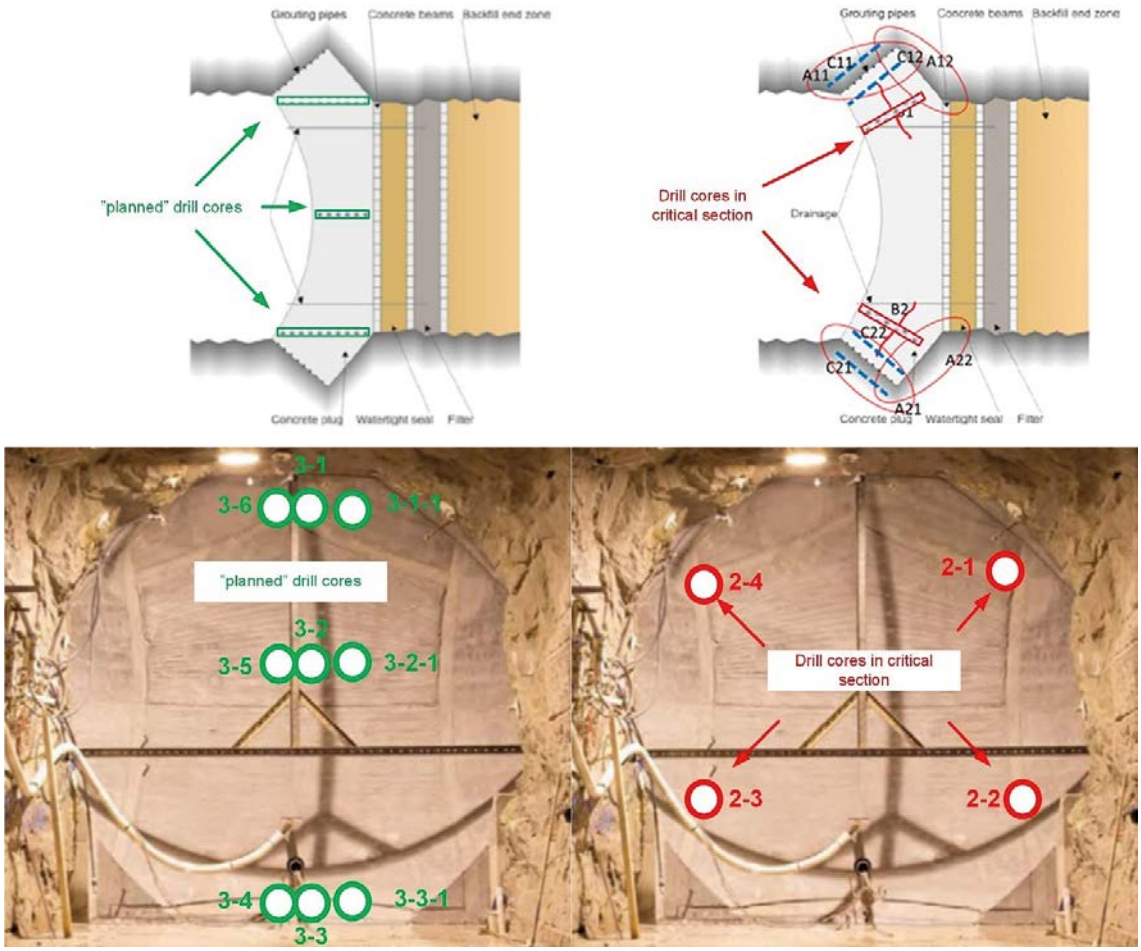

Figure 6-1. *Drill cores with diameter 95 mm for the investigated concrete properties, from Vogt (2019).*

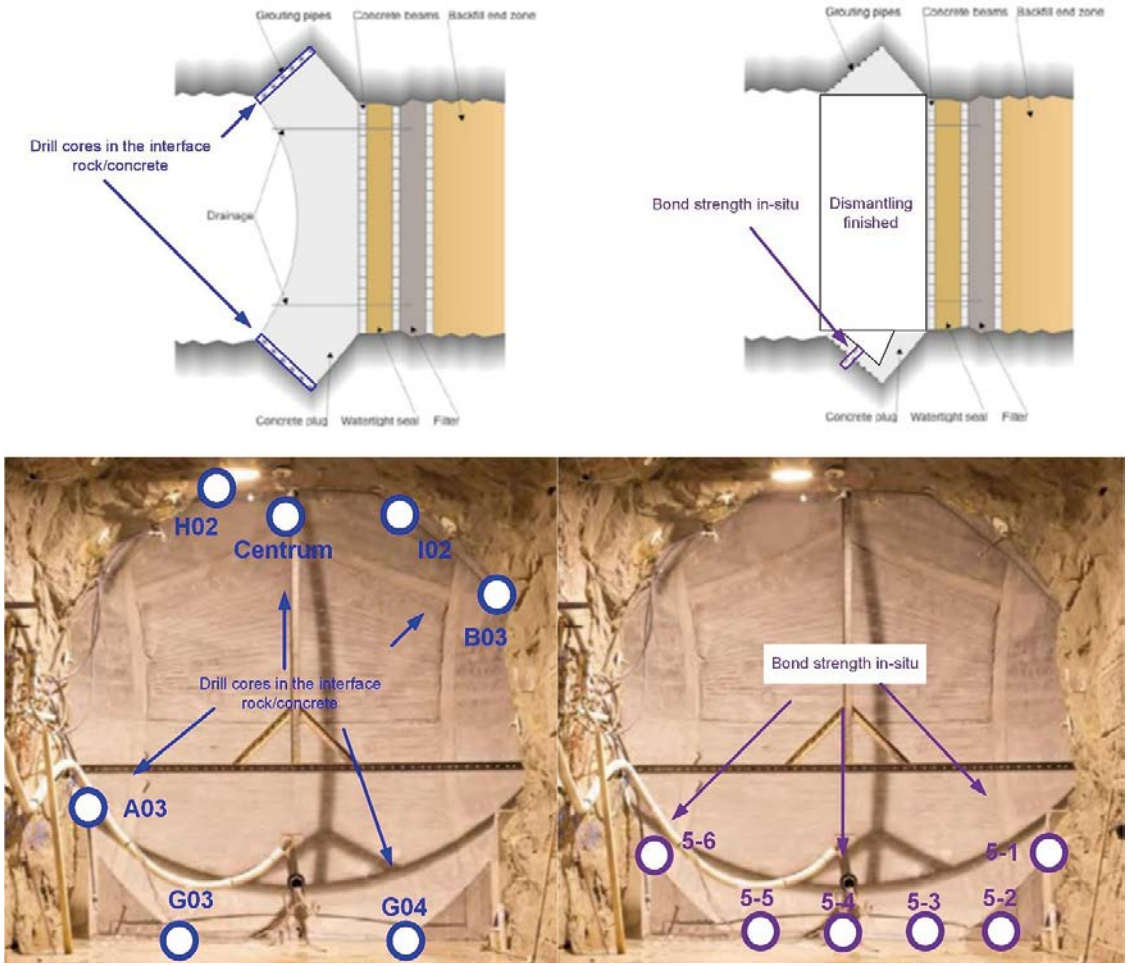

Figure 6-2. *Drill cores with diameter 150 mm for investigation of the interface between rock and concrete (left). In-situ test of bond strength between rock and concrete on the upstream face of the slot in the rock (Vogt 2019).*

6.2 Test plan

The length of the cores was at least 2 m, which made it possible to take several samples from each core. From each core, three samples were created for test of the mechanical properties; one close to the upstream surface, one in the centre and one close to the downstream surface. In addition, from all the cores along the centre line (see Figure 6-1) samples were also created for the tests related to the durability.

In summary, the following properties were tested:

Mechanical properties

- Compressive strength.
- Tensile strength.
- Bond strength to rock, tested in laboratory and in-situ (also visual inspections of the gap between rock and concrete).
- Density.
- Young's modulus (elastic modulus).

Other material properties

- Permeability.
- pH by leaching.
- Carbonation.
- Microstructure.
- Degree of capillary saturation.

The tests were performed according to test standards as far as those are available or valid for the type of tests performed, and in some cases some modifications had to be made were best practice methods were chosen instead. More information about the test procedures and the test plan can be found in Vogt (2019). The results from these tests are described in the following section.

6.3 Test results from the concrete cores

In this section, the main conclusions from all material tests performed on the concrete material are presented.

6.3.1 Mechanical properties

Compressive strength

A total of 21 samples were tested obtained from the cores presented in Figure 6-1. The test results showed relatively large scatter for compressive strength. There is a clear tendency that the samples from the central parts of the dome have a higher compressive strength than samples situated close to the upstream or downstream surface. The average of the samples close to the surface is 69 MPa and the central samples have a strength of 75 MPa. The average for all samples is 71 MPa with a standard deviation of 5 MPa. The central parts of the concrete dome also show similar strength as the results obtained from the monolith, placed outside of the test tunnel. The average strength is also in line with the material classification tests performed during development of the concrete mix presented by Vogt et al. (2009).

Tensile strength

The tensile strength was determined from 21 samples taken from the cores presented in Figure 6-1. The test results show a relatively large scatter in tensile strength with an average tensile strength of 2.6 MPa and a standard deviation of 0.5 MPa. In contrast to the test of the compressive strength, the tendency of lower strength closer to the surfaces was not as significant for the tensile strength. The average for the centre was 2.7 MPa and 2.6 MPa for the surface. Overall, the tensile strength is lower in the dome than reported from the previous laboratory tests where about 3.2 MPa was expected. It is difficult to assess the cause for this difference, but it could for instance be a result of on-going aging or a result of loading conditions and/or an effect of restrained shrinkage. According to Vogt (2019) it is however unlikely that aging is the reason, since this effect was not seen in the compressive strength.

The concrete mix used in the concrete dome had higher air content than normal which also could be a reason. Considering that the measurements of the concrete dome showed much smaller shrinkage deformations than expected, it is likely that restrained shrinkage (i.e. that the concrete dome did not fully release from the rock prior to contact grouting) is primary reason for the lower tensile strength.

Bond strength to rock, tested in laboratory and in-situ (also visual inspections of the gap between rock and concrete)

During sampling, the 50/50 cores were mainly intact where the concrete was bonded to the rock. However, despite careful handling, these cores debonded during the transport to the laboratory or during preparation for the splitting tensile test. This shows that the bond strength must have been low. Only one, out of 21 specimens, was possible to test for bond strength. The obtained splitting strength from this test was 1.2 MPa, which is less than half the tensile strength.

Due to the low bond strength and problems with handling the specimens, additional tests were performed where the bond strength was measured in-situ. After the concrete dome had been breached, the concrete in the lower part of the slot had been saved and thereby, left unaffected. A surface of the remaining part of the plug at the downstream part of the slot was prepared at six locations at the same angle as the rock surface in the slot. The thickness of remaining concrete varied approximately between 100–240 mm. A core was drilled through concrete and rock and the concrete part was gripped with a special tool and pulled off. However, all cores except one came loose during drilling while the last core came lose when fixating the gripping tool. Thereby, no values of the in-situ bond strength were possible to obtain.

Thereby, the bond strength was very limited in the downstream part of the slot. This area transmitted the forces during the test mainly through compressive forces from the water pressure. The bond in the upstream side of the slot abutment had to a great extent already been lost during the testing with increasing water pressure. This was later shown during the demolition, where the concrete near the upstream part had no bond that could keep the concrete parts hanging from the slot, see Section 7.1.2.

From the 50/50 cores, it was also possible to measure the thickness of the grout material. This shows the gap that occurred between the concrete dome and the rock due to the early shrinkage and the thermal contraction prior to contact grouting. In general, the grouted gap varied between 0.2 and 0.7 mm. The grouting thickness is shown in Figure 6-3. This was far from the expected gap that would have occurred if the dome had released completely from the rock. In addition, no clear correlation between the grout thickness and the height of the dome could be detected, which would be expected if the dome was subjected to unrestrained shrinkage. This further indicates that the dome did not completely release from the rock during the cooling stages.

Density

The density was measured for all samples tested for compressive and tensile strength and all samples that were tested for elastic modulus. In total, 63 specimens were tested, where the average was 2 253 kg/m^3 with a standard deviation of 118 kg/m^3. This value was lower than expected during design (2 336 kg/m^3 according to Vogt et al. (2009)) and this is likely caused by the fact that higher air content was measured during construction of the concrete dome, as reported by Grahm et al. (2015). The increased air content of the concrete in the plug can also explain certain observations such as lower average compressive strength than earlier laboratory tests.

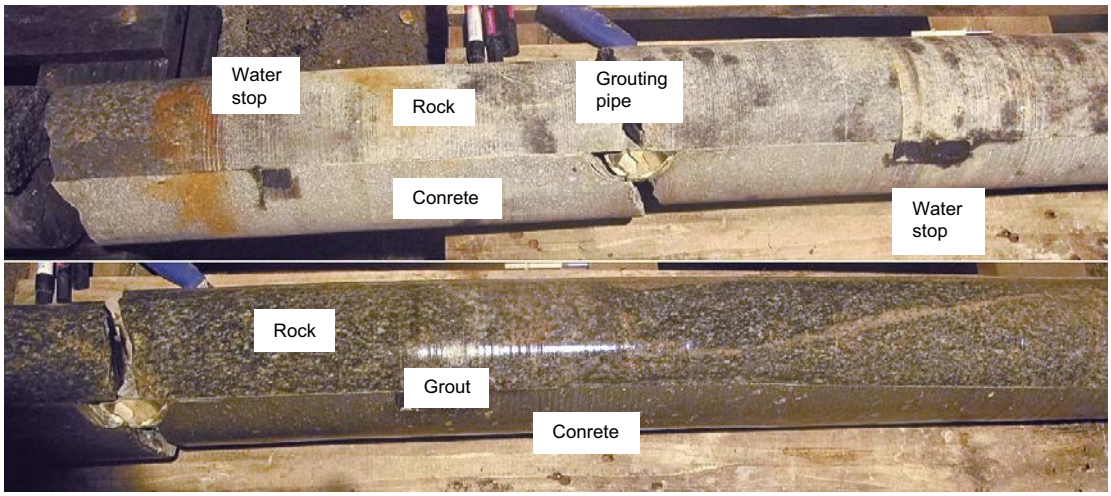

Figure 6-3. *Examples of drill cores (A03) from the interface between rock and concrete immediately after drilling. The water stops (dark squares) and grouting pipes (light coloured halve-circles) are clearly visible. Also, a thin layer of grout (light colour) at the interface. These cores seemed to be attached to each other after drilling, i.e. a certain bond strength existed. From Vogt (2019).*

Elastic modulus

The elastic modulus was measured from nine specimens taken from the cores in the centre, see Figure 6-1. One specimen, located close to the surface showed significantly lower elastic modulus than the rest, especially for the initial tangential modulus but also to some extent for the secant modulus ($E_{initial}$ = 12.3 GPa and E_c = 24.4 GPa respectively). No irregularities regarding the specimens have however been documented in the test report. This deviation leads to lower average and larger standard deviation. Even if this value is included the average secant modulus is 34 GPa with a standard deviation of 4.5 GPa. With this value excluded the average is 35 GPa with a standard deviation of 3.0 GPa. The obtained elastic modulus is in line with the elastic modulus used for the design which was 34 GPa.

6.3.2 Other material properties

In this section the other tested material properties, not related to the mechanical properties are presented.

Permeability

The permeability was measured on nine specimens taken from the cores in the centre of the plug. The average permeability of the concrete was 2.2E–12 m/s and the test results showed relatively large spread within each core but also between different cores. The test results obtained from the concrete dome are significantly higher than the corresponding values that were obtained in the laboratory tests by Vogt et al. (2009), typically 3 to 15 times higher. There are some differences between the concrete used in the previous laboratory tests and the concrete mix used in the full-scale test, such as the higher air content. It is difficult to assess the influence from the differences in mix designs, however Vogt (2019) states that it is clear that the long-term water pressure, quick unloading during drainage for the gas tightness test and the final strength test have had negative influence on the water tightness of the concrete dome.

It can also be concluded that the highest permeability is obtained close to the downstream surface of the dome and primarily for the cores at an elevation corresponding to the upper half of the dome. As shown in the following section regarding the microstructure, this area is more subjected to micro-cracking and as previously shown in Section 4.2.2 this region is subjected to highest stresses during unloading due to drainage in the gas tightness test.

In the design, a conservative value of 1E–11 m/s was stipulated and despite the influence from these micro cracks, the permeability of the concrete dome is still lower than this.

pH by leaching

Nine samples with a height of 12 mm and diameter 30 mm were extracted from the centre cores. These were submerged in artificial saline water and the pH was measured with a glass electrode. During the first two weeks of the test, the pH value increased due to leaching of alkalis, but stabilized after about one month. The pH values typically varied between 9 and 9.5, which is well below the requirement of pH ≤ 11 as seen in Figure 6-4.

Carbonation

The depth of carbonation was measured with two different approaches. In the first one, it was determined on freshly broken surfaces of drill core pieces with a pH indicator. Based on these tests, the depth was typically between 7 and 9 mm but for some samples could be up to 17 mm. However, it should be noted that this approach is somewhat difficult to use for low-pH concrete due to the relatively low difference in pH between carbonated and uncarbonated concrete. Therefore, these results can be considered to have a relatively high degree of uncertainty compared for conventional concrete.

In the second approach, the carbonation depth was determined based on thin sections where the depth was determined between 4.5 and 7.5 mm. This approach is considered more exact while these values can be considered as rather high for a humid environment and five years of exposure according to Vogt (2019). The low-pH concrete closer to the surface, i.e. the carbonated layer, had higher degree of capillary porosity than in the low-pH located at greater depth. It is not possible to determine if the carbonation caused increased porosity or if the increased porosity caused increased carbonation.

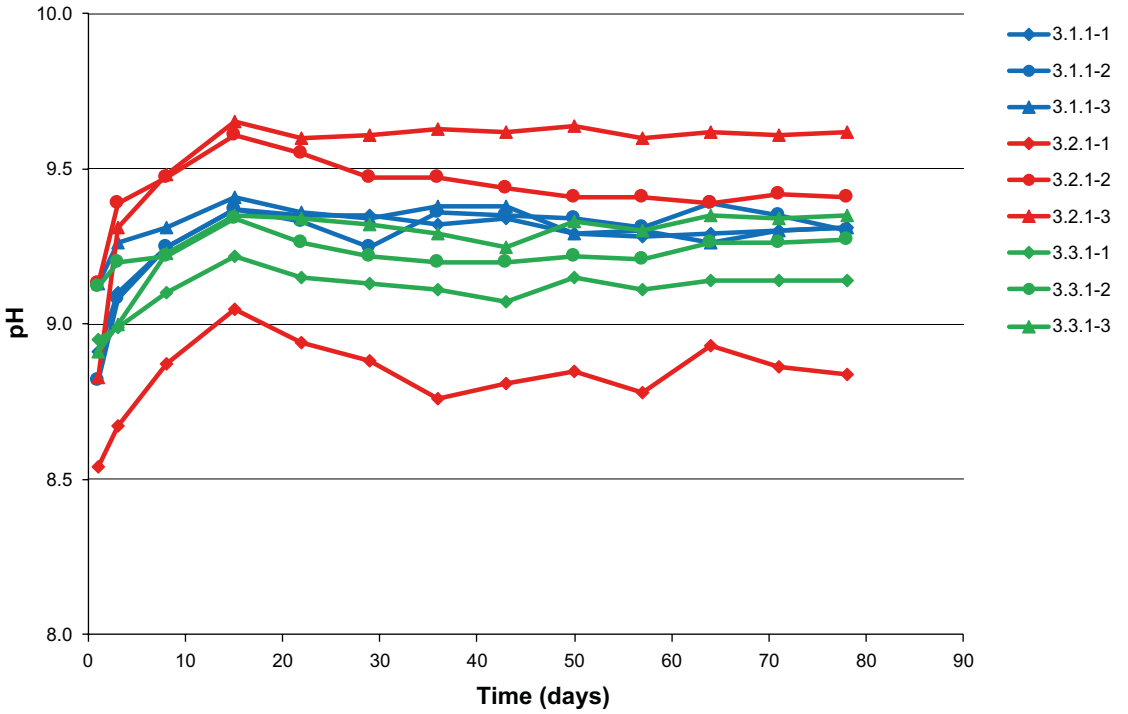

Figure 6-4. *Measured pH by leaching, from Vogt (2019).*

Microstructure

Thin sections were analysed to determine the microstructure of the low-pH concrete. These thin slices were obtained from three cores in the central part of the dome, see Figure 6-1. Three thin slices were created for each core, resulting in nine thin slices.

Overall, all thin slices showed larger extent of micro cracking closer to the downstream surface both regarding the frequency of cracks and the maximum observed crack width. In addition, the cores obtained from higher elevation of the dome showed higher degree of micro-cracks, where the core taken at the top of the dome showed both high frequency of micro-cracks and large maximum crack width of 0.001 mm.

A UV photo of the concrete located close to the downstream surface of the dome is shown in Figure 6-5. In the upper part of the photo, the concrete has a brighter colour than in the bottom. The reason for this is that the concrete closer to the surface (in the top of the figure) has higher degree of porosity compared to the concrete at greater depth (in the bottom of the figure). It is also possible to see a micro-crack that goes from the surface and in the concrete, which are illustrated with a bright green colour in the figure. The micro-cracks run around the ballast grains, which indicates lower fracture energy. The observed micro-cracks have according to Vogt (2019) probably formed due to restrained shrinkage of the cement paste. Vogt (2019) also states that based on observations made in thin sections, there is no evidence of reduced durability of the concrete.

The personnel responsible for performing the non-destructive testing also pointed out that the concrete surface was softer than normally which also indicates higher porosity of the surface layer. Possible explanations of the higher porosity of the surface layer of the concrete was discussed by Vogt (2019):

Leaching – caused by running water on the concrete surface. Normally, leaching involves decomposition and loss of calcium oxide. However, for the concrete dome, no increased levels of calcium oxide were found in these areas. In addition, the gradient and depth of the porous layer appears to be the same for all three thin sections that were taken from different locations of the dome. According to Vogt (2019), equivalent leaching over the concrete surface seems unlikely since this would imply identical water exposure on the concrete surfaces.

Water in the formwork – if there was water in the formwork that got mixed into the surface layer of the concrete this could be a plausible explanation. However, as stated by Vogt (2019) this is considered unlikely since this would most likely result in varying thickness of the surface layer with higher porosity in different parts of the dome.

Reduced curing of the concrete surface – this could occur if substances applied to the formwork hindered adequate hydration of the surface layer. According to Vogt (2019) some paint coating was applied to the wooden formwork and these types of paints may have an effect of the hydration of the surface.

Degree of capillary saturation

The degree of capillary saturation was measured on nine specimens obtained from three centre cores as shown in Figure 6-1. All samples showed high degree of water saturation (> 90 %). This was expected considering that the concrete dome was subjected to water pressure on the upstream side and was subjected to an environment with high relative humidity on the downstream surface.

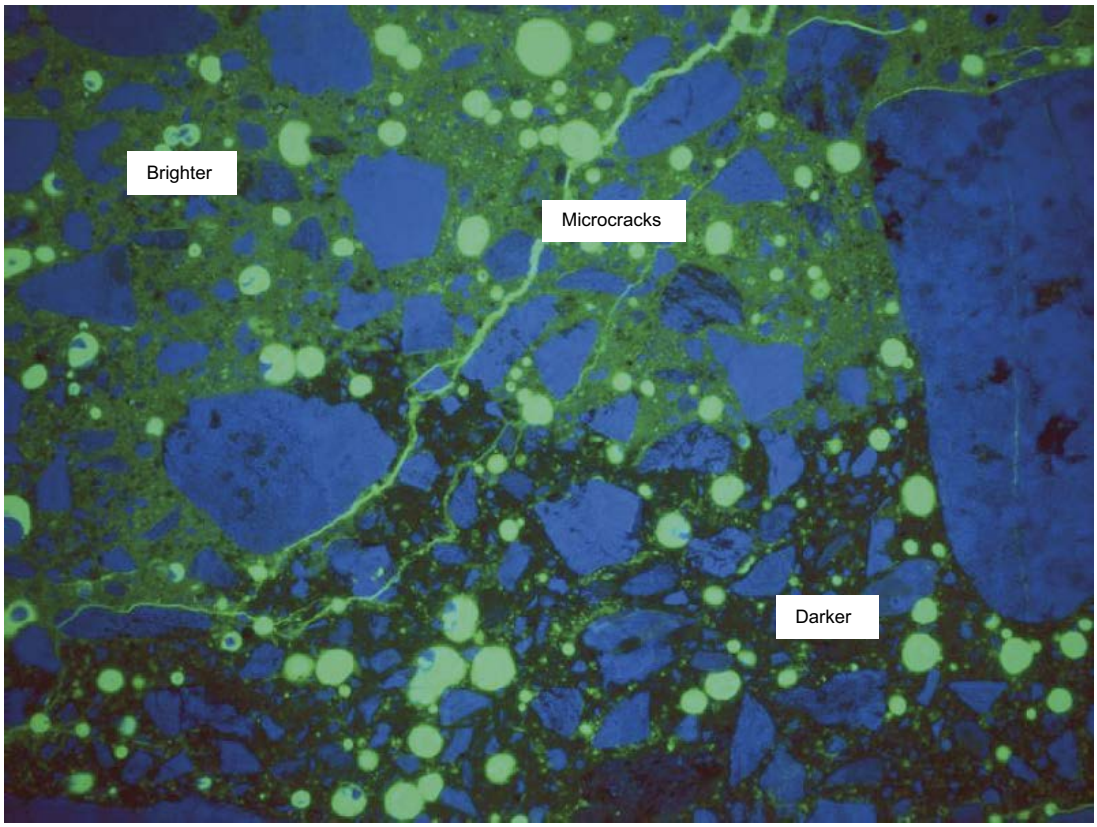

Figure 6-5. *UV light of the sample 3.2.1-I located 5–10 mm from the downstream surface. Width of the figure is 6.7 mm. The brighter area in top of the figure illustrates higher porosity compared to the darker area in the bottom area.*

6.4 Observations during sampling

Core sampling and visual observations did not show any obvious defects such as cracks, honeycombing or large voids in the concrete. However, in the top of the dome, a triangular void was detected during core drilling of the core denoted H02 as previously shown in Figure 6-2. This void showed that the casting of the dome had not completely filled the volume. In Figure 6-6 a), the placement of the drilled core is illustrated. The height of the void was about 0.4 m and it was observed during core drilling that top of the dome was partially filled with grout material as shown in Figure 6-6 b).

The same observations were then made for all 50/50 cores sampled near the top of the dome and in Figure 6-7 the cores from H02 and I02 are shown. The grout material can be seen as a brighter grey colour with absence of larger aggregates. One additional core was sampled in the centre (denoted Centre in Figure 6-2) of the dome and is shown in Figure 7-11a. For clarification, a picture of the void taken during dismantling of the dome is presented in Figure 7-11b. An additional drill core and a photography of the void are presented in Figure 6-8. Further discussion regarding the detected void in the top of the concrete dome is presented in Section 7.2.

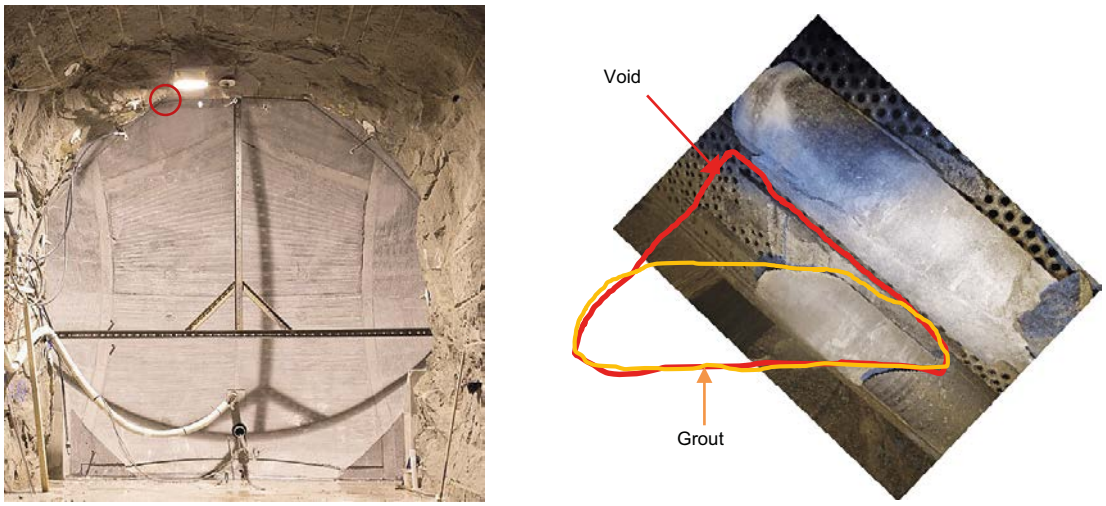

Figure 6-6. *Detected void in the top of the dome. a) Location of the drill core. b) A drill core showing the amount of grout filling the void, the hand drawn lined represents the size of the void and the outline of the abutment.*

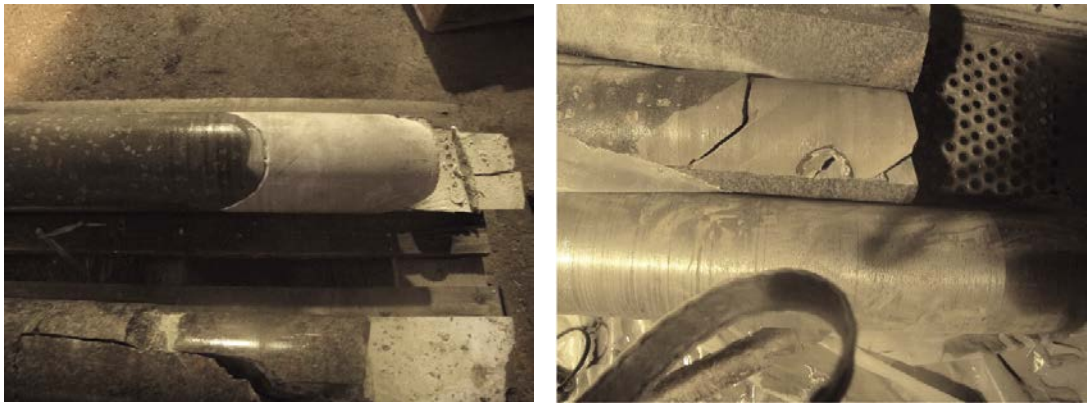

Figure 6-7. *a) Drill cores H02 and b) I02. The top part of the cores is displayed.*

a) b)

Figure 6-8. *a) Drill core "centre" and b) void on top of the concrete.*

6.5 Evaluation

The testing of the concrete has shown that the material properties of the dome is more or less the same as the properties defined by Vogt et al. (2009) and that were assumed in the design. The tested properties contained both mechanical properties such as tensile and compressive strength and stiffness (elastic modulus) as well as other properties such as permeability, pH, water content etc. The results showed no significant decrease in mechanical properties despite that the dome was subjected to challenging conditions. However, some indications have been found that the properties in the downstream surface layer in certain areas has been influenced negatively. The reason for this is that this concrete has higher capillary porosity and is exposed to micro-cracking. The exact cause for this could not be determined, however several plausible reasons have been identified. According to Vogt (2019), the most likely reason is that this occurred during pouring and is due to insufficient curing.

One important property that has been tested in this report is the bond between concrete and rock. The monitoring of the concrete dome, as well as the fact that the void was water filled shows that the bond had been lost on upstream side already during the initial pressurization, Grahm et al. (2015). However, in the downstream side of the slot, the bond seemed to be intact. This was verified by the concrete cores taken at the interface between concrete and rock. However, this bond was low considering that it failed already during transport and handling of the specimens. These specimens also showed the extent of grouting that had penetrated the gap between the concrete and rock that had occurred due to shrinkage and the cooling of the dome.

6.6 Comparisons with requirements

The material tests have shown that properties of the concrete used in the dome are similar to the properties used for design and the previous testing. This shows that it possible to develop the concrete mix B200 in a concrete factory that has similar properties as in the laboratory. This also shows that no significant decrease in mechanical properties due to aging, loading or restrained shrinkage has occurred after 5 years even though the dome has been subjected to high water pressure.

In addition, the self-compacting concrete has filled the form and the distribution of the aggregates in the concrete seems to be good. Figure 6-9 show the distribution of aggregates in the concrete and that the cooling pipes were well embedded in the concrete.

One thing that deserves to be mentioned regarding the concrete properties and difference in design assumptions are the shrinkage. In the design the autogenous shrinkage was quite high and would result in quite large gap that could be grouted between the concrete and rock. In the full-scale test, the shrinkage seems to have been significantly smaller and thereby only resulted in partial release of the concrete dome due to shrinkage and cooling. This resulted in smaller gap that needed to be grouted but also that larger stresses were induced in the concrete dome than assumed in the design.

The core drilling also revealed that the concrete was not pumped all the way up to the top of the dome. The casting stopped about 0.4 m from the top. Venting pipes were installed to prevent an air pocket in the top but apparently this did not work sufficiently. One conclusion that can be drawn from this is however that the design of the concrete dome is robust which allows for defects like this and still works as intended. Different suggestions for improvement of the production of the concrete dome are discussed and presented in Chapter 9.

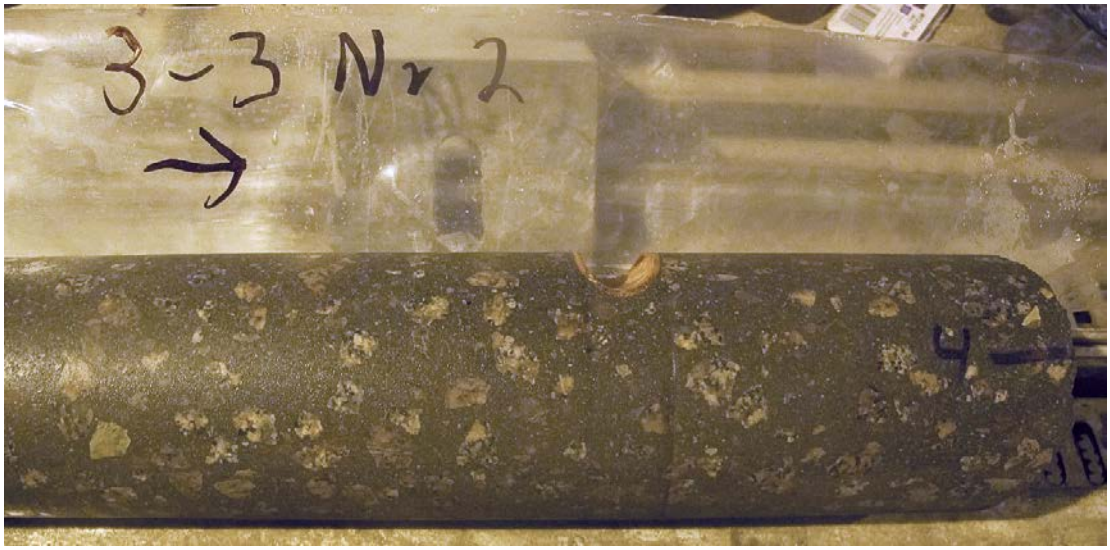

Figure 6-9. *Core 3-3-1, part 2. The large aggregates seem very well distributed, the cooling pipe is well embedded in concrete.*

7 Demolition of the DomPlu

After all core samples were collected, the demolition of the plug commenced. A square section of the plug was first seam drilled and removed for future reference. The remaining concrete dome was then removed with a hydraulic hammer. The seam drilled section was removed on 23rd November 2017, and the demolition commenced 27th November 2017 and was carried out over 17 days.

7.1 Demolition of the concrete dome

7.1.1 Core drilling

To save an intact sample of the concrete dome, which was not damaged by the hydraulic hammer, a square section of the concrete dome was cut by seam drilling. The section was taken in the centre of the plug, slightly below mid-height, as illustrated in Figure 7-1a. Figure 7-1b shows the seam drilling in progress and Figure 7-2 shows the result of the seam drilling. The sample section was removed with a wheel loader, this is illustrated in Figure 7-3. The final sample and the resulting hole in the concrete dome can be seen in Figure 7-4.

a) b)

Figure 7-1. *a) Location of the sample section. b) Seam drilling in progress.*

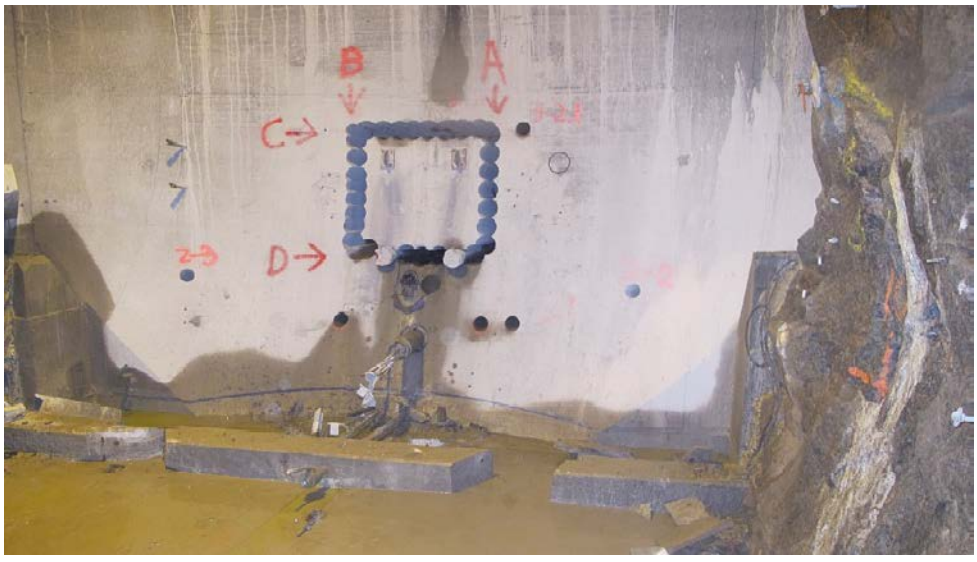

Figure 7-2. *The seam drilling is finished, and the section is awaiting extraction.*

a) b)

Figure 7-3. *Extraction of the square sample, using a wheel loader.*

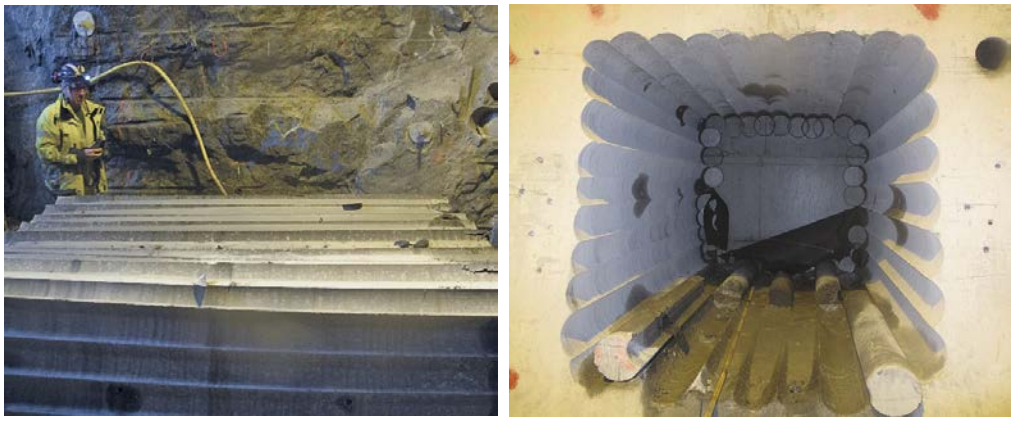

a) b)

Figure 7-4. *a) The extracted section and b) The hole left in the concrete dome.*

7.1.2 Hydraulic hammer

The hydraulic hammering was carried out with a remote controlled, electric BROKK 400 demolition robot. The demolition robot was equipped with a hydraulic hammer with 1 250 kg impact force. The demolition commenced on 28 November 2017 and required 17 days. The demolition robot and the result after the first day of demolition can be seen in Figure 7-5.

The demolition caused a lot of dust from the broken off concrete. To handle the dust, a nozzle was mounted to spray water and bind the dust. The hydraulic hammer also proved to be too small, since the concrete in the concrete dome had a very high strength. However, the demolition robot could not carry a larger hammer. The contractor estimated that the demolition would be faster if a larger hammer could have been used.

The layout of the test area also proved to be a challenge for the removal of the demolition rubble. The demolition robot had to be moved out of the test tunnel to make room for the excavator and truck, which were used for the removal. The tunnels are quite narrow for this type of machinery and moving them about was time consuming. In addition, the excavator was under dimensioned. The contractor estimated that the demolition would be 2 days faster if the logistics were better and a larger excavator was used.

Figure 7-6, Figure 7-7, and Figure 7-8 shows the state of the concrete dome after 4, 9 and 14 days respectively. Figure 7-9 shows the upstream face of the slot abutment where a thin layer of grout from the contact grouting is visible in certain areas. If this area had any bond between concrete and rock, then pieces of concrete would have been seen on the rock surface. In addition, in Figure 7-6a, the concrete on the upstream in the top-right corner of the photo has fallen from the slot. This shows that the bond in this area was lost, most likely during the increasing water pressure as previously discussed.

Figure 7-5. *Demolition Robot BROKK 400 and the concrete dome after the first day of demolition.*

a) b)

Figure 7-6. *a) Concrete dome during the fourth day of demolition (2017-12-04). b) The head of the hydraulic hammer.*

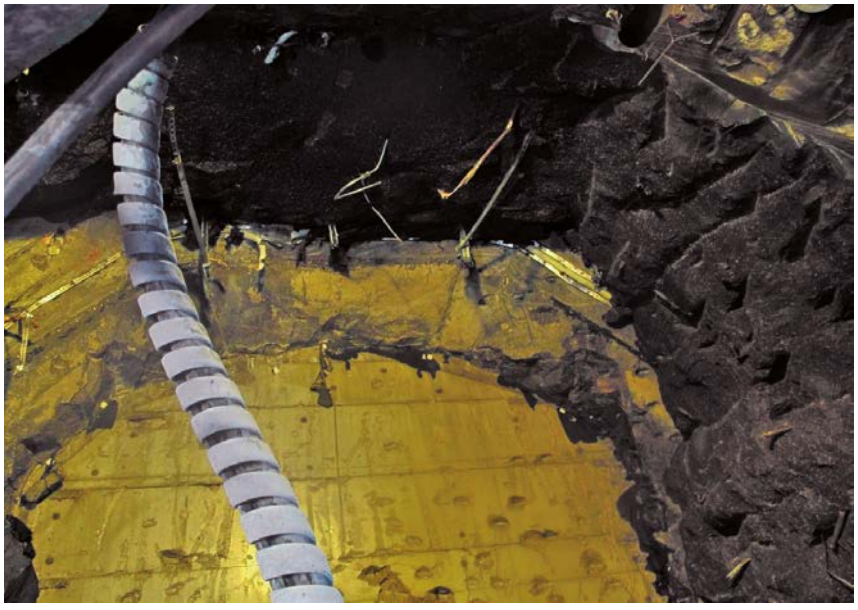

Figure 7-7. *The concrete dome after the 9th day of demolition, the concrete beams behind the dome are visible.*

Figure 7-8. *The concrete dome after the 14th day of demolition.*

Figure 7-9. *Some areas are visible with a thin layer of grout on the upstream side of the slot.*

7.2 Finding the large void in the top of the concrete dome

As previously presented in Chapter 5 and Chapter 6, a void was detected in the top of the concrete dome during sampling of concrete drill cores. During demolition of the concrete dome, it was possible to take a closer look at the cavity, as seen in Figure 7-10 and Figure 7-11. The width of the void was about 1 m, the length of the wedge was about 3.8 m and the height of about 0.4 m results in a volume of about 0.8 m^3.

As mentioned previously, this void was partially filled with grout, where the grout thickness was estimated to be about 10 cm as seen in Figure 7-11. This corresponds to about 380 litres of excess grout that had been placed in the top of the dome. As mentioned in Grahm et al. (2015), it was noticed during grouting that significantly more grout than expected was used. According to Grahm et al. (2015) 654 litres of grout was used compared to the estimated 260 litres. The difference between the used and estimated amount of grout is 394 litres which corresponds to the amount of grout found in the top of the dome.

Figure 7-10. *Measuring the width of the large void, about 1 m.*

Figure 7-11. *Measuring the height of the void, about 40 cm whereof 10 cm is filled with grout.*

Considering that several sensors were installed in the top of the concrete dome, it is also important to assess whether these have been completely cast in concrete or not. In Figure 7-12, one of the joint-meters installed in the top of the dome is shown. As can be seen in the figure, the joint-meter and its fixation in the rock was barely covered with concrete and then further covered by 10 cm of grout. Thereby, the sensor was embedded in concrete, but it is likely that the void has influenced the measurements in the top. Considering that the top of the dome was filled with air after casting, the restraint in the top was much lower than it should have been. This would have allowed for larger displacements due to the early shrinkage. Considering that it took a few hours before the concrete bonded to the sensor, it is therefore likely that some part of the shrinkage deformations occurred prior to this. However, the initial shrinkage cannot explain the small displacements measured in the top since the development of shrinkage was expected occur for about 90 days. Even if a few hours were missed in the beginning that does not explain the smaller shrinkage measured at the dome.

Figure 7-12. *Photo of the void and the joint-meter JM01 to the right.*

A few sensors were mounted on reinforcement bars installed in the rock near the top of the slot. One of these bars is for instance shown in Figure 7-11 and Figure 7-12 These sensors failed recording during the pressure increase to 4 MPa performed in the beginning of 2014. Considering that the void was waterfilled and pressurized, the water has propagated along the reinforcement bars to the sensors and then also followed the bundle of cables out through the plug. This explains why leakage occurred through the cables for the sensors in the concrete dome.

The void in the top also explains other observations made during the monitoring the behaviour during pressurization of the dome. Leakage was detected in the area in the top as shown in Figure 7-13. This leakage was detected near the drill hole I02, see Figure 6-2. This seems reasonable considering that the void in the top was water filled and had a water pressure of about 3 MPa, as previously shown in Figure 4-24.

Figure 7-13. *Illustration of leakage at the concrete rock interface during the initial pressurization up to 4 MPa, from Grahm et al. (2015).*

7.3 Removal of the concrete beams, bentonite seal and filter

The uppermost concrete beam was at the time for installation casted around the periphery i.e. concrete was pushed into the remaining gap between the beam and the rock. The beam was crushed with a hydraulic hammer, the same that was used for removal of the concrete dome. The beam was then removed. The other beams were removed by using a hydraulic hammer carried by an excavator. The hammer was used to crush the ends of the beams which then could be lifted away, see photos in Figure 7-14. After removal of one concrete beam the bentonite behind was sampled and removed before the work with removal of the next concrete beam was started.

Once the concrete beams were removed, samples was taken of the bentonite according to Section 8.1. The remaining bentonite was removed by use of a special hook carried by an excavator, see photos provided in Figure 7-15 and Figure 7-16. No material tests were performed in the filter. The filter material was removed using a hose from a vacuum truck, see Figure 7-17.

a) b)

Figure 7-14. *a) A hydraulic hammer was used on both ends of each concrete beam to crush the concrete. B) After crushing the concrete at both ends the steel anchoring to the rock was cut and the beam could then be lifted away by a large loading machine. From Åkesson et al. (2019).*

a) b)

Figure 7-15. *a) A scissor platform was used during sampling of the bentonite. b) The exposed bentonite has been sampled. From Åkesson et al. (2019).*

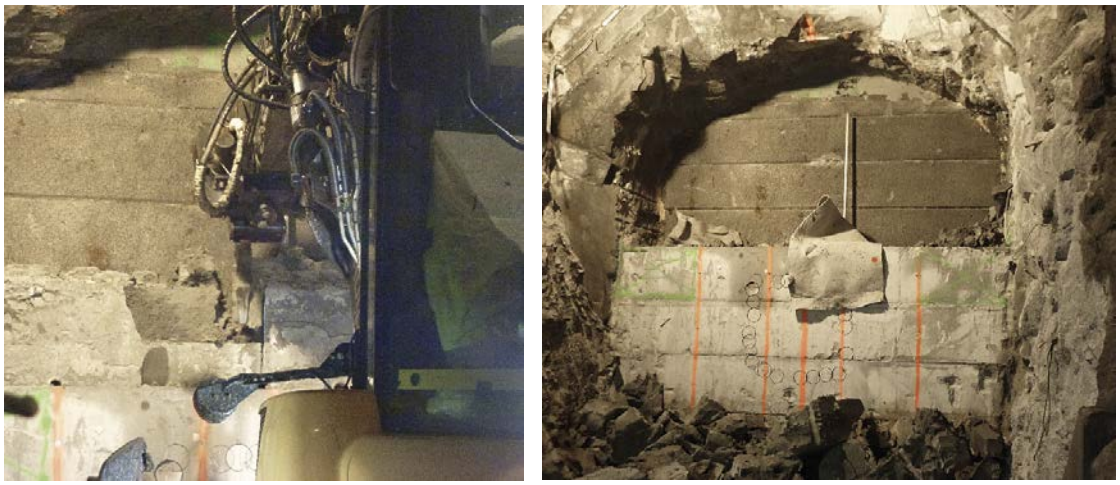

a) b)

Figure 7-16. *a) A special "hook" was used to remove the remaining bentonite above the next concrete beam. b) The main part of the bentonite has been removed, leaving the outer parts close to the rock wall for sampling. From Åkesson et al. (2019).*

Figure 7-17. *A vacuum truck was used to remove the filter material. From Åkesson et al. (2019).*

7.4 Removal of the backfill and LECA beams

The LECA beams were removed using a wheel loader, see Figure 7-18. The backfill was thereafter sampled according to the scheme described in Section 8.1. Once the sampling was finished, the backfill was removed. The drill used for sampling is illustrated in Figure 7-19. The backfill and LECA beams are is illustrated in Figure 7-20 after the sampling.

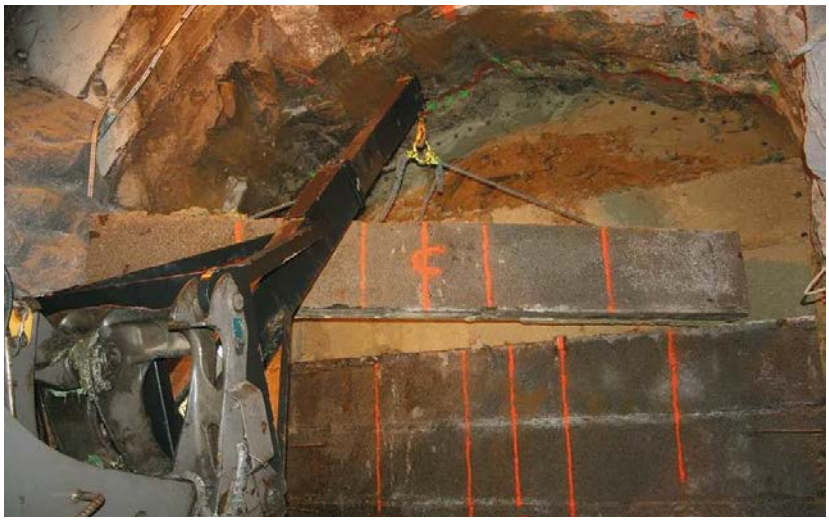

Figure 7-18. *Removal of a LECA beam.*

Figure 7-19. *Drill used for sampling of the backfill. From Åkesson et al. (2019).*

Figure 7-20. *The upper part of the backfill after two LECA beams has been removed a number of samples have been taken. From Åkesson et al. (2019).*

7.5 After demolition

In Figure 7-21, the experiment tunnel is shown after the demolition. In the photo, the concrete back wall is visible in the back of the tunnel. The three lead-through pipes for cables and pressurization pipes can also be seen. The location of the concrete dome is shown with orange spray paint in the figure. The orange pipes show the location of the in-situ bond strength tests that were presented in Chapter 6.

7.6 Evaluation

To get a large number of undisturbed samples for material testing, the demolition of the plug was carried out carefully and it was therefore time consuming. In the spent fuel repository, a malfunctioning plug could be demolished quicker and less carefully. The demolition of the concrete dome using a hydraulic hammer is representative of the demolition that would be carried out in the repository and important experience was obtained. However, the demolition of the bentonite could have been carried through much quicker, using an excavator.

Some important experiences were gathered during the demolition of the concrete dome. The hydraulic hammer used was too small, if a larger hammer was used, the demolition would have been quicker. The hydraulic hammering also produced a lot of dust. This was helped by mounting a nozzle on the hydraulic hammer and binding the dust with water.

The logistics of the test site was also an issue. The access tunnels will be larger in the final repository than in Äspö HRL, so the logistics would likely be better. However, it would be desirable to have a plan for the demolition if a plug would malfunction in the final repository. As a part of improving the logistics, it would be desirable to use the same machine for removal of the hydraulic hammering and the demolition rubble. Ideally, the same machine should also be used to remove the remaining plug and the backfill.

7.7 Comparisons with requirements

A deposited canister containing spent nuclear fuel should be possible to retain during the operation of the repository. The full-scale test has shown that the demolition of the concrete dome can be achieved within a reasonable time frame to access the rest of the plug system and the backfill in the case of a malfunction in any of the included systems.

Figure 7-21. *Photo of the tunnel after demolition of the plug.*

8 Results from bentonite tests

8.1 Core sample plan

A large number of samples were taken from the bentonite seal and the backfill. In total 450 samples were taken from the bentonite seal and 360 samples for the backfill. The sampling plan for the bentonite seal is shown in Figure 8-1. The samples were taken in a grid pattern (0.6 m × 0.8 m) over the whole tunnel cross-section where the seal blocks were installed. In addition, samples were also taken in the pellet filled slot between the blocks and the rock wall. In all these grid points, samples were taken at five different depths in the 500 mm thick bentonite seal.

The sampling plan for the bentonite backfill is shown in Figure 8-2. The samples were taken in a grid pattern (0.6 m × 0.8 m) over the whole tunnel cross-section where the backfill blocks were installed. In addition, samples were also taken in the pellet filled slot between the blocks and the rock wall. In all these grid points, samples were taken at four different depths in the bentonite backfill.

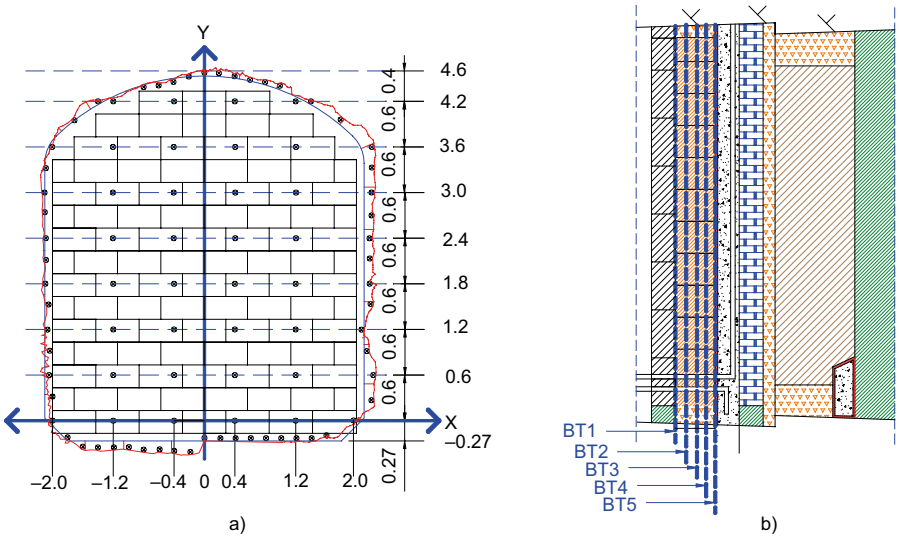

Figure 8-1. *Schematic showing the planned sampling of the bentonite seal. a) The sampling of the vertical bentonite seal surface. b) The vertical sampling was performed in five different sections of the seal (Åkesson et al. 2019).*

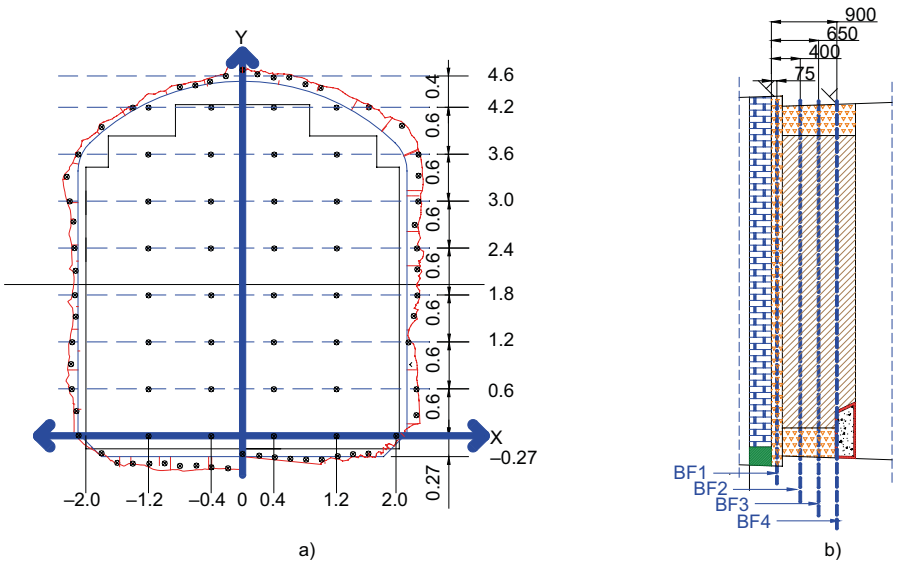

Figure 8-2. *Schematic showing the planned sampling of the backfill section. a) The sampling of the vertical backfill surface. b) The vertical sampling was performed in four different sections of the backfill. In addition, extra samples were also taken from the innermost part of the backfill section (Åkesson et al. 2019).*

8.2 Test plan

Several material tests were performed in the bentonite to determine the following properties:

- Water content.
- Density.
- Determination of exchangeable cations.

In addition to these tests, observations were made during the removal and sampling to study internal movements between the different material layers etc.

8.3 Test results

In the following section, the test results from Åkesson et al. (2019) are summarized where the main findings are presented.

8.3.1 Water content

The water content was measured in all samples in the bentonite seal and the results have been summarized in contour plots for each section as seen in Figure 8-3. As seen in the figure, the water content is highest in BT5 (closest to the filter) and in BT1 (closest to the concrete dome). If no leakage occurred in the rock, then the water content is expected to have its highest in BT5 and decrease over the thickness of the bentonite seal. Considering that the section closest to the concrete dome shows almost as high water-content as the section closest to the filter, this indicates that the bentonite seal has been by-passed in the full-scale test. Furthermore, the pore pressure sensor installed in the slot showed that the water pressure on the concrete dome was about 3 MPa while the filter pressure was 4 MPa. This also indicates that the bentonite seal was by-passed.

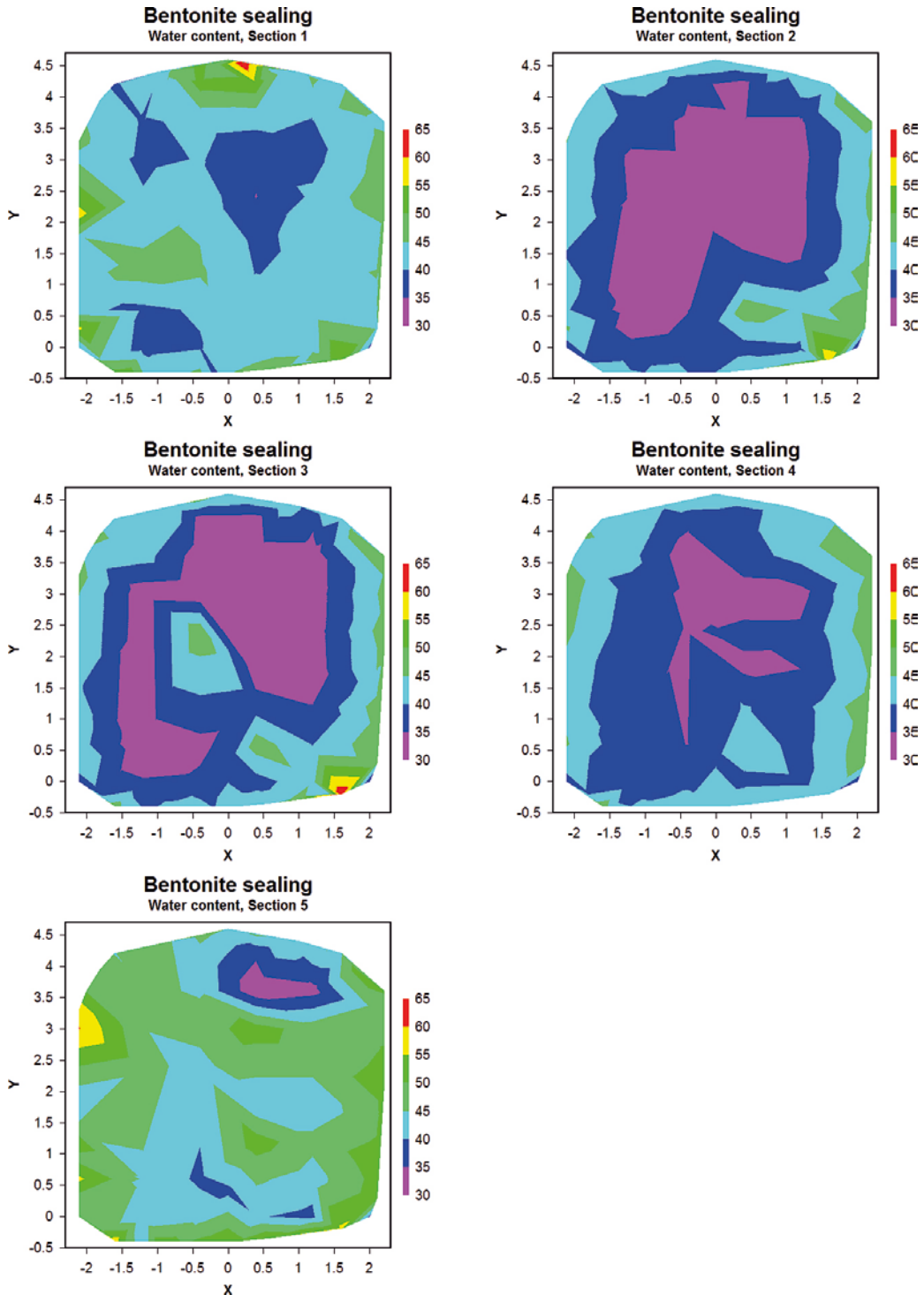

Figure 8-3. *Graphs showing the water content distribution in the bentonite seal in the five different sections sampled, Åkesson et al. (2019).*

The visualization of the results has been done in a similar way for the backfill which are presented in Figure 8-4. As can be seen from the results, the highest water content is obtained in section BF1 (closest to the filter) and BF4 (closest to the concrete wall). In this case, it was expected that the section denoted BF4 should show a high water-content since water also was pumped in to the macadam pocket located next to the concrete wall.

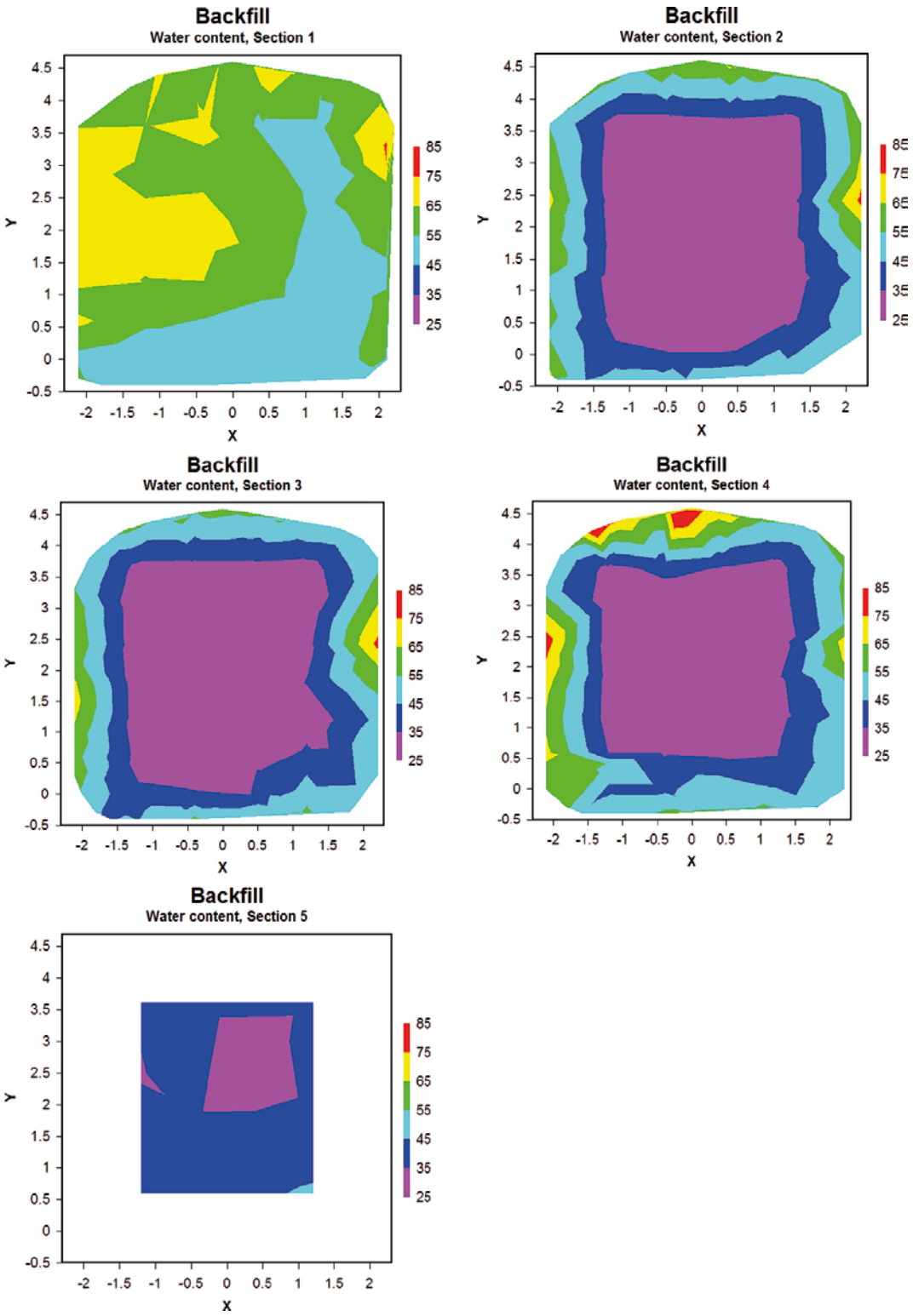

Figure 8-4. *Graphs showing the water content distribution in the backfill in the five different sections sampled, Åkesson et al. (2019).*

8.3.2 Density distribution

Bentonite seal

The dry density was determined for all samples in the bentonite seal and are presented for each section in Figure 8-5. In the figure, all samples taken from the central parts of the tunnel cross-section (i.e. where the blocks were stacked) are illustrated with black dots. All samples that were taken at the periphery, near the rock interface (i.e. where the pellets were installed) are illustrated with blue dots. As expected, the dry density is higher in the regions where the blocks were installed compared to where the pellets were installed. It is also reasonable that the sections closer to the middle of the bentonite seal shows less scatter and especially higher density of the former pellets filled slot. This is caused by the confining effect where the pellets closer to the upstream or downstream surfaces easier can expand towards the other materials.

Overall, the density in the bentonite seal varied between 1 020 and 1 460 kg/m^3. The lowest density was found in the periphery, where the dry density at installation was 900 kg/m^3. The density in these regions had after termination of the test increased to between 1 020–1 370 kg/m^3. This means that the central blocks, with an installed dry density of 1 682 kg/m^3 had swelled and compressed the pellet filling. The variation in density in the central parts varied between 1 120 and 1 460 kg/m^3.

The resulting dry density is also presented as contour plots in Figure 8-6 for each section. It can be seen in the figure that the dry density is lowest in section BT5 which is located closest to the filter. This indicates that the swelling of the bentonite seal has caused movement towards the filter, i.e. the bentonite seal has compressed the filter. The density is also lower in section BT1 which is located closest to the concrete beams. According to Åkesson et al. (2019), this is likely caused by flowing water during the initial pressurization to 4 MPa, where the water entered the bentonite seal from the initial gaps between the concrete beams (and through the mesh of the geo-textiles). This may have caused early swelling of the bentonite in this section.

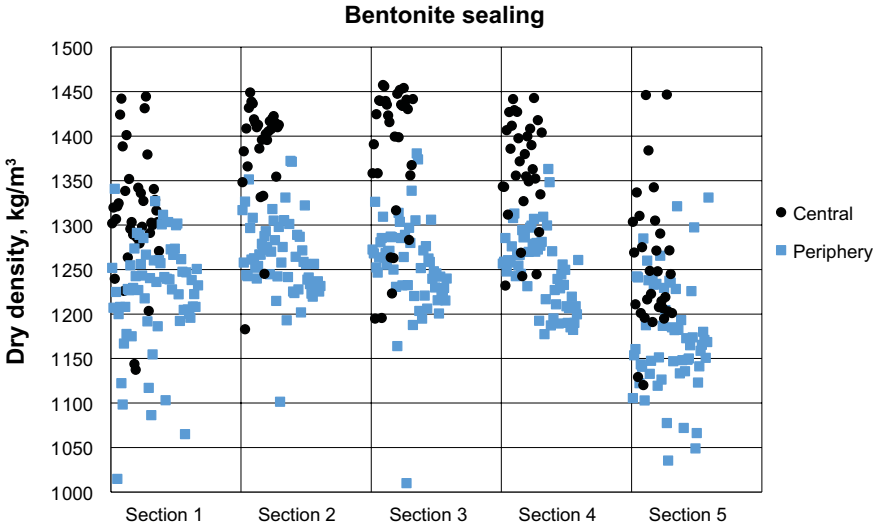

Figure 8-5. *Graph showing the results from all measurements on dry density in the bentonite seal. The results are divided after measuring section on the x-axis. The samples taken from the central parts (former block stack) are marked with black dots and the samples taken in the periphery (former pellet filled slot) are marked with blue cubes, Åkesson et al. (2019).*

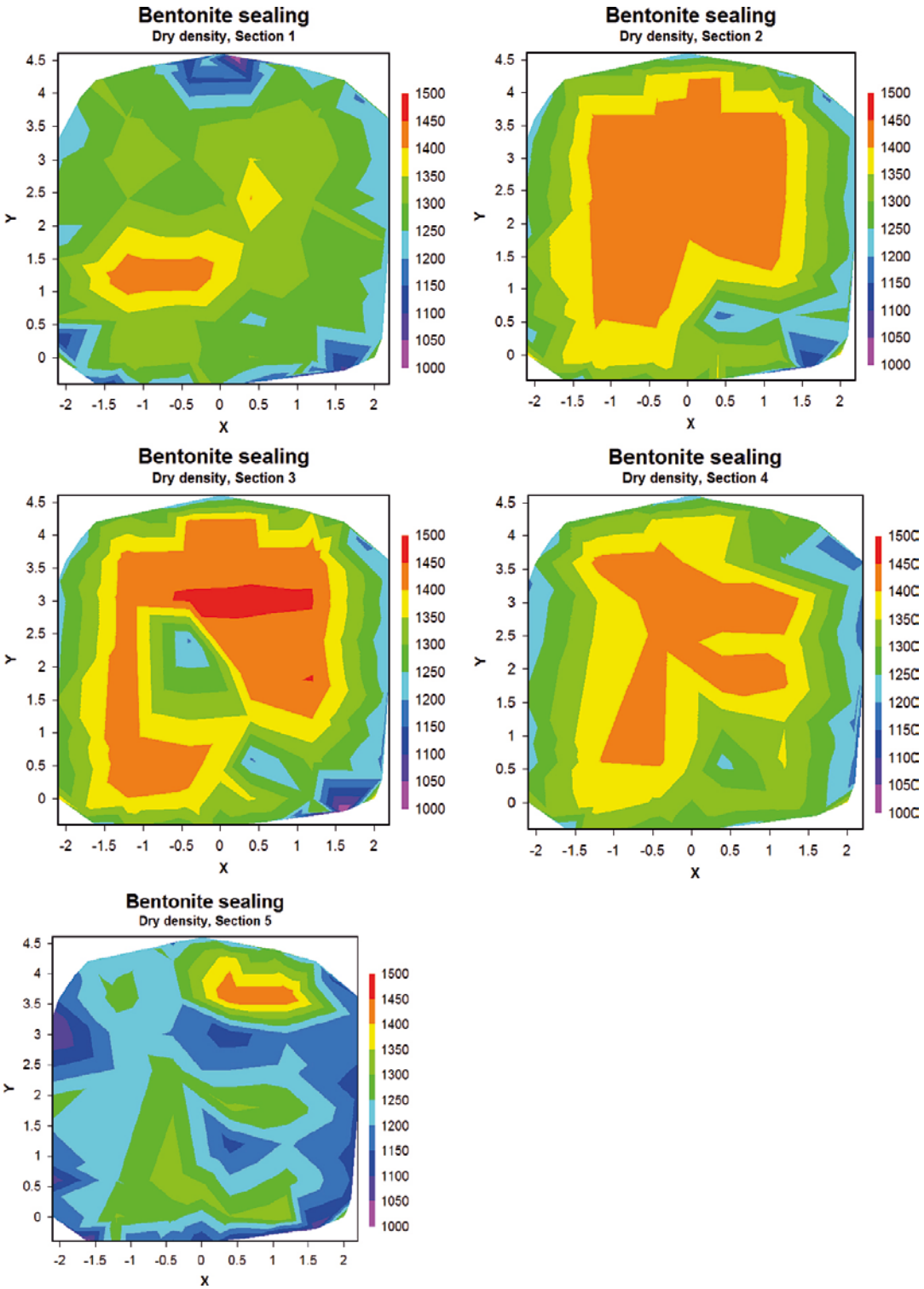

Figure 8-6. *Illustration of the distribution of dry density in the bentonite seal, Åkesson et al. (2019).*

Bentonite backfill

The dry density was determined for the samples in the bentonite backfill and the results are presented for each section in Figure 8-7. The results are presented in the same way as for the bentonite seal where the samples from the central parts of the tunnel cross-section (i.e. where the blocks were stacked) are illustrated with black dots. The samples that were taken at the periphery, near the rock interface (i.e. where the pellets were installed) are illustrated with blue dots.

The results show large difference between the periphery (i.e. where the pellets were installed) and the central part (i.e. where the blocks were stacked) for all sections except BF1 which is located closest to the LECA beams. The density for the periphery samples is between 875 and 1 225 kg/m^3. The density for the central parts was between 1 200 and 1 600 kg/m^3, with exception of Section 1 but also Section 5. The reason why the inner section is lower is because pellets were installed between these blocks and the concrete wall. According to Åkesson et al. (2019) these large differences in density shows that the backfill has not homogenized.

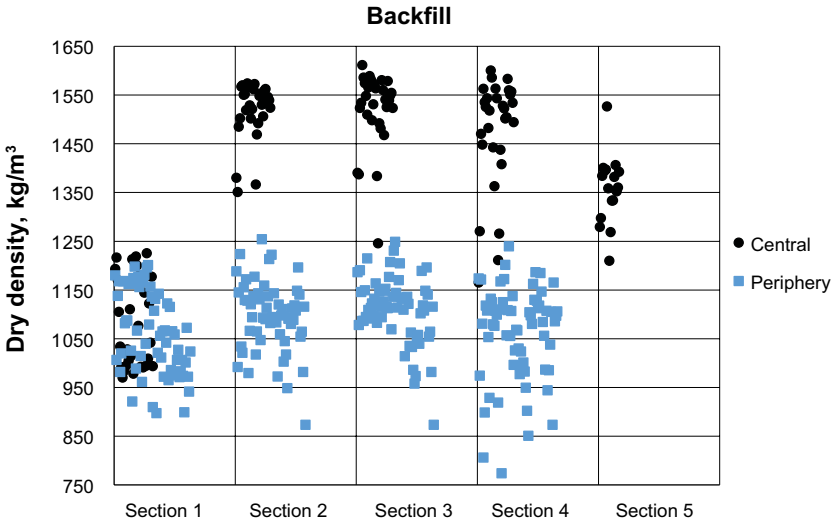

Figure 8-7. *Graph showing the results from all measurements on dry density in the backfill. The results are divided after measuring section on the x-axis. The samples taken from the central parts (former block stack) are marked with black dots and the samples taken in the periphery (former pellet filled slot) are marked with blue cubes, Åkesson et al. (2018).*

Results are also presented as contour plots for each section, see Figure 8-8. These results clearly show the high density of the central parts in Section 2 to 4. This is likely a result of that the bentonite backfill has not homogenized even after five years after construction.

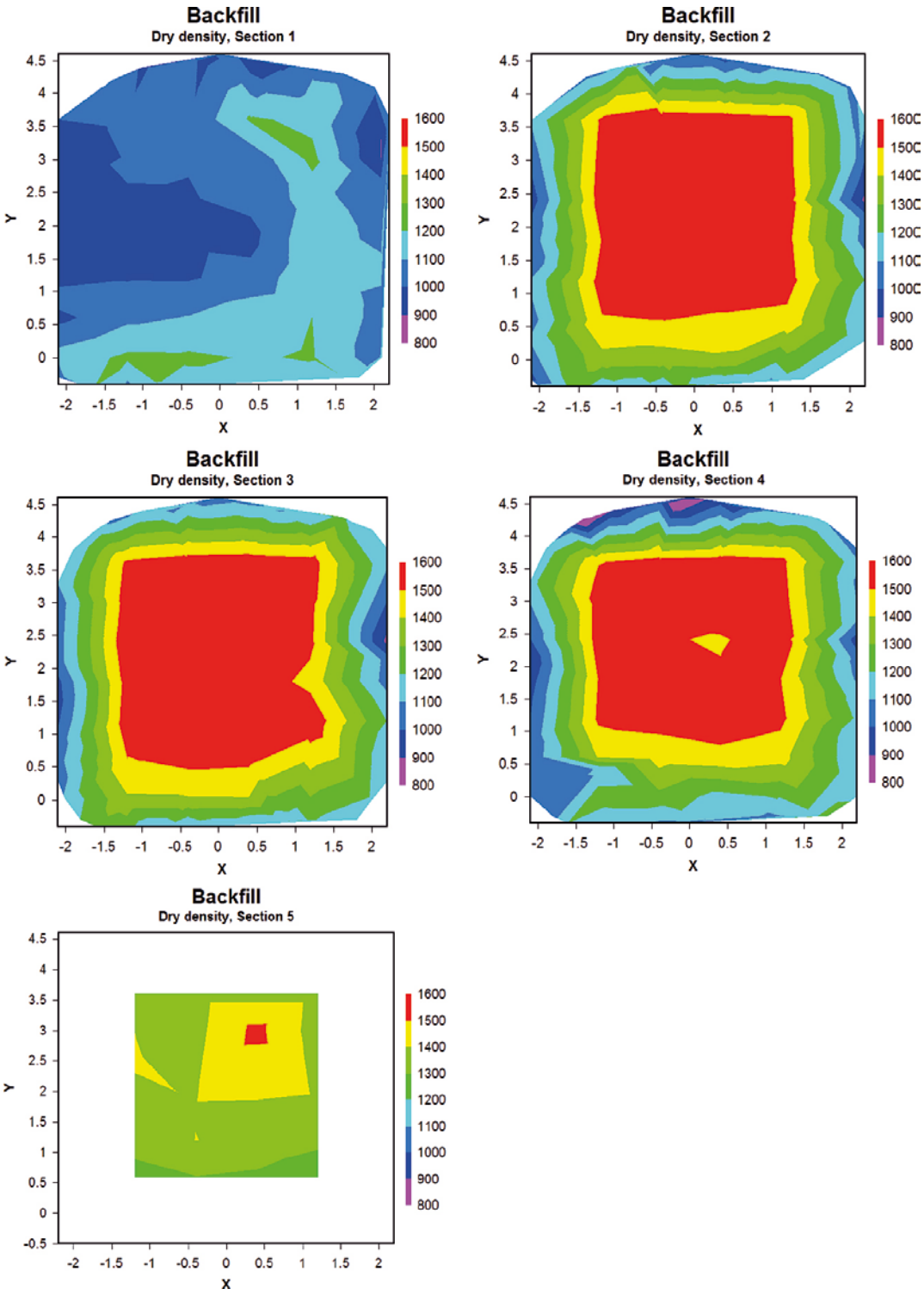

Figure 8-8. *Illustration of the dry density in the bentonite backfill, Åkesson et al. (2019).*

8.4 Evaluation

Based on the obtained density distribution and the water content, the degree of saturation was also calculated by Åkesson et al. (2019). Overall, the water saturation in the bentonite seal was between 96 and 102 % according to Åkesson et al. (2019). It should however be noted that the density and water content has not been determined on exactly the same samples since this is impossible. Instead these samples are taken as close to each other as possible. This may have resulted in some uncertainty and deviation in the calculated degree of saturation.

Similar calculation of the degree of saturation has also been performed for the backfill. The results show that the backfill is in general saturated except for the central parts of Section 3 and 4 that have lower degree of saturation, typically between 85 and 95 %. The density distribution confirms that both the back fill and bentonite seal have not had time to homogenize. However, homogenization was not expected during the time frame for the full-scale test since this is a slow process. The bentonite seal was designed to produce a swelling pressure slightly below 2 MPa during the time period of the experiment, which was well achieved.

9 Conclusions and experiences

This report summarizes the final phase of the DomPlu full-scale test of end plugs for the deposition tunnels in the KBS-3V reference disposal concept. The first part of the project was carried out in cooperation between SKB and Posiva Oy. The project has also received funding from the DOPAS project between 2012–2014. In the full-scale test, a deposition tunnel end plug was constructed in the Äspö HRL and installed in the crystalline rock at the intended depth of the planned deposition tunnels in the KBS-3V repository in Forsmark. The system design, construction of the plug and the early results were reported on by Grahm et al. (2015). In this report, the final phase of the project is described, where a gas leakage and a strength test were carried out. The plug was there after depressurized and deconstructed. Material tests were also performed for the included components in the plug. A summary will be given in this section, thereafter, the results will be discussed based on the purposes of the project, given in Section 1.2.

During the gas leakage test, the plug was depressurized as the filter was drained. When the filter was drained, it was filled with helium and the gas pressure was continually recorded. The filter was pressurized for 18 hours and during that time, the gas pressure increased slightly. The increased pressure was likely caused by inflow of groundwater leaking into the filter. A sniffer device was also used to examine if gas was leaking to the downstream side of the plug, but no helium was detected. It was concluded that the bentonite seal was gas tight.

During the gas leakage and strength tests, the plug was first depressurized to conduct the gas leakage test. The water pressure was thereafter increased to 8.1 MPa to evaluate the strength of the concrete dome. With the addition of swelling pressure from the bentonite seal the acting total pressure on the dome was up to 10.0 MPa. By evaluating the measurements from the instrumentation, it was concluded that the concrete dome exhibited some nonlinear behaviours, where the displacements increased after the tests. The nonlinearity was most likely caused by cracking or loss of bond in the interface between the rock and concrete dome. The numerical FE-simulations predicted the displacements and strain of the concrete dome quite well, even though they lacked the nonlinear material models.

Many sensors had failed in the backfill and bentonite seal at the time of the gas leakage and strength test. However, the one remaining extensometer showed some considerable nonlinear displacements in the LECA beams. The pore pressure sensors gave a pore pressure that was quite evenly distributed over the backfill and bentonite seal. The pore pressure in the slot abutment was also quite high, which shows that the bentonite seal was quite likely by-passed. The total pressure sensors gave a swelling pressure of 0.2 and 1.9 MPa in the bentonite seal, which is less than the maximum expected swelling pressure of 2 MPa. A similar swelling pressure was recorded in the backfill except in one sensor, which showed a significantly higher swelling pressure. No conclusion could be drawn regarding the nonconformant pressure sensor. However, it is believed that this area experienced high local deformations early in the project or that the water pressure in the filter as transmitted over a smaller section area in the backfill at this location.

Different numerical analyses were performed to predict the evolution of saturation, homogenization and swelling pressure in the bentonite seal and backfill. According to Åkesson et al. (2019) the numerical models showed fairly good ability to predict the overall evolution of relative humidity, swelling pressures and displacements. The hydro-mechanical model was performed with lower pressure compared to the experiment (only atmospheric pressure) due to convergence issues which resulted lower hydration rate. The lowest dry densities in the hydro-mechanical model significantly exceeded the lowest values observed in the in experimental data, which may be a model simplification.

The plug showed limited leakage from the beginning and was observed to be tighter than the rock at the test site. The main part of the leakage was due to experiment-related causes, such as the cable lead-through at the front of the concrete dome, the surrounding rock mass and a fracture in the rock, which surfaced in the access tunnel 14 m downstream of the plug. During the monitoring phase the leakages decreased further and stabilized after a few years. During the gas leakage test, when the plug was depressurized, the leakage almost stopped entirely. During the strength test, however, when the pressure was increased to 8.1 MPa, the leakage increased dramatically. The strength test did not leave

any permanent damage that influenced the leakage since it returned to its original leakage value when the pressure was resumed to 4 MPa. The test results show that a leakage of 1–2 l/h should be considered as an upper limit of the expected leakage of a plug, but a lower value can be expected, since the natural water head is lower than the artificial pressure applied in this full-scale test. Moreover, the rock at Forsmark is expected to be less fractured than at the test site.

The measurements of the concrete dome show that it behaved overall elastic, during both gas tightness test and the strength test, since the strain is about the same before and after a load event. This means that no cracking is expected in the concrete dome at the locations where these sensors were installed. However, the global sensors such as displacements (LVDT and joint-meters) showed that some non-linear effects had occurred during these tests. The numerical model of the concrete dome validated these results and also showed high risk of loss of bond between concrete and rock in the slot, which could explain the non-linear effects measured by the displacement sensors. This was later confirmed with tests during the demolition. The FE-simulation gave good predictions of the behaviour of the concrete dome regarding all measured behaviours, e.g. temperatures, strains and deformations.

Non-destructive tests were performed on the concrete dome to search for manufacturing defects such as material separation, delamination and honeycombing. No such defects were detected but some methods were able to locate the cooling pipes and the periphery of the concrete dome. It should be mentioned that no defects were found inside the concrete dome, except a void in the top. The instruments used were not well adapted for the curved surface and massive thickness of the concrete dome and the abutments of the concrete dome could not be examined. However, it was deemed likely that MIRA and GPR could be used in future projects and that a NDT-programme for continuous monitoring could be implemented in the spent fuel repository.

To evaluate the state of the concrete dome after the depressurization of the plug, an extensive core drilling campaign was performed in the concrete dome. The core samples were tested for mechanical properties, bond strength at the interface with the rock and properties related to durability. The mechanical properties were close to the expected values, however, the bond strength between the rock and concrete was low. The properties related to durability were also close to the expected values even though it was noted that the concrete had a slightly higher permeability than expected which likely was caused by micro cracks in the cement paste.

The demolition of the concrete dome was performed with a remote controlled electric demolition robot equipped with a hydraulic hammer. The demolition took 18 days and went well, even though it could have been faster if for instance a larger hydraulic hammer had been used. The logistics of the test tunnel also turned out to be an issue and the removal of the demolition rubble took quite some time and delayed the demolition. The demolition of the backfill was carried through very carefully in order to perform undisturbed material tests and did not reflect a failure scenario where a plug has to be retrieved in the final repository.

During the drilling of the core samples, a large void was detected in the top of the concrete dome. The void occurred during the pouring of the concrete dome because the formwork was not top filled. The void had an estimated volume of about 0.8 m^3. During the contact grouting, a 10 cm thick layer of grout was collected in the void. The concrete dome performed as expected despite the void. Finding the void did however explain why some sensors in the top of the concrete dome failed prematurely and why there was an increased leakage in the top of the dome.

The bentonite material tests showed that the bentonite was not saturated through. The central parts of the bentonite seal and the backfill had a quite low degree of water content, while the periphery contained more water. The downstream side of the bentonite seal had a quite high degree of saturation, along with the measurements of pore water pressure in the abutment of the concrete dome, this shows that the bentonite seal quite likely was short circuited. The short circuiting means that water was able to travel past the bentonite seal, most likely in cracks and possibly to some extent in micro cracks in the rock. The dry density of the bentonite seal and backfill shows that the bentonite had a quite low degree of consolidation. The central parts of the bentonite seal and backfill had a high density, while the periphery and the pellet filled section had quite a bit lower density.

9.1 Discussion of results

9.1.1 Feasibility of the plug structure

The full-scale test demonstrated that the DomPlu is a feasible design method for deposition tunnel end plugs. A large waterfilled cavity was found in the top of the concrete dome, where the concrete was not top filled. Despite of the cavity in the top of the concrete dome, the plug system performed as expected.

The intention of the bentonite seal is to create a water tight section to prevent leakage and the main task of the concrete dome is to resist the hydrostatic pressure load. However, in the full-scale test, water could likely bypass the bentonite seal through cracks or microcracks in the rock. The function of bentonite seal is reduced if the water can travel through the rock and the concrete dome therefore provided more to the water tightness than was intended in the design.

It cannot be concluded from the full-scale test if the water by-passed the bentonite seal trough the fracture network at the test location or through microcracks caused by the EDZ. It is, however, most probable that the water transport that by-passed the bentonite seal occurred due to the network of natural fractures in the rock. Thereby, it is important to choose adequate plug locations without fractures that can become water transmissive in the spent fuel repository. In addition, SKB is currently investigating alternative methods for excavation of the deposition tunnels with a technique that will significantly reduce the EDZ in the rock. The design of the bentonite seal may also be revised in future designs, if for instance larger swelling pressure is allowed, etc.

9.1.2 Evaluation of construction methods

The construction methods were presented and discussed in Grahm et al. (2015). Only findings made during this project will be discussed in this section. The large cavity in the top of the concrete dome occurred during the casting. Future construction should make certain that this issue does not arise again. This is further discussed in Section 9.2.1.

The shrinkage of the concrete dome was smaller than expected during the design. The result was that the interface between the concrete dome and the rock was only partially filled during the contact grouting. The partial grouting resulted in a smaller prestress than expected. The low shrinkage could result from a lower autogenous shrinkage, that the cooling was not sufficient or that the shrinkage was restrained. A combination of factors is also possible.

The formworks used for the casting of the concrete dome was designed for much higher pressures than necessary. A slimmer and more optimized form would make the construction easier to perform. This is further discussed in Section 9.2.1.

9.1.3 Load bearing capacity and behaviour during normal operation

The full-scale test was performed with a lower water pressure than initially intended, due to large leakage in the fractured rock. The strength test performed in 2017 showed that the concrete dome can withstand the intended design loads without sustaining serious cracks or damage. Some nonlinear behaviour was noticed, likely cracking or loss of bond in the interface between the concrete dome and the rock. However, this is considered normal in concrete structures and does not constitute an issue for the structural integrity of the concrete dome.

The plug was pressurised to 4 MPa of water pressure for three years, during this time some small displacements occurred in the concrete dome as seen in Section 4.2.1. The displacements were nonlinear to some extent and depended on increased swelling pressure and creep in the concrete dome. However, some long-term displacements are expected in concrete structures and the recorded displacements does not cause a threat to the function or the structural safety of the concrete dome.

9.1.4 Leakage

The rock at the test site was highly fractured. This led to large leakages that was related to the experiment setup rather than the design of the plug. Large leakage was also observed in the cable bundle to the sensors used to monitor the test inside the concrete dome. The leakage through the concrete dome was 1–2 l/h at 4 MPa. This should, however, be considered a maximum value, since the water head will be considerably lower when an external water pressure is not applied.

When the plug was depressurized for the gas test and before the demolition, the leakage stopped. Which shows that the leakage came from the pumps and not the inflow of water from the surrounding rock. During the strength test, when the water pressure was increased from 4 MPa to 8.1 MPa, the leakage increased about 20 times. However, after the strength test when the water pressure returned to 4 MPa, the leakage returned to the same level as before the test. This shows that no nonlinear damage, which affected the leakage occurred.

9.1.5 Gas tightness

The plugs in the spent fuel repository should be gas tight and have the ability to stop convection of air between a plugged deposition tunnel and the operating repository. A gas leakage test was performed, to test the gas tightness of the plug. Helium gas was pumped into the depressurized and drained filter and an overpressure was maintained for 18 hours. The plug held the gas pressure and the gas sniffer was not able to detect any helium in the experiment tunnel. The plug was therefore considered to be gas tight.

9.1.6 Evaluation of control and measurement tools

The instrumentation in bentonite seal, backfill and concrete dome was used in the DomPlu test to monitor its behaviour. The plugs in the spent fuel repository will not have these sensors installed, which eliminate the risk for leakage in cables or the cable lead-through. However, for the sake of the full-scale test, the instrumentation has been considered a success and much knowledge has been gained even though many sensors failed during the operation.

Several methods for non-destructive testing were used. The tests with Ultra-sonic pulse-echo concrete tomography (MIRA) and Ground Penetrating Radar (GPR) were quite successful even though more testing is required if the methods should be considered for use in the repository. Some development, modification and automatization of the hardware used might also be required. In addition, the software for interpreting the data would have to be updated to handle the curved surface of the concrete dome.

9.1.7 Evaluation of analysis methods

The FE-models used for predicting the behaviour of the concrete dome and the bentonite were developed before the full-scale test commenced and was reported on in Grahm et al. (2015). During this final part of the project, there were several chances to control if the predictions made were correct.

The FE-simulations for the concrete dome did not incorporate a nonlinear material model or the swelling pressure from the bentonite. However, during the depressurization for the gas leakage test and the subsequent loading in the strength test, the FE-model predicted the displacements and strains with good accuracy.

9.2 Lessons learned

The full-scale test of the dome plug has shown that the design concept works and that it is possible to build a plug that meets the defined requirements. Some areas of improvement have been identified during this project, which will be discussed in the following section.

9.2.1 Improvements of the concrete dome design

Casting of the concrete dome

The main area of improvement regarding the concrete dome is to ensure that the void detected in the top of the dome does not occur in future plugs. This is essential considering that the casting of the dome showed that air was trapped in the top of the dome and thereby the number of venting tubes in the DomPlu test was not sufficient to evacuate the air. To prevent this, improved measures are required regarding the venting pipes; either with larger diameter tubes or additional tubes in the top. A method for controlling that the concrete dome is top filled should also be incorporated. This can be done, either by using sensors for monitoring the casting or using a camera in the top that allows for visual inspection inside the formwork during casting. All these measures are intended to prevent that pumping of concrete is not stopped before the slot is filled to the top.

The venting tubes could be placed within the concrete body and should be removed after casting is finished to prevent possible leakage paths. Alternatively, the venting pipes could be placed in the rock, but also in this case it is important to prevent that these form leakage paths in the future. Two examples for placement of venting tubes are illustrated in Figure 9-1. It could also be possible to use grouting tubes in the positions shown in Figure 9-1 for additional grouting as a complement to the circular grouting tubes placed in the slot.

It should also be possible to cast the top of the dome with a modified concrete mix, consisting of smaller aggregates and higher amount of super-plasticizer. This would improve the flowability of the low-pH concrete and could thereby simplify top filling of the slot. This is however, difficult to perform with the pumping technique used in the DomPlu test. The concrete was pumped in the top of the formwork and thereby pumped in at a lower elevation than the slot, see Figure 9-2a. To use a modified concrete mix would require additional pumping pipes at the top of the slot. Same as with the venting pipes, it is important that these are removed after casting and that the volume is filled with concrete to avoid future leakage paths.

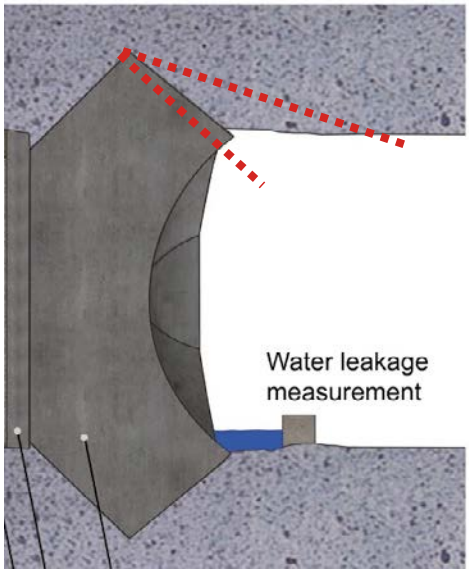

Figure 9-1. *Illustration of possible placements of venting tubes or grouting tubes to fill the slot.*

The used technique of pumping in concrete in the formwork at a lower elevation meant that the surface of the concrete always was above the pumping position. This means that the surface of the rising casting-front obtained a hardened skin which was pushed upwards during casting. During the sampling of cores, this hardened skin of the casting surface was detected in one of the cores as seen in Figure 9-2b. Vogt (2019) pointed out that this has not affected the performance of the concrete dome. However, to prevent this, it is recommended that pumping of concrete occasionally is pumped in from above the free surface.

Improved formwork

The formwork used was quite extensive and was designed according to normal praxis, i.e. to carry the full hydrostatic pressure of the concrete, see Figure 9-3. Due to the low casting rate, the maximum obtained pressure on the formwork was only about 25 % of the maximum hydrostatic pressure, see Grahm et al. (2015). It should therefore be possible to design the formwork based on a lower pressure than the full hydrostatic pressure. In addition, it would be beneficial if the formwork could be adjusted to make it easier to re-use and adapt to varying tunnel geometry. Finally, the NDT testing showed that the irregularities of the downstream surface caused problems during testing and assessment of the dome. Therefore, a smoother surface is desired for the downstream part of the dome.

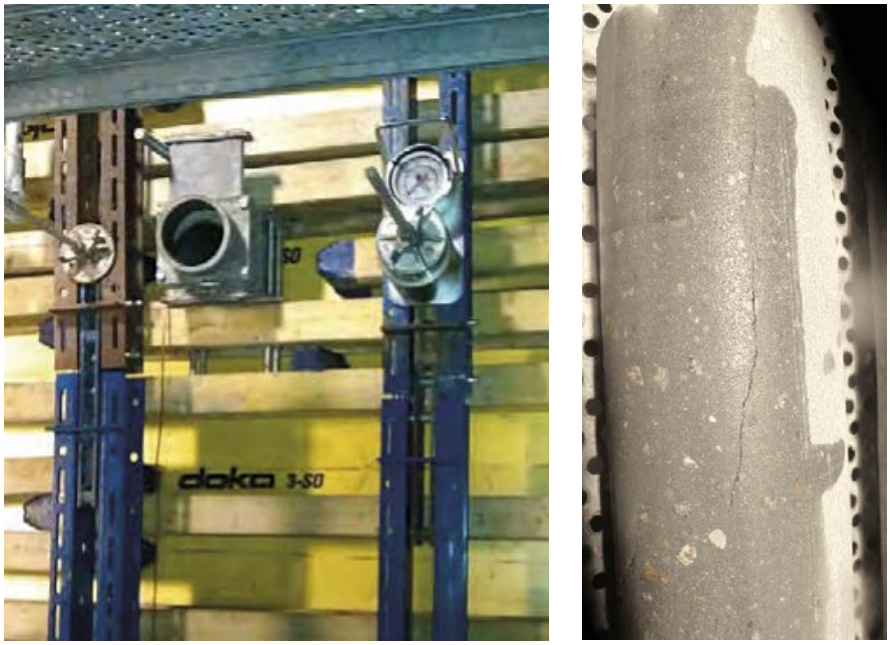

a) b)

Figure 9-2. *a) Illustration of the formwork with the connection for pumping hose, b) The observed hardened skin from casting seen in one concrete core.*

a) b) c)

Figure 9-3. *Illustration of the formwork used for casting the concrete dome.*

Simplify the installation procedure

One of the design premises of the concrete dome was that it should completely release from the rock as a result of the shrinkage and cooling procedure. As shown in this report, this was not the case where only partial release may have been obtained. One possible reason for this could be that the shrinkage was lower than expected, which is indicated by the measurements and simulations of the concrete dome. Another explanation could be that micro-cracking occurred within the cement matrix of the concrete material instead of loss of bond in the top of the dome.

Regardless, the initial state of the concrete dome should be further analysed and especially regarding improvements in the cooling scheme and the need for breaking the bond between concrete and rock prior to contact grouting.

Updated geometry of the concrete dome

There are several on-going investigations and suggested design modifications that may influence the loads acting on the concrete dome or its load carrying capacity. One of these, is that the excavation method of the deposition tunnels is currently investigated. Based on a targeting decision, the cross-sectional area of the tunnel will be decreased. Decreasing the tunnel cross-section results in lower total pressure loads acting on the concrete dome. This means that it is necessary to evaluate how the current design can be transferred to a case with smaller tunnel.

Another aspect that will influence the design of the concrete dome is changes to the bentonite seal, especially if they lead to changes in the expected swelling pressure. One discussion that has been on-going is to allow for higher swelling pressure in the bentonite seal, which would allow for a more robust construction. The design assumption of the concrete dome was that the swelling pressure should be 2 MPa. However, considering the uncertainties in the pressure load (regarding its size, distribution and when the pressure occurred) a safety factor of 2 was used, e.g. a design swelling pressure of 4 MPa. This was not a designing factor for the dome as the current design have significantly higher load capacity than this as shown by Malm (2012). However, it is important to remember that these analyses assumed that the concrete dome was stress-free prior to contact grouting, e.g. complete loss of bond in the concrete rock interface was assumed.

Further analyses of the geometry of the concrete dome are also needed, especially with the purpose to redesign the downstream surface to allow for easier formwork design and easier evaluation with non-destructive testing methods.

Breaching / demolition of the concrete dome

The DomPlu project showed that it is possible to breach and demolish the concrete dome if needed. The technique used with a hydraulic hammer worked as intended. However, a few areas for improvement have been identified:

- Using a larger demolition machine with a more powerful hydraulic hammer is recommended.
- The logistics in the experiment tunnel and the access tunnel was not optimal and the demolition was delayed because of this. In the final repository, the access tunnels will be larger and the logistics less challenging. However, the demolition should be planned in advance with logistics in mind.
- It would be beneficial if the same machine could be used for the hydraulic hammering and removing the demolition rubble.
- The demolition work produced a large amount of dust from the broken off concrete, this was helped by spraying water to bind the dust. To further improve this, the nozzle for the hose should be mounted on the hydraulic hammer.

9.2.2 Improvements of the bentonite seal, filter and backfill

Updating the bentonite seal section

The bentonite seal is designed to constitute the water tight part of the plug and to ensure that the swelling pressure acting on the concrete dome should be 2 MPa. As mentioned previously, the plug structure would be more robust if higher swelling pressures could be allowed and this would further increase the water tightness of the plug. The results from the full-scale test indicate that the bentonite seal was water tight. However, the high permeability of the adjacent rock resulted in that the leakage by-passed the bentonite seal to a great extent. The risk for this can be reduced with the following revisions:

- A new excavation method for the deposition tunnel that results in smaller excavated damaged zone (EDZ) in the rock. It however, not possible to quantify if leakage past the bentonite seal in the EDZ from the full-scale test and therefore, it is unknown how much this would affect the results.
- Another important factor is that fractures in the rock that may by-pass the plug should not be allowed at the plug location.
- The third action is to ensure that the bentonite seal intersects the EDZ in the rock. It is not possible to quantify the existent or extent of leakage in EDZ from this test. However, if this is an issue then this could be achieved by excavation a larger tunnel diameter at the location of the filter and seal using a method that yields minimal EDZ, such as wire-sawing. This was already proposed in Malm (2012) and is illustrated in Figure 9-4.

Regarding the size of the swelling pressure, which varied between 0.2 and 1.9 MPa in the bentonite seal, it is important to remember that the full-scale test had a limited duration and the swelling pressure in the bentonite seal was expected to increase further if the test would continue for many more years, see Grahm et al. (2015). In the full-scale test the intention was to achieve a swelling pressure that produce a swelling pressure in the region that was less than the maximum allowed swelling pressure of 2 MPa.

In the current design, different types of bentonite blocks are used for the backfill and for the seal. From a logistic perspective, it would be easier if it is possible to use the same type of blocks for the bentonite seal as for the bentonite backfill. This would likely result in higher swelling pressures acting on the concrete dome.

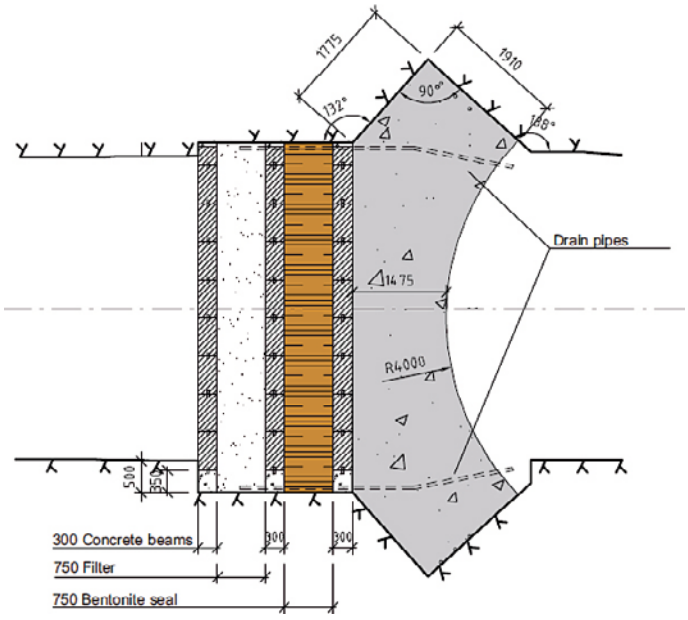

Figure 9-4. *Illustration of plug design with larger bentonite seal section, from Malm (2012).*

Optimizing the filter section

Drainage of the filter is an important function of plugs for the spent fuel repository to facilitate the construction of the concrete dome. If the water pressure is not relieved during curing (hardening) and contact grouting of the concrete dome, there is a large risk that the structure would be damaged. A drainage function is also important in case of demolition of a malfunctioning plug. The demolition would be very dangerous if the plug was exposed to a large water pressure.

The filter was also used to saturate the bentonite seal artificially before the full water pressure was applied. This proved to be quite successful and it will be necessary to perform the same operation in the spent fuel operation. Especially because the expected natural water flow will be substantially lower.

The inlet of the drainage pipes clogged during the full-scale test due to the use of a fine copper mesh at the end of the pipe which is installed in the filter. This also proved to be an issue when the drainage pipes were used for pumping in water into the filter for the initial filling of the filter and during subsequent drainages. The copper mesh was clogged several times and had to be back-flushed. Alternatives to the fine copper mesh should therefore be investigated further. In addition, increasing the number of drainage pipes would increase the robustness of the plug. The improvements of the drainage pipes should also be incorporated for the venting pipes that were installed in the filter section.

Backfill end zone

A one-meter thick bentonite backfill was part of the DomPlu full-scale test. In the reference design, the backfill closest to the plug is denoted as backfill end zone. The intention of the backfill end zone is to gradually decrease the swelling pressure that occurs in the deposition tunnel towards the plug. In the full-scale test the swelling pressure in the backfill varied between 0.2 and 1.9 MPa except for one sensor, which showed a significantly higher pressure. Structurally, the concrete some can handle a considerably higher pressure, as mentioned in Section 9.2.1. When evaluating if an increased pressure on the concrete dome should be allowed, the possibility to exclude the backfill end zone should also be investigated. Using the same backfill blocks in the entire deposition tunnel, all the way to the filter section of the plug would simplify the installation and reduces the need for storage of different kinds of bentonite blocks that needs to be installed in different regions.

9.3 Future activities

In addition to the activities discussed in the previous section, some future activities should be investigated further to simplify the plug and to increase its robustness. These activities are discussed in the following section.

Evaluate possibility to use a grout curtain at the plug location

One method to reduce leakage through the rock would be to install a grout curtain at the plug location prior to the excavation of the slot. The design life-span of the plug is relatively short and therefore a grout curtain could be a suitable measure. A grout curtain would increase the robustness and flexibility of the plug and reduce the water transport caused by poor rock quality that could short circuit the plug. It is important to consider the long-term effect on the water transport in the rock if the grout degrades, and therefore this need to be analysed further before such a solution could be considered as acceptable. The possibility to use a grout curtain should therefore be investigated further, and also if this has any possible implication on the long-term safety of the repository.

Evaluate the possibility to use rock bolts at plug location to secure the rock

The occupational safety of workers from the risk of rock blocks falling down, is an important aspect to consider at the slot abutment. In the DomPlu test, this was achieved by building a support frame with a mesh that prevented falling blocks, see Figure 9-5. In a future repository, the slot can either be excavated directly after the excavation of the deposition tunnel or just before installation of the plug. Depending on when the slot is excavated, the need for occupational safety measures varies. Keeping a rock excavation open for a longer period of time increases the risk of large deformations, rock spalling or falling blocks.

Installation of a supporting steel structure, may interfere with transportation in the tunnel to some extent. A steel frame might therefore not be viable in a case where the tunnel area is reduced, since it could result in a size restriction of the transport past the plug location.

Installing rock bolts could be one method to stabilize the rock at the plug location. However, it needs to be further analysed if the installation of bolts can affect the performance of the plug system.

a) b)

Figure 9-5. *a) Erected safety scaffolding including a mesh to protect workers from falling rocks. b) Detail of the scaffolding with two of the Ø 250 mm boreholes for the wire-sawing are also visible. From Grahm et al. (2015).*

References

SKB's (Svensk Kärnbränslehantering AB) publications can be found at www.skb.com/publications. SKBdoc documents will be submitted upon request to document@skb.se.

Börgesson L, Sandén T, Andersson L, Johannesson L-E, Goudarzi R, Åkesson M, 2015. System design of Dome Plug. Preparatory modelling and tests of the sealing and draining components. SKB R-14-25, Svensk Kärnbränslehantering AB.

Chandler N A, Cournut A, Dixon D, Fairhurst C, Hansen F, Gray M, Hara K, Ishijima Y, Kozak E, Martino J, Masumoto K, McCrank G, Sugita Y, Thompson P, Tillerson J, Vignal B, 2002. The five year report of the Tunnel Sealing Experiment: an international project of AECL, JNC, ANDRA and WIPP. AECL-12127, Whiteshell Laboratories, Canada. Available at: https://inis.iaea.org/collection/NCLCollectionStore/_Public/41/057/41057251.pdf?r=1&r=1

Dahlström L-O, 2009. Prototype Repository. Experiences from the design and construction of plug II in the Prototype Repository. SKB R-09-49, Svensk Kärnbränslehantering AB.

Dixon D A, Priyanto D, Korkeakoski P, Farhoud R, Birch K, Man A, 2016. Full-Scale tunnel and shaft seals: Tunnel Sealing Experiment (TSX) and Enhanced Sealing Project (ESP). Presentation at DOPAS – Full Scale Demonstration of Plugs and Seals 2016 Workshop, Turku, Finland, 24–27 May 2016. Available at: http://www.posiva.fi/files/4148/3.2_Dixon_DOPAS_2016_TSX_ESP.pdf

Germann Instruments, 2018. MIRA. Available at: http://germann.org/products-by-application/flaw-detection/mira

Grahm P, Karlzén R, 2015. System design of Dome Plug. Experiences from full-scale wire sawing of a slot abutment for the KBS-3V deposition tunnel plug. SKB R-14-24, Svensk Kärnbränslehantering AB.

Grahm P, Malm R, Eriksson D, 2015. System design and full-scale testing of the Dome Plug for KBS-3V deposition tunnels. Main report. SKB TR-14-23, Svensk Kärnbränslehantering AB.

Kristensen A L, 2018. Revised replacement report. Examination of Vault Plug. Report 117-30437, Force Technology. SKBdoc 1618653 ver 1.0, Svensk Kärnbränslehantering AB.

Magnusson J, Mathern A, 2015. System design of Dome plug. Experience of low-pH concrete mix B200. Material properties from laboratory tests and full-scale castings. SKB P-14-26, Svensk Kärnbränslehantering AB.

Malm R, 2012. Low-pH concrete plug for sealing the KBS-3V deposition tunnels. SKB R-11-04, Svensk Kärnbränslehantering AB.

Malm R, 2015a. Instrumentation and evaluation of the concrete dome plug DOMPLU. TRITA-BKN, Report 147, KTH Royal Institute of Technology, Sweden.

Malm R, 2015b. Evaluation of the concrete dome plug DomPlu – follow-up 2015. TRITA-BKN, Report 156, KTH Royal Institute of Technology, Sweden.

Malm R, 2016. Evaluation of the concrete dome plug DomPlu – follow-up 2016. TRITA-BKN, Report 161, KTH Royal Institute of Technology, Sweden.

Malm R, 2017. Evaluation of the concrete dome plug DomPlu – follow-up 2017. TRITA-BKN, Report 167, KTH Royal Institute of Technology, Sweden.

Malm R, 2018. Full-scale test of an unreinforced concrete dome plug for the spent nuclear fuel repository. Nordic Concrete Research Journal 58, 55–75.

Malm R, Enzell J, Hassanzadeh M, 2019. Full-scale test of the Dome Plug for KBS-3V deposition tunnels, structural response of the concrete dome. NDT, FE-simulations and evaluation of measurements during the leakage and strength test. SKB P-18-14, Svensk Kärnbränslehantering AB.

Martino J B, Dixon D A, Holowick B E, Kim C-S, 2011. Enhanced Sealing Project (ESP): seal construction and instrumentation report. APM-REP-01601-0003, Nuclear Waste Management Organization, Canada.

Posiva SKB, 2017. Safety functions, performance targets and technical design requirements for a KBS-3V repository. Conclusions and recommendations from a joint SKB and Posiva working group. Posiva SKB Report 01, Posiva Oy, Svensk Kärnbränslehantering AB.

SKB, 2010a. Design and production of the KBS-3 repository. SKB TR-10-12, Svensk Kärnbränslehantering AB.

SKB, 2010b. Design, production and initial state of the backfill and plug in deposition tunnels. SKB TR-10-16, Svensk Kärnbränslehantering AB.

SKB, 2014. Svar till SSM på begäran om komplettering rörande grundvattenkemi på kort och medellång sikt. SKBdoc 1437441 ver 1.0, Svensk Kärnbränslehantering AB. (In Swedish.)

Svemar C, Johannesson L-E, Grahm P, Svensson D, Kristensson O, Lönnqvist M, Nilsson U, 2016. Prototype Repository. Opening and retrieval of outer section of Prototype Repository at Äspö Hard Rock Laboratory. Summary report. SKB TR-13-22, Svensk Kärnbränslehantering AB.

Vogt C, 2019. Sampling, testing and properties of low-pH concrete in the KBP1016 dome plug. SKB P-18-16, Svensk Kärnbränslehantering AB.

Vogt C, Lagerblad B, Wallin K, Baldy F, Jonasson J-E, 2009. Low pH self compacting concrete for deposition tunnel plugs. SKB R-09-07, Svensk Kärnbränslehantering AB.

Åkesson M, 2017. Full-scale test of the Dome Plug for KBS-3V deposition tunnels. Gas tightness test. SKB P-17-37, Svensk Kärnbränslehantering AB.

Åkesson M, Sandén T, Goudarzi R, Malmberg D, 2019. Full-scale test of the Dome Plug for KBS-3V deposition tunnels. Monitoring, function tests and analysis of bentonite components. SKB P-18-15, Svensk Kärnbränslehantering AB.

Arkitektkopia AB, Bromma, 2019

SKB is responsible for managing spent nuclear fuel and radioactive waste produced by the Swedish nuclear power plants such that man and the environment are protected in the near and distant future.

skb.se